The
Massachusetts Bay Water Quality Model:
2006-2007 Simulation

Massachusetts Water Resources Authority
Environmental Quality Department
Report 2009-11

The Massachusetts Bay water quality model: 2006-2007 simulation

Prepared by:

Rucheng Tian, Changsheng Chen, Qichun Xu, Pengfei Xue,
Geoffrey Cowles, Bob Beardsley, Brian Rothschild

Department of Fisheries Oceanography
School for Marine Science and Technology
University of Massachusetts Dartmouth
706 South Rodney French Blvd
New Bedford, MA 02744

submitted to
Massachusetts Water Resources Authority
Environmental Quality Department
100 First Avenue, Building 39
Charlestown Navy Yard
Boston, MA 02129
(617) 242-6000

July 2009

Citation:

Tian R, Chen C, Xu Q, Xue P, Cowles GW, Beardsley RC, Rothschild BJ. 2009. The Massachusetts Bay water quality model: 2006-2007 simulation. Boston: Massachusetts Water Resources Authority. Report 2009-11. 124 p.

Executive Summary

Under contract with Massachusetts Water Resources Authority, the University of Massachusetts Dartmouth's Marine Ecosystem Dynamic Modeling team conducted model simulations for the Massachusetts Bay system. These models simulate the water motion (hydrodynamics) and the biologically-driven changes in carbon and nutrients (water quality) of the study area -- Boston Harbor, Massachusetts Bay and Cape Cod Bay -- for the years 2006 and 2007. This report presents the simulation, validation, and interpretation for the water quality model; a separate report describes the hydrodynamic model. Projection of the impact of the MWRA effluent on water quality parameters such as algal development and dissolved oxygen level and sensitivity analysis on surface wind forcing are presented as well.

The model generally reproduces field observations of an array of biological, environmental and water quality variables in both magnitude and seasonal variation. The model reproduces the spring and fall phytoplankton blooms with their high chlorophyll concentration and primary production. Although there was good agreement in general between the simulation and observations, the model tended to underestimate chlorophyll when it was high and overestimate chlorophyll when it was low; this could result from an inaccurate carbon to chlorophyll ratio. Also, the model tended to underestimate dissolved oxygen (DO) in the deep layer during summer, which probably resulted from underestimation of vertical mixing strength.

Sensitivity analysis did not reveal a substantial impact of the MWRA outfall on the ecosystem function in general. Although the simulation without the MWRA outfall predicted slightly lower primary production in summer and fall, DO in the bottom layer was practically the same between the two runs. Effluent dispersion was determined by water movement, which was subject to both local and remote forcing. Local currents had a strong response to wind forcing so that the influence of effluent on ecological function was partly controlled by the prevailing wind. Indeed, sensitivity analysis shows that forcing the model with a high-resolution wind field corrected to some extent the discrepancy between simulation and observation by increasing the DO level in the bottom layer by 9-18% in 2007. Biological responses to upwelling and storm events depend not only on the strength and direction of the wind, but also on the timing of events and the availability of light and nutrients. Our simulations revealed that south-southwesterly upwelling wind is unfavorable to effluent dispersal from the MWRA outfall whereas north-northeasterly downwelling wind is favorable .

Table of Contents

List of Figures

List of Tables

1. Introduction

1.1. Project overview

The Massachusetts Water Resources Authority (MWRA) has established a long-term monitoring program to evaluate the impact of MWRA sewage treatment plant effluent on the ecosystem function and water quality in the Massachusetts Bay system (MBS) including Boston Harbor (BH), Massachusetts Bay (MB) and Cape Cod Bay (CCB). The monitoring program primarily consists of an array of field observations, but is complemented by water quality modeling as required by the MWRA permit for effluent discharge into MB. The water quality model was initially developed by HydroQual and USGS by coupling the RCA model (Row-Column Advanced Ecological Systems Operating Program) and the 3D hydrodynamic model ECOMsi (HydroQual, 2000). The coupled simulation system was then entitled "Bays Eutrophication Model" (BEM). BEM has been applied to MBS for the years 1994-1999 by HydroQual and 2000-2005 by University of Massachusetts Boston (UMB) (HydroQual, 2000; HydroQual, 2003; HydroQual and Signell, 2001; Jiang and Zhou, 2004b, 2008).

We obtained a full set of field data to run the BEM for both 2006 and 2007 from MWRA and other sources. This report presents the details of data treatment, model set up, model-data comparison and interpretation of the simulated results. In addition to simulating 2006 and 2007, we have conducted a sensitivity analysis by driving the model with spatially- and temporally-resolved wind fields for both 2006 and 2007; the results showed significant improvement in the model prediction in terms of DO concentration in the deeper layer. We have also examined the biological response to storm events in the MBS.

1.2. Physical background

The MBS comprises the Boston Harbor in the west, Cape Cod Bay in the south and Massachusetts Bay in the central region (**Figure 1.1**). It is a semi-enclosed coastal embayment with a length of approximately 100 km and a width of 50 km. The water depth averages about 35 m, with the maximum depth of 90 m in Stellwagen Basin, but only 20 m on Stellwagen Bank. Stellwagen Bank, located on the east side of the MB, limits deep-water exchange between MB and the Gulf of Maine (GOM). Deep water exchange occurs mainly through the North Passage off Cape Ann and the South Passage off Race Point. (**Figure 1.1**).

The hydrodynamic circulation in MBS is subject to both local forcing such as wind and tide and remote forcing through the intrusion of the Western Maine Coastal Current (WMCC) (Bigelow, 1927; Butman et al., 2002). The general circulation pattern within MBS is counterclockwise with inflow through the North Passage and outflow through the South Passage. The inflow is primarily determined by a) the WMCC which bifurcates near Cape Ann with one branch flowing into MBS (Bigelow, 1927; Lynch et al., 1996) and b) coastal freshwater discharges, particularly from the Merrimack River located north of the bay (Butman, 1976). Local wind forcing can significantly alter the current pattern and velocity (Geyer et al., 1992; Butman et al., 2002; Jiang and Zhou, 2004a). Wind-induced upwelling and downwelling activities were observed and simulated in previous studies (e.g., Geyer et al., 1992; HydroQual and Signell, 2001; Jiang and Zhou, 2004a). However, the water column stratification changes primarily following seasonal variations in net surface heat flux, and freshwater discharge. Water stratification usually starts in spring due to increased insolation and freshwater discharge, intensifies in summer due to surface

heating, and erodes in fall due to surface cooling and increased wind stress following which the water column becomes well mixed again in winter.

1.3. Biological background

Phytoplankton development in the MBS generally shows seasonal cycles typical of temperate regions due to the seasonality in solar radiation, water column stratification and nutrient availability (Libby et al., 1999; Libby et al., 2000). During winter when the water column is well-mixed and solar radiation is weak, phytoplankton growth is restricted due to limited light exposure in most of the MBS. Phytoplankton usually bloom in spring following the establishment of water column stratification and increases in solar radiation. However, spatial differences and interannual variations in the timing of the phytoplankton spring bloom can occur due to local forcing and the physical environment. For example, the spring phytoplankton bloom often develops earlier in CCB than in the Stellwagen Basin due to shallow water depth. During the post-bloom season in summer, phytoplankton biomass is low in most of the MBS due to nutrient limitation. Local phytoplankton development can occur due to, for example, wind-driven upwelling activity and river discharge. The fall bloom in MBS usually occurs in late September and early October when increased wind stress and cooling at the sea surface erode the stratification and as such increase vertical mixing and replenish nutrients from the deeper layer to the euphotic zone. With further increases in vertical mixing and decreases in solar radiation, phytoplankton development is limited again, leading to high nutrient concentrations and low phytoplankton abundance in winter.

The seasonal cycle of phytoplankton production is accompanied by succession in phytoplankton species. Diatoms dominate the spring phytoplankton bloom under nutrient-replete conditions, particularly with high silicate concentrations. On the other hand, phytoflagellate species prevail during the summer stratified season under nutrient-depleted conditions. With the replenishment of surface nutrients in fall, a phytoplankton assemblage of different sizes and species develops. Phytoplankton seasonal succession results in variations in biological parameter values and carbon: chlorophyll ratio. The seasonality in phytoplankton production and biomass can in part be traced to the secondary production level with variations in zooplankton abundance and species through bottom-up control (Turner, 1994; Libby et al., 2000; Libby et al., 2001).

Benthic biological and biogeochemical dynamics directly affect nutrient supply and oxygen demand and thus the water quality of MBS. BH, CCB and Stellwagen Basin are characterized by a soft sea floor with fine sediment and high organic matter content, whereas the coastal regions are mostly covered by coarse sediment and rocks (Kropp et al., 2001; Kropp et al., 2002; Maciolek et al., 2003). In regions of soft floor with fine sediments, biological oxygen demand (SOD) is higher than that in the hard-floor region. In BH, for example, high values of SOD and nutrient flux have been observed. Outside of the harbor in MB and CCB, physical processes significantly affect benthic biogeochemical processes where aerobic conditions dominate (Maciolek et al., 2003; Tucker et al., 2002; Jiang and Zhou, 2008). Most of these biological and biogeochemical processes are parameterized in the BEM (see next section).

2. Model description

2.1. Model domain and grid

Orthogonal curvilinear grids were used for both the hydrodynamic model and BEM in the MBS (**Figure 2.1**). The hydrodynamic model grid consists of 68 rows and columns. BEM used a subset of the hydrodynamic model grid with the first 54 columns and the same 68 rows. As such, the BEM simulation domain covers the entire MBS with an open boundary running from Cape Cod to Cape Ann. In the vertical, the hydrodynamic model used 13 sigma levels and BEM used 10 sigma levels by combining the first top 3 sigma levels in the hydrodynamic model grid.

2.2. Model structure

BEM was based on the HydroQual RCA Water Quality Model (**Figure 2.2**) coupled with the hydrodynamic model ECOMsi. Dissolved oxygen (DO) is the primary state variable of environmental concern in the simulation system. In the model, DO is computed by the reaeration flux at the sea surface, sediment oxygen demand (SOD) at the bottom and internal biological and biogeochemical dynamics in the water column such as phytoplankton photosynthetic production, respiration consumption, biogeochemical oxygen demand through the mineralization of particulate and dissolved organic matter and nitrification. Phytoplankton growth is sustained by solar radiation and dissolved inorganic nutrients including ammonium NH_4^+, nitrate NO_3^- and nitrite NO_2^-, phosphate PO_4^{3-} and dissolved silica ($Si(OH)_4$). Nutrients are formed through the mineralization of organic substances and at the sediment-water interface (**Figure 2.2**). In the model, organic matter is divided into dissolved and particulate forms with each being further divided into refractory and labile categories, as illustrated by the nitrogen cycles in **Figure 2.3**. Zooplankton grazing is not explicitly modeled with trophodynamics, but represented by a linear function leading from phytoplankton to particulate and dissolved organic matter. Phosphorus and silicon were parameterized in a similar way as the organic carbon pools and the total number of state variables amounted to 26 (**Table 2.1**): Salinity, three phytoplankton groups (spring, summer and fall groups), four nutrients (ammonia, nitrate+nitrite, phosphate and dissolved silica), four organic phosphorus forms, four organic nitrogen pools, six organic carbon pools (four labile and refractory dissolved and particulate forms plus the reactive and exudates components), biogenic silica, dissolved and aqueous oxygen and total active metal. For this application in MBS, the last state variable (total active metal) was not modeled.

As an example, the nitrogen biogeochemical dynamics is parameterized as the following (**Figure 2.3**): Dissolved inorganic nitrogen (DIN) is transformed into organic forms through phytoplankton photosynthesis. Phytoplankton is then disintegrated into non-living dissolved and particulate organic forms through grazing, mortality and exudation. Particulate organic nitrogen is first disintegrated into dissolved organic forms which are then mineralized into DIN. The sinking of phytoplankton and non-living particulate organic matter conveys organic nitrogen to sediments where diagenesis transforms organic nitrogen into DIN which is then dispersed into the water column through vertical mixing and upwelling. Meanwhile, denitrification in the sediment can transform some nitrate into gas nitrogen and thus make it unavailable for biological uptake. On the other hand, river runoff, effluent discharges, and inflows at the open boundary can add nutrients to the system. Carbon and phosphorus have similar dynamics to that of nitrogen in the model and as a result, more than 100 controlling parameters are involved in the water quality model (**Table 2.2**). Detailed model description and model parameter estimations

can be found in previous MWRA reports (HydroQual, 2000; HydroQual, 2003; HydroQual and Normandeau, 1995; Jiang and Zhou, 2007).

The sediment module in BEM is essentially based on the model developed by DiToro (2001). It is designed to capture the sinking flux of organic matter from the water column to sediments, sedimentary diagenesis transforming organic matter into inorganic nutrients, nutrient feedback from sediment to the water column, sediment oxygen demand during sedimentary diagenesis, and denitrification which converts nitrate into gaseous nitrogen (N_2) and thus leads to nitrogen loss from the system through outgassing to the atmosphere.

2.3. Forcing

2.3.1. Surface forcing

The BEM requires surface forcing of downwelling short-wave solar radiation through the sea surface, wind speed and fraction of daylight (**Figure 2.4**). The model calculates the daily total insolation which is then partitioned according to the daylight fraction to calculate photosynthesis. Wind speed is used by RCA primarily for the determination of oxygen exchange at the sea surface, i.e. the oxygen reaeration flux. However, the wind effect on the function of the whole system is far more than the reaeration flux through the influence on the hydrodynamics prediction of ECOM_si. First, wind speed and direction can directly affect the current pattern and speed, and thus influence the dispersion of effluent in the region and energy exchange at the open boundary. Secondly, wind energy can penetrate into the water column and strengthen the vertical mixing that determines nutrient supply from deeper layers to the euphotic zone. Thirdly, specific wind can generate upwelling or downwelling that advect nutrients and biogenic substances in the water column. Fourthly, the erosion of the thermocline by surface wind forcing can replenish oxygen in deep layers.

The initial wind data were downloaded from the NOAA Buoy 44013 deployed in Massachusetts Bay at 42.35 N 70.69 W. Data were collected at 4 m above the sea surface and then converted to wind speed at 10 m elevation. The initial file contains hourly wind data, but some data were missing, for which prediction by the MM5 meteorological model was used. Dr. Payne (WHOI) provided shortwave radiation data in W m-2 which were converted into langleys per day for model use (1 langley = 1 cal cm^{-2} = 41840 J m^{-2} = 41840 W). Finally, the forcing file (model.pcv.2006 and model.pcv.2007) were prepared by combining the daily-averaged wind, daily total radiation in langley (ly) and day length expressed as a fraction (**Figure 2.4**)

The daily average solar radiation exhibits typical seasonal cycles with low values in winter and high values in summer. Due to variations in cloudiness, however, low solar radiation occurs through out the year. The wind speed also shows seasonal cycles, with low values in summer and high values in winter and fall. Daily variations in wind speed are much higher than seasonal variations. Daylight fraction varies from 0.37 in winter to 0.63 in summer at the latitude of the MBS.

2.3.2. Nutrient loadings

Nutrient and carbon loadings include the MWRA effluent outfall from the Deer Island Treatment Plant (DITP), Non-MWRA point sources, non-point sources, river discharge and atmospheric

sources. We describe below the determination of each source based on observed data and historical assessment.

MWRA collects daily measurements of treated sewage flow in gallons per day and concentrations of various effluent constituents in ug l^{-1}. Some of the data can be directly used to drive the model such as NO_3^-, NO_2^-, NH_4^+ and PO_4^{3-}, but other bulk-parameter data need to be converted and partitioned into model variables including carbonaceous biochemical oxygen demand (CBOD), total Kjeldahl nitrogen (TKN) and total phosphorus (TP). CBOD was first converted into total organic carbon using the function TOC = 0.7CBOD+18 (HydroQual and Normandeau, 1993) and then partitioned to each organic matter pool using the functions listed in **Table 2.3**. In a similar way, TKN and TP were first converted into total organic nitrogen and phosphorus and then partitioned into their respective organic pools (**Table 2.3**). Silicate was not analyzed at the MWRA outfall and we followed the previous work by assuming a silicate concentration of 12.5 mg l-1. (HydroQual, 1993, p.3-6).There is no update for non-MWRA point sources and previous estimates conducted by Menzie-Cura (1991) and Alber and Chan (1994) were used.

Non-point source loadings comprise runoff and groundwater inputs. For runoff from combined sewer systems, loads were estimated using the combined sewer overflows (CSOs) at the Mystic/Chelsea confluences, the upper Inner Harbor, the lower Inner Harbor, Fort Point Channel, North Dorchester Bay, South Dorchester Bay, and the Neponset River estuary. Data of total annual CSO discharge at the above locations were provided by MWRA via the help from Wendy Leo, and were then partitioned into each month based on the Charles River discharge in each year as a proxy for precipitation, as has been done in previous years (Wendy Leo, personal communication, Mar 13, 2008). CSO effluent has not recently been analyzed for nutrients, so CSO effluent concentrations reported by Alber and Chan (1994, **Table 2.3**.6) and the conversion and partitioning functions listed in **Table 2.3** were used to estimate contaminant loadings. For ground water input, the previous estimates by Menzie-Cura (1991) were used.

For river loadings, daily discharges of Charles River, Neponset River and Merrimack River were initially downloaded from the USGS internet site. http://waterdata.usdgs/ma/ nwis. However, the Merrimack River is located outside the BEM sub-domain and only used for the hydrodynamic model. There are no accurate river flow data for the Mystic River near the river mouth and its discharge was assumed to equal 0.195 of that of the Charles River. Three rivers (Charles, Neponset and Mystic rivers) were thus taken into account in preparing nutrient loads for the 2006 and 2007 runs.

Few river nutrient data were available for 2006 and 2007; the data do not allow monthly estimations of nutrient concentration but it is unlikely that nutrient concentration considerably changed from 2004 to 2006 and 2007. Thereby, nutrient concentrations in the Charles River measured in 2004 downloaded from the USGS internet site were used to estimate river loadings. Data for most nutrients were directly used for the river loading computation, but that of total organic phosphorus was converted into model variables using the same functions listed in **Table 2.3**. Data for particulate organic nitrogen (PON) and dissolved organic nitrogen (DON) were equally split into refractory and labile pools (RPON, LPON and RDON and LDON, respectively).

The atmospheric loadings were based on the previous estimates reported by Menzie-Cura (1991), and were the same as used previously by HydroQual and the UMB group (HydroQual and Normandeau, 1995; HydroQual, 2000; HydroQual, 2003; Jiang and Zhou, 2004b). These estimates included both dryfall and wetfall of inorganic and organic nitrogen, phosphorus, and carbon.

The MWRA outfall was the largest nutrient source of nitrogen and phosphorus to the MBS in 2006 and 2007 (**Figure 2.4**). Non-MWRA sewer operation systems constituted the second largest loadings for phosphorus, but the atmospheric input accounted for the second large loading for nitrogen. In terms of carbon, however, non-MWRA sewage treatment plants contributed the largest loading, followed by the MWRA outfall and atmospheric input. Rivers and non-point sources contributed smaller shares compared to other sources.

2.3.3. Open boundary conditions

Bi-weekly open boundary conditions were established with the objective analysis (OA) procedure and the MWRA field observation data. The OA software, called OAX, was initially developed by Bedford Institute of Oceanography (Hendry and He, 1996) and is available on their internet web site. The covariance function (R) between data and estimation site is based on their pseudo-distance (r) determined as:

$$R(r) = (1 + r + \frac{r^3}{3})e^{-r} \tag{2.1}$$

$$r = \sqrt{\left(\frac{x_d - x_m}{a}\right)^2 + \left(\frac{y_d - y_m}{b}\right)^2 + \left(\frac{z_d - z_m}{c}\right)^2 + \left(\frac{t_d - t_m}{T}\right)^2} \tag{2.2}$$

where x ,y, z, and t are the four spatial and temporal coordinates, the subscripts d and m indicate data and model positions, respectively, and the parameters a, b, c, and T are the decorrelation scales for their corresponding coordinate.

Field observations were conducted at seven stations near the MWRA outfall (called "nearfield" stations indicated by "N") and 25 far-field stations indicated by "F" (**Figure 2.6**). Approximately monthly observations were conducted at the near-field stations, while the far-field stations were occupied 6 times per year including the two stations in Cape Cod Bay (F01 and F02) and five stations in the southern part of Mass Bay (F03, F29, F05, F06 and F07). In 2006, data collected for the Stellwagen Bank National Marine Sanctuary during two cruises at four stations (SW1-4) close to the open boundary in North Passage were also included in determining the open boundary condition. Given the low frequency of field observations and their long distance from the open boundary, relatively large decorrelation scales were used, 30 km in the horizontal, 15 m in the vertical and 45 days in time. The OAX package allows a larger decorrelation scale along-isobath than perpendicular to the isobath. However, the difference in decorrelation scale between along- and perpendicular to the isobath is effectively almost insignificant given the gentle changes in topography in the simulation domain.

Bi-weekly open boundary conditions were computed for 14 measured parameters: Chlorophyll (Chl), DO, NH_4^+, NO_3^-, PO_4^{3-}, $Si(OH)_4$, DON, DOC, DOP, PON, POC, POP, Biogenic silica and salinity. DON was estimated as the difference between the total dissolved nitrogen (TDN) and total dissolved inorganic nitrogen (NO_3^-, NO_2^-, NH_4^+). Similarly, DOP was estimated as the difference between total dissolved phosphorus (TDP) and dissolved phosphate (PO_4^{3-}), and particulate phosphorus (PARTP) was used as POP. The OA-mapped chlorophyll field was then partitioned to the three phytoplankton groups using the partition coefficients listed in **Table 2.5**. From January to April, all the chlorophyll was considered consisting of winter-spring phytoplankton with zero partition coefficient to the other two phytoplankton groups. May was considered as a transition period with the chlorophyll being equally split into winter-spring and summer phytoplankton groups. In June and July, all chlorophyll belonged to the summer phytoplankton group and August was another transitional period with chlorophyll being split into the summer and fall phytoplankton groups. Chlorophyll consisted of only fall phytoplankton in September through November, and was split into winter-spring and fall phytoplankton in December. Each phytoplankton had a specified carbon to chlorophyll ratio: 40, 65 and 15 for winter-spring, summer and fall phytoplankton, respectively (HydroQual, 2000; HydroQual, 2003; Jiang and Zhou, 2004b). DON and PON were split equally into labile and refractory pools; the partition coefficients for organic carbon and phosphorus are listed in **Table 2.6**.

Examples of OA-mapped open boundary conditions in April and August 2006 and 2007 are presented in **Figures 2.7**-2.14. In 2006, chlorophyll concentration was higher in the northern passage off Cape Ann than in the southern passage off Cape Cod in April (**Figure 2.7**) and a subsurface chlorophyll maximum appeared in August (**Figure 2.8**). Nutrients showed high concentration in the deeper channel and depletion in the surface layer (**Figures 2.7** and 2.8). Particulate organic matter showed higher values in the surface layer than in the deeper layer in April (**Figure 2.9**) and a subsurface maximum in August (**Figure 2.10**). Differences in organic matter concentration between the northern and the southern passages appeared as well in certain cases. Similar to chlorophyll, DO concentration had higher surface values in April and slightly higher values in the subsurface layer in August.

In 2007, chlorophyll had high values from surface down to the deeper layer in North Passage in April (**Figure 2.11**). The field survey on April 22 detected 8.88 $\mu g\ l^{-1}$ chlorophyll at 103 m at Station F27 and 9.91 $\mu g\ l^{-1}$ at 50 m at Station F26. High values of chlorophyll concentration were also observed in the deeper layers in South Passage. Subsurface maximum chlorophyll concentration developed in August in North Passage, but with high surface values in the surface layer in South Passage (**Figure 2.12**). Most of the nutrients had higher values in the deeper layer than in the surface layer except for NH_4^+ which showed a subsurface maximum (**Figures 2.11** and 2.12). DO had high values in the surface layer in April and high values in the subsurface layer in August.

Readers should bear in mind that the above results were obtained by OA analysis. Given the low frequency of field observations and the large distance between the open boundary and the observation sites, particularly for the Southern Passage, the OA-mapped results should be interpreted with caution.

2.4. Numerical scheme

The advection/diffusion terms in the RCA simulation were driven by the hydrodynamic model ECOMsi (HydroQual, 2000). The hourly-averaged temperature, salinity, currents and turbulent diffusivity were stored in HD output files and then loaded into RCA during the simulation. Due to the fact that the RCA used 10 sigma levels in a smaller domain whereas ECOMsi used 13 sigma levels in a larger domain, the output data from ECOMsi were first treated by a collapse program which extracted the RCA sub-domain and combined the top 3 sigma levels of ECOMsi to a single level in RCA. The RCA was integrated over an annual cycle with a time step of 4.14 minutes with the surface forcing presented above, the physical forcing computed by ECOMsi and the open boundary conditions determined through objective analysis.

2.5. Model parameters

The model parameter values were fully based on the previous studies without any adjustment (**Table 2.2**). Readers are referred to the previous reports for parameter value estimation and validation (HydroQual, 2003, Jiang and Zhou, 2004b; 2008).

2.6. Initial conditions

The initial conditions for 2006 were based the final results of the 2005 run that was provided by the UMB group, and that for the 2007 simulation were based on the final results of the 2006 simulation.

2.7. Adjustments to model code

As we began to use the last version of the code used by UMB, we found there was a shift in time between the physical and biological simulation in the initial code. Therefore we modified the code so that physical and biological simulations matched. Before the modification, the biological module had a time clock independent from the physical output for transport loadings. As the time lag in the physical transport files was longer than the time step specified in the biological module at the boundary between two months, a time shift between the physical and biological simulations occurred at the end of each month and the total accumulated shift reached about 10 hours in December, i.e. the biological simulation during the daytime actually used the transport field of the nighttime. After the modification, the biological clock was removed and the transport loading was only determined by the physical clock so that the biological simulation strictly followed the physical simulation whatever time step was used in the physical transport.

3. Validation and discussion

3.1. Data description

As stated earlier, the MWRA monitoring program consists of seven stations near the MWRA outfall and 25 stations in Mass Bay and Cape Cod Bay (**Figure 2.6**) and 19 stations in the Boston Harbor sampled through the Boston Harbor Water Quality Monitoring project (e.g., Taylor et al., 2004). The far-field stations were sampled roughly bi-monthly, near-field stations approximately monthly, while the harbor stations were visited on a weekly basis. Water samples were collected at five standard levels at all the near- and far-field stations except for the far-field stations F30 and F31 close to the harbor where only 3 standard levels were sampled due to shallow water depth (< 15 m). Two layers (surface and bottom) were sampled at the harbor stations, but when the total depth is too shallow (e.g. < 5m), only surface samples were collected. Nutrients, organic substances, pigments, and dissolved oxygen were analyzed in the collected water samples based on the protocol described in Libby et al. (2006). Primary productivity was measured at the stations F23, N04, and N18 close to the MWRA outfall (**Figure 2.6**). Following the protocol used previously in this project, only a subset of the field observation data were used for model validation (Jiang and Zhou, 2004b; 2008). Nutrients fluxes and sediment oxygen demand were measured at four stations in the harbor , four stations in MB around the MWRA outfall, and one in Stellwagen Basin (Tucker et al., 2007; Tucker et al., 2008), which were also used for model validation. Examples of model-data comparisons were presented in the following sub-sections.

3.2. Data-model comparison for the 2006 simulation

Chlorophyll concentration generally exhibited typical seasonal cycles in both observation and simulation with high values in early spring and fall (**Figure 3.1**). The spring bloom occurs mostly at the end of February or early March and lasts till end of March (e.g., Station F23 and F01) or early April (e.g., Stations N04, N07, N10 and F06). At shallow stations (e.g., F01, F06, F23, and N10), the spring bloom occurred simultaneously in both the surface and the bottom layers, with chlorophyll concentration slightly higher in the bottom layer than in the surface layer. At deeper stations (e.g., N04 and N07), there was a delay in the timing of phytoplankton development from the surface to the bottom layer, and usually the magnitude of the bloom was slightly higher in the surface layer than in the bottom layer. The fall phytoplankton bloom started in late September and lasted until November; it occurred simultaneously in both the surface and the bottom layers at shallow stations, but was almost indiscernible in the bottom layer at deeper stations. The model successfully reproduced the phytoplankton seasonal cycles and predicted compatible magnitudes in phytoplankton blooms. However, the model seemed to underestimate the surface chlorophyll concentration at near-field stations (e.g., N10) and overestimate chlorophyll concentration at certain far-field stations (e.g., F01 and F06).

Nutrients also displayed seasonal cycles following phytoplankton development (**Figures 3.2** and 3.3). DIN (equal to the sum of NH_4^+, NO_2^- and NO_3^-) and silicate were replenished in the whole water column in winter, depleted in spring due to phytoplankton consumption during the spring bloom, and increased in later fall due to strengthened vertical mixing. During summer and early fall when chlorophyll concentration was typically low, high nutrient concentrations were observed in the bottom layer at both near-field and far-field stations, which indicated that phytoplankton development was light-limited in the bottom layer. Nutrient concentration in

surface waters remained at a low level from late spring to early fall and increased in late fall and early winter. The late fall increase in nutrient concentrations in the surface layer corresponded to a decrease in the deeper layer, indicating a redistribution of the nutrients in the water column by increased vertical turbulence.

The model successfully reproduced both the timing and the magnitude of the seasonal cycle in nutrients. Given that phytoplankton development was primarily determined by nutrient availability and subsequent uptake from spring to fall, any deviation in chlorophyll concentration between model and data is most likely due to deviation in the carbon to chlorophyll ratio, which can vary considerably depending on the environmental conditions and phytoplankton species assemblages. If the model had dynamically underestimated phytoplankton development, the nutrient concentrations would have been overestimated.

DON had limited seasonal variations (**Figure 3.4**). A common feature was that DON concentration increased during the spring phytoplankton bloom, after which variations were generally small except at station F23 where DON increased during fall as well. As this station was close to the harbor, horizontal advection might dominate instead of internal biogeochemical dynamics. Nevertheless, the model predicted compatible DON level over an annual cycle. PON showed similar seasonal variation to that of chlorophyll (**Figure 3.5**), with high values in spring and fall and low values in summer and winter. In most cases, the model prediction matched the data in both seasonal variations and magnitudes.

DO had seasonal variations that differed from that of chlorophyll, with high values during the spring phytoplankton bloom, but stayed at a low level in fall without responding to the fall bloom (**Figure 3.6**). The high DO values in spring reflected photosynthesis production through phytoplankton growth. However, the highly energetic turbulence and reaeration in fall prevented DO accumulation in the surface layer. Meanwhile, remineralization of organic substances remained active so that DO stayed at a low level in the bottom layer. This can be better explained by DO saturation (**Figure 3.7**). During the spring phytoplankton bloom, DO was mostly over-saturated in the surface layers and also in the bottom layer at shallow stations. In fall, however, DO saturation was around 100% indicating an equilibrium with the atmosphere through surface reaeration, but under-saturated in the bottom layer due to remineralization consumption. High surface temperature in early fall represent another reason the lower DO level than in spring due to the decrease in the DO saturated solubility. Water mass inflow through the open boundary and horizontal advection can also alter bottom DO concentration in the region (Libby et al., 2008). The model reproduced well the seasonal variations and concentration of DO (**Figure 3.6**), but some scattered data of DO saturation were not simulated by the model (**Figure 3.7**).

Good correlations were found between the modeled and observed results for NO_3^- and $Si(OH)_4$ in the surface layer and DO in the bottom layer, but the correlation between the two data sets significantly deteriorated for chlorophyll in the surface layer (**Figure 3.8**). In the case of surface chlorophyll, the model tended to overestimate chlorophyll abundance at low concentrations and underestimate chlorophyll abundance at high concentrations. This deviation in chlorophyll concentration between the model and the observation was not translated into nutrient concentration for which modeled and observed results compared relatively well, though the

observed data were scattered at the low end of the concentration range. This is in agreement with our interpretation that the deviation between the model and the observation likely results from an inaccurate carbon to chlorophyll ratio used in the model. In the case of DO in the bottom layer, the modeled and observed results were relatively well correlated with a correlation coefficient of 0.85.

Time-series data of key variables (temperature, DIN, chlorophyll and DO) in the water column are shown for two near-field stations (**Figures 3.9** and 3.10) and two far-field stations (**Figures 3.11** and 3.12). At the near-field stations N04 and N10, the model reproduced the observed homogeneous water column in winter and stratification in summer and early fall (**Figures 3.9** and 3.10). DIN displayed a similar seasonal cycle between the model and the data: replenished in winter in the whole water column, depleted fully in spring and early summer, regeneration through remineralization and input from the sediment to the bottom layer, and vertically mixed again in late fall and winter. The model seemed to underestimate nutrient concentration in mid-depth layers in late summer and early fall, which can be caused by underestimation of remineralization or of horizontal advection fluxes. Similarly, the model reproduced the observed chlorophyll seasonal variations, with high values during the spring bloom, low values in summer, and increases again in late fall. The modeled surface chlorophyll concentration in spring and mid-depth concentration in early fall was lower than that observed, in accordance with the overall correlation showing that the model underestimated chlorophyll at high concentrations. DO matched well between the model and observation in the water column. The highest values of DO were observed and modeled during the spring phytoplankton bloom and the lowest values appeared in the bottom layer in summer when remineralization consumption and sediment oxygen demand were highest within an annual cycle. A particularly high DO event in surface water was observed at station N10, which was not reproduced by the model. As a similar event was not observed at the station N04, it appeared to be a local event that model overlooked.

The model seems to overestimate the surface mixed layer depth in summer at the far-field stations F06 and F23 (**Figures 3.11** and 3.12). The model predicted a thermocline down to 20 m while data showed stratification around 10 m. DIN was almost depleted in the entire water column during the summer season at these two far-field stations, when chlorophyll concentration remained at a low level. Similarly, DO showed a strong seasonal cycle, but weak stratification at these two far-field stations. Given the low frequency of observations at the far-field stations (bi-monthly), it is not straightforward to draw any conclusion from the small-scale mismatches between the model prediction and the data.

Model-data comparison of chlorophyll and DO in Boston Harbor (BH) is presented in **Figures 3.13** and 3.14 as examples. Seasonal cycles in chlorophyll concentration were observed and predicted in BH. The spring phytoplankton bloom was similar to that in the MB in terms of magnitude and duration, but the fall bloom in BH lasted a much longer period of time with higher magnitudes than that in MB. In fact, chlorophyll concentration stayed at a high level throughout summer and fall. Possible processes include anthropogenic and terrestrial inputs of nutrients, high regeneration in the harbor and increased nutrient fluxes at the sediment-water interface. As in MB, the model tended to overestimate chlorophyll at high concentrations in BH.

Good model-data comparison was obtained for DO in BH (**Figures 3.14** and 3.15). DO showed high values during the spring bloom, but remained at low levels during summer and fall when high chlorophyll concentration was observed and simulated. DO was also under-saturated in late summer and fall, which indicated that the massive development of phytoplankton in BH during summer and fall was more likely due to increased nutrient regeneration instead of new nutrient input from outside the system. The model-data deviation remained at a low level in most cases.

Primary production near the outfall exhibited similar seasonal cycles to that of chlorophyll with spring and fall phytoplankton blooms (**Figure 3.16**). A large fall bloom was also observed at station F23, which is close to BH. The model prediction was in general comparable with the observations. At station F23, however, the model appeared to overestimate the primary production. Observations of nutrient and oxygen fluxes at the sediment-water interface were mostly reproduced by the model without large discrepancies (**Figures 3.17**-3.21). Unlike biological production in the water column which had a bimodal distribution with high values in spring and fall, the nutrient flux and SOD on the bottom displayed a unimodal distribution with high values in summer and early fall and low values in winter. Although biodeposits provide organic substances to the sediments through the sinking of biogenic detritus, the diagenesis of these deposited materials functioned independently from the biological production in the water column. The dominant forcing determining the speed of sedimentary diagenesis and remineralization was the temperature, which reached high values in summer and fall and thus accelerated diagenesis in the sediment.

3.3. Data-model comparison for the 2007 simulation

As biological and biogeochemical seasonal cycles were discussed in the previous section, we will focus in this section on the difference between the 2007 and 2006 simulation and on the data-model comparison for the 2007 simulation.

Chlorophyll concentration in 2007 displayed seasonal cycles similar to 2006 (**Figure 3.22**), but at stations F23, N04 and N10, the magnitude of the spring bloom was slightly lower than that in 2006 (**Figure 3.1**). Extreme high values of chlorophyll data were not reproduced by the model, but most of the data were within the model-predicted range. DIN and $Si(OH)_4$ were quite similar between the two years in terms of seasonal variations and model-data compatibility (**Figures 3.23** and3.24 for 2007 and 3.2 and 3.3 for 2006). However, DON concentration, both observed and modeled, was significantly higher during summer and fall in 2007 than in 2006, particularly at station F23 close to the harbor (**Figures 3.25** vs 3.4). PON and DO were mostly the same between the two years (**Figures 3.26**-28 for 2007 and 3.5-7 for 2006). The overall model-data correlation was comparable between the two years for NO_3^- and DO, but deteriorated for chlorophyll and improved for $Si(OH)_4$ in 2007 as compared to 2006 (**Figures 3.29** vs. 3.8).

Time-series of the key parameters (T, DIN, chlorophyll and DO) exhibited similar patterns in the water column between the two years (**Figures 3.30**-3.33 for 2007 and 3.9-3.12 for 2006). At station N04, however, the observation showed lower chlorophyll in spring without a significant subsurface maximum in summer and fall in 2007 (**Figure 3.30**) as compared to 2006 (**Figure 3.9**). At station N10, the model predicted higher DIN concentrations in the bottom layer in summer 2007 than that in 2006, but the chlorophyll concentration was very similar between the two years (**Figures 3.31** and 3.10). At Station F23, the model predicted high DIN concentration at the end of the year (**Figure 3.33**). As these stations are close to the MWRA

outfall or close to BH, local perturbations can generate anomalies from the general biological seasonal cycles.

In the harbor, the seasonality of chlorophyll was muted, with a continuously high concentration in summer and fall and a barely perceptible the spring phytoplankton bloom (**Figure 3.34**). The model underestimated the chlorophyll data in spring, but the high simulated concentration in summer and fall was supported by observations at certain stations. The DO simulation fitted the data better than that of chlorophyll (**Figure 3.35**), but in most cases, DO was undersaturated in the harbor, particularly in the deeper layer (**Figure 3.36**). The magnitude and seasonal cycle of primary production were similar between the two years (**Figure 3.15** for 2006 and **Figure 3.37** for 2007). The model tended to underestimate the primary production as compared with data when the production was high, such as during the spring phytoplankton bloom at all three stations and during the fall bloom at station F23. There were no discernable differences between the two years in terms of nutrient and oxygen fluxes at the sediment surface (**Figures 3.38**-3.42 for 2007 and 3.17-3.21 for 2006). The model reproduced the data relatively well; the seasonal variations described for the year 2006 were found for the year 2007, mainly high values during summer and early fall and low values in late fall and winter, primarily driven by the bottom water temperature.

4. Projection of the influence of the MWRA outfall on the ecosystem function in Mass Bay

In order to assess the potential influence of the MWRA outfall on ecosystem function in the MBS, we have conducted a simulation without MWRA effluent for both 2006 and 2007. In this chapter, we call the initial run with the MWRA outfall as the "Control run" and the sensitivity-analysis run as the "Non-sewage" run. We compare the major ecological variables between the two runs including chlorophyll concentration in surface waters, DO concentration and saturation in the bottom layer, and integrated primary production in the water column at the monitoring stations, and map the differences between the two runs at mid-depth (15 m) within the flow field near the MWRA outfall site.

The simulated chlorophyll concentration in surface waters and DO concentration and saturation in the bottom layer were almost identical between the two runs, which means that the MWRA outfall does not have notable impact on phytoplankton development in surface waters or DO level in the bottom layer (**Figures 4.1**-4.3). The Non-sewage run predicted slightly lower primary production during the summer and fall seasons, but the difference between the two runs was minor (< 15%; **Figure 4.4**). As a general pattern, the MWRA outfall did not have substantial influence on the ecological function of the MBS. Local influence is discernable, however, around the MWRA outfall (**Figures 4.5** and 4.6). On February 15 as a winter scenario, a higher NH_4^+ concentration was simulated at 15 m by the Control run than the Non-sewage run (**Figure 4.5**, upper right panel), but no signal of the chlorophyll anomaly was detected at the same place and time (**Figure 4.5**, upper left panel). On May 15, the NH_4^+ anomaly at the MWRA site was almost imperceptible (**Figure 4.5** lower right panel). Compared to the upper panel where south-southwesterly wind dominated, a strong north-northeasterly wind created a strong coastal current that dispersed rapidly the MWRA effluent away from the region. Wind forcing can thus directly influence the stagnation or dispersion of the MWRA effluent and thereby its impact on ecological function. On August 15 as a summer scenario, the MWRA effluent was translated into biological production and chlorophyll concentration (**Figure 3.6** upper panel). On November 15, when north-south wind prevailed, only a NH_4^+ anomaly was simulated while chlorophyll concentration was at a low level all around the MWRA outfall (**Figure 4.6** lower panels). Based on the above results, a north-northeasterly wind is the most favorable for effluent dispersion from the MWRA outfall, while south-southwesterly wind is unfavorable for effluent dispersion. Moreover, south-southwesterly wind can generate upwelling and thus bring effluent from deeper waters to the euphotic zone, while north-northeasterly wind can create downwelling and thereby help further restrict the effluent to the deeper layers. Wind forcing appears to be of a primary concern in order to have an adequate modeling assessment of the MWRA outfall influence on MBS ecosystem function.

For 2007, the Control and the Non-sewage runs predicted almost identical time-series data of chlorophyll in the surface layer and DO in the bottom layer at the MWRA monitoring stations (**Figures 4.7**-4.9). Similar to 2006, the vertically integrated primary production in the water column was slightly lower in the Non-sewage run than that in the Control run (< 17%; **Figure 4.10**), but this difference was not translated into other state variables such as surface chlorophyll concentration and bottom DO concentration and saturation. Nevertheless, NH_4^+ and chlorophyll anomalies can be recognized at the mid-depth (15 m) around the MWRA outfall

(**Figures 4.11** and 4.12). On Feb 15, the dispersion pattern of NH_4^+ traced well the current pattern whereas chlorophyll anomaly was not discernable (**Figure 4.11** upper panel). During this period of time, the phytoplankton production was probably limited by light exposure so that nutrient effluents were not effectively transformed into biological production. On May 15, however, the chlorophyll dispersion was well traced in the current system whereas the NH_4^+ anomaly was restricted to the MWRA site (**Figure 4.11** lower panel). Under this scenario, phytoplankton production was apparently more rapid than current dispersion so that nutrient effluents were first translated into biogenic detritus which were then dispersed by the current system.

5. Sensitivity analysis with wind-field

As mentioned above, wind forcing plays a major role in determining the MWRA effluent dispersion and consequently the impact on MBS ecosystem function. The previous runs were driven by uniform wind forcing with the data collected at NOAA Buoy 44013. On the other hand, the Marine Ecosystem Dynamic Modeling group (MEDM) routinely conducts forecast and hindcast of meteorological field with the WRF meteorological model. Spatially resolved data for wind and heat fluxes have been established for three decades, from 1978 to the present. Using this forcing data set, we have conducted sensitivity analysis for both 2006 and 2007; we call this run as the "Wind-field run" in the following text while the previous run with uniform-wind forcing as the "Uniform-wind run".

In 2006, the chlorophyll concentration was comparable between the two runs, with slightly higher values in the Wind-field run at certain stations in summer (**Figure 5.1**). DO was also similar between the two runs at most of the monitoring stations (**Figures 5.2** and 5.3). At station F23 close to the harbor, however, the Wind-field run predicted slightly higher DO concentration than the Uniform-wind run during the summer season, and the Wind-field run improved the fit between simulation and observation. Primary production was mostly similar between the Wind-field and the Uniform-wind runs (**Figure 5.4**), but during the summer season, the Wind-field prediction tended to be slightly higher than that of the Uniform-wind run. The general pattern of the simulation appeared thus comparable using the two sets of forcing, but the spatially-resolved wind field improved the model prediction on local scales.

Significant differences were produced between the two runs during storm events. For example, on August 20 2006 when a cyclone passed the region, the Wind-field run predicted lower temperature and higher chlorophyll concentration over a great part of the simulation domain (**Figure 5.5**). The difference was particularly large close to the coastal region and in the northern region of Cape Cod Bay (CCB). Although the NO_3^- concentration was mostly similar between the two runs, the Wind-field run predicted higher DO concentration in the deeper layer than the Uniform-wind run in most of the simulation domain, with the largest difference in CCB. Transect plots showed that the Wind-field run predicted lower temperature in surface layers and higher temperature in deeper layers than the Uniform-wind run, particularly on the eastern side of Stellwagen Bank (**Figure 5.6**). Increased vertical mixing can lead to lower temperature in surface layer and higher temperature in deeper layers, but horizontal advection can also redistribute oceanic fields and thereby alter parameter distribution on a particular transect. This is particularly true for the coastal areas where upwelling and vertical mixing are conditioned by topographic features. The Wind-field run predicted higher DO concentration in both the surface and the bottom layers, but lower DO concentration at mid-depth close to the coast. Also the Wind-field run predicted higher DO production and consumption in the surface layer than the Uniform-wind run, but the two runs were practically identical in the deeper layer in terms of DO source and sink prediction. The higher DO concentration in surface layers can be explained by the higher production in the Wind-field run, but the higher DO concentration in deeper layers is caused by physical processes such as vertical mixing and horizontal advection.

For 2007, the chlorophyll prediction was mostly similar between the two runs during the spring bloom, but the Wind-field predicted significantly higher values in summer and early fall than the

Uniform-wind run (**Figure 5.7**). The difference in DO prediction was even larger than that in the 2006 simulation (**Figures 5.8** and 5.9). At four (stations F23, N10, F01 and F06) of the six stations shown, the Wind-field run predicted higher DO concentration and saturation by 9-18% than the Uniform-wind run during the summer season. Time-series data showed that the reaeration flux of DO at the sea surface was higher in winter and fall and lower in spring and summer when the ocean released a small amount of oxygen to the atmosphere (Figure 10). The difference between the two runs was minimal in spring and fall. At the bottom, the Wind-field run predicted slightly higher SOD than the Uniform-wind run, which indicated higher DO consumption by sediment diagenesis in the Wind-field run (Figure 10). As a result, the higher DO in the bottom layer predicted by the Wind-field run must be linked to internal physical and biological processes in the water column. The Wind-field run predicted higher DO production and consumption in surface layers than the Uniform-wind run, but the difference between the two runs was minimal in the bottom layer in terms of DO source and sink. The increased DO production in surface layers in the Wind-field run provided an additional DO source, but this had to be advected to the bottom layer through physical processes. Apparently, the Wind-field run predicted stronger vertical exchange in the water column, resulting in higher nutrient supply to the euphotic zone followed by higher phytoplankton and DO production, which were then redistributed to the bottom layer as compared to the Uniform-wind run. As mentioned earlier, water mass inflow through the open boundary and horizontal advection can also alter bottom DO concentration in the region (Libby et al., 2008).

6. Biological response to upwelling and storm events

The water quality monitoring program reported multiple upwelling events in the MBS in 2006 and 2007 (Libby et al., 2007, 2008) based on the surface water temperature measured at the Boston Buoy, and the wind stress. An upwelling event was identified when the surface temperature dropped more than 1.2 ºC per day and the south-north wind stress was higher than 0.04 Pa. Upwelling can potentially bring nutrients from deep layers to the euphotic zone and thus stimulate phytoplankton development. Chen et al. (2009) identify multiple passages of storms in the region. In this section we analyze the impacts of these upwelling and storm events on the distribution of key variables (temperature, chlorophyll and NO_3^-) predicted by RCA.

Upwelling events were identified on Jul 1 and Oct 1 2006 and Aug 4 and Sep 2 2007 (Libby et al., 2008, their Figure 4-2). The event on Jul 1 2006 was characterized by moderate but persistent south-southwesterly wind (**Figure 6.1**). The model predicted low temperature near the coastal region on both the western and northern sides of the simulation domain. Chlorophyll concentration was slightly higher in the coastal region while nitrate concentration remained low all through the event.

The model predicted low temperature on both the west and north coast of the bay on Oct 1 2006, which was enlarged on Oct 4 and covered a large area over the entire bay on Oct 7 (**Figure 6.2**). High chlorophyll concentration was simulated throughout the coastal region during this period of time. It is noteworthy that high NO_3^- concentration was simulated on Stellwagen Bank, particularly on the eastern side of the bank.

An atmospheric cyclone passed the MBS from May 9 to 14 2006 which created persistent strong northerly wind (**Figure 6.3**). Theoretically, north-northeasterly wind can generate downwelling in the coastal region, but also strong wind strengthens vertical mixing regardless of wind direction. The model predicted low temperatures over almost the entire simulation domain on May 9 and 11, but increased surface temperature was simulated on May 14 with decreased wind. Chlorophyll concentration evolved similarly, with high values over most of the simulation domain on May 9 and 11, but significantly decreased on May 14. No spatial variation was simulated in NO_3^- distribution.

An anticyclone passed the region late October with first strong north-northwesterly wind followed by a change in wind direction to south-southwesterly wind (**Figure 6.4**). The surface water temperature started to drop first in the coastal region and then extending to the entire domain. High chlorophyll concentration was simulated throughout the region near the coast, and low concentration toward the open boundary, with a sharp inshore-offshore gradient. Similarly, sharp contrast in NO_3^- concentration was also simulated, with high values toward the open-sea region and low values toward the coast.

Upwelling events were also reported on Aug 4-10 and Sep 2-8 2007 (Libby et al., 2008). The model predicted low temperatures during these periods of time, particularly in the west coastal region and on Stellwagen Bank (**Figures 6.5** and **6.6**). Chlorophyll and NO_3^- concentrations were practically unchanged from Aug 4 to 10 (**Figure 5.5**, middle and lower panels). During the second upwelling event from Sep 2 to 8, a tongue of high chlorophyll concentration was

simulated extending from BH to the northern side of Stellwagen Bank. Similarly to the upwelling early October 2006 (**Figure 6.2**), high NO_3^- was predicted on Stellwagen Bank during the upwelling event from Sep 2 to 8 2007 (**Figure 6.6**).

In summary, phytoplankton development significantly responded in general to upwelling and storm events. However, the biological responses depend not only on wind strength and direction, but are also determined by the timing and ecosystem status. According to our model prediction, the effect of the north and northeasterly wind in May 2006 was not from the downwelling that the wind created, but from the strengthened vertical mixing that led to an increase in phytoplankton abundance (reflected by high chlorophyll concentration) basin wide (**Figure 6.3**). Upwelling can potentially bring nutrients from deeper layers to the euphotic zone and thus stimulate phytoplankton development, but this depends on the timing of the event and the ecosystem function in general. Given that the MBS is a shallow system, nutrients are depleted in the whole water column in early summer. Upwelling in the coastal region in early summer cannot effectively supply nutrients to the euphotic zone even though it brings water from deeper to surface layers (examples **Figures 6.1** and 6.5). Biological responses to upwelling events manifest the most in late summer and early fall, when surface water remains nutrient-depleted while deep water is nutrient replenished (examples **Figures 6.2**, 6.4 and 6.6). Under these conditions, upwelling effectively advects nutrients from deep layers to the euphotic zone and stimulates phytoplankton development. In late fall, however, although upwelling can bring nutrients to the surface layer, the strong vertical mixing generated by the increased wind stress redistributes phytoplankton cells in the water column in deep regions. Given the limited insolation at that time, phytoplankton are basically light-limited and cannot transfer nutrients into biomass (see for example **Figure 6.4**). As far as the dispersal of the MWRA effluent is concerned, upwelling accompanied by north-northwestward current is unfavorable to effluent dispersion whereas downwelling accompanied by south-southwestward current helps to restrict the effluent to the deeper layer and disperse the effluent away the region.

7. Summary

We have conducted a series of numerical simulations to analyze the basic ecological function of MBS and the possible impact of the MWRA outfall in 2006 and 2007 using the eutrophication model initially developed by HydroQual. The key variable as a measure of ecosystem health is the dissolved oxygen (DO) which is regulated by internal biological and biogeochemical dynamics in the water column, reaeration at the sea surface, sediment oxygen demand at the bottom, and hydrodynamics such as vertical mixing and advection. A unique skill of this simulation system resides in the sediment module which effectively captures nutrient and DO fluxes at the sediment-water interface.

Superimposed upon the natural function of the MBS ecosystem are anthropogenic perturbations through discharges of nutrients and organic substances. Anthropogenic sources include the MWRA and non-MWRA effluents, non-point sources, and atmospheric inputs. The MWRA outfall dominated the anthropogenic sources in 2006 and 2007.

Environmental parameters were monitored at 36 stations in MB and CCB including 7 stations near the MWRA outfall, plus 11 stations in BH. These data were used to establish the bi-weekly open boundary conditions using objective analysis and the simulation was validated by comparing with the field observations. The model has mostly reproduced the magnitudes and seasonal cycles of an array of monitored variables. Basically biological processes were dominated by spring and fall phytoplankton blooms reflected by high chlorophyll concentration and primary production. Following phytoplankton development, nutrients were depleted in surface waters from late spring to mid fall. However, nutrients in deeper water showed a different seasonality from that in the surface layer, with high values during summer and early fall. Although the spring phytoplankton bloom consumed most of the nutrient stock in the water column, nutrients in the deeper layer were primarily controlled by the remineralization of organic matter during the summer and fall season. With increased temperature in summer, regeneration was accelerated leading to a net production of nutrients in the deeper layer. The level of DO in the water column was regulated by both the production of phytoplankton photosynthesis and the consumption of remineralization. As such, the DO seasonality differed from that of phytoplankton and nutrients. During the spring phytoplankton bloom, photosynthesis production prevailed, leading to high DO concentration in both surface and deep layers. During summer, remineralization consumption dominated, resulting in low DO concentration, particularly in the deep layer. During the fall bloom, photosynthesis production did not compensate for the loss of remineralization so that DO remained at a low level. As was also the case for remineralization in the water column, diagenesis of biodeposits was essentially controlled by temperature and generated high fluxes of nutrients and SOD during the summer season. With good agreement in general between the simulation and observation, the model tended to underestimate chlorophyll at high concentrations and overestimate chlorophyll at low concentrations. An inaccurate carbon to chlorophyll ratio can lead to deterioration in the model-data comparison, but the mechanism leading to this discrepancy remains to be analyzed. Also the model tended to underestimate DO in the deep layer during summer, which could be caused by biased vertical mixing strength.

Sensitivity analysis did not indicate a significant impact of the MWRA outfall on the ecosystem function in general. On a local scale close to the MWRA outfall, effluent nutrients can be traced to the mid-depth and in some cases translated into an anomaly in chlorophyll concentration. The

dispersion and stagnation of effluent were primarily determined by the current system, which was subject to both local and remote forcing. The local current had a strong response to wind forcing so that the influence of effluent on ecological function was partly controlled by the prevailing wind. Indeed, sensitivity-analysis shows that using a high-resolution wind field corrects to some extent the discrepancy between simulation and observation by increasing the DO level in the bottom layer by 9-18%.

Biological responses to upwelling and storm events in the MBS depends not only on the strength and direction of the wind, but also on the timing of the event and the general function of the ecosystem. Neither in early spring when the water column is nutrient-replenished, nor in early summer when the water column is nutrient-depleted, can upwelling events have significant influence on biological production in the MBS. Biological responses to upwelling events manifest the most in the late summer and early fall when surface water remains nutrient-depleted while deeper waters are nutrient-replenished. In late fall and early winter when phytoplankton are light-limited, upwelling can advect nutrients from deeper to surface layers, but the advected nutrients cannot be converted to biomass so that the upwelling influence on biology is limited in deep regions. Concerning the dispersal of the MWRA effluent, upwelling can bring the effluent to the surface layer while downwelling events help to restrict the effluent to the deeper layer and disperse the effluent away from the near-field region.

8. References

Alber, M. and A. Chan. 1994. Sources of contaminants to Boston Harbor: revised loading estimates. Boston: Massachusetts Water Resource Authority. ENQUAD 1994-01, 113pp.

Bigelow, H.B. 1927. Physical oceanography of the Gulf of Maine (Part II). Bulletin of the Bureau of Fisheries, 40: 511-1027.

Butman, B. 1976. Hydrography and low frequency currents associated with the spring runoff in Massachusetts Bay Memoires. Societe Royale des Sciences de Liege, 6: 247-275.

Butman, B., Bothner, M.H., Lightsom, F.L., Gutierrez, B.T., Alexander, P.S., Martini, M.A., and Strahle, W.S. 2002. Long-term Oceanographic Observations in Western Massachusetts Bay offshore of Boston, Massachusetts: Data Report for 1989-2000, U.S. Geological Survey Digital Data Series 74.

Di Toro, D. M. 2001. Sediment Flux Modeling, Wiley-Interscience, New York, 624 pp.

Geyer, W. R., Gardner, G. B., Brown, W. S., Irish, J., Butman, B., Loder, T., and Signell, R. P. 1992. Physical oceanographic investigation of Massachusetts and Cape Cod Bays. Massachusetts Bay Program. MBP-92-03, 497pp.

Hendry, R., and I. He (1996). Technical report on objective analysis (OA) project, Bedford Institute of Oceanography, Dartmouth, Nova Scotia, 105pp.

HydroQual, Inc. 2000. Bays Eutrophication Model (BEM): modeling analysis for the period 1992-1994. Boston: Massachusetts Water Resources Authority. ENQUAD 2000-02, 158pp.

HydroQual, Inc. 2001. Boundary sensitivity for the Bays Eutrophication Model (BEM). Boston: Massachusetts Water Resources Authority. Report ENQUAD 2001-14. 90pp.

HydroQual, Inc. 2003. Bays Eutrophication Model (BEM): modeling analysis for the period 1998-1999. Boston: Massachusetts Water Resources Authority. ENQUAD 2003-03, 318pp.

HydroQual, Inc. and Normandeau Associates, Inc. 1993. A water quality model for Massachusetts and Cape Cod Bays. Boston: Massachusetts Water Resource Authority. ENQUAD 93-05, 222pp.

HydroQual, Inc. and Normandeau Associates, Inc. 1995. A water quality model for Massachusetts and Cape Cod Bays: Calibration of the Bay Eutrophication Model (BEM). Boston: Massachusetts Water Resource Authority. ENQUAD 1995-08, 402pp.

HydroQual, Inc. and Signell, R.P. 2001. Calibration of the Massachusetts and Cape Cod Bays Hydrodynamic Model: 1998-1999. Boston: Massachusetts Water Resources Authority. ENQUAD 2001-12, 170pp.

Jiang, M.S. and Zhou, M. 2004a. The summer Ekman pumping and its implications to the deep water renewal in Massachusetts and Cape Cod Bays. Proceedings of the 8th Estuarine Coastal Modeling. San Francisco. 11-3-0003. p929-948.

Jiang, M.S. and Zhou, M. 2004b. Calibration of the Massachusetts and Cape Cod Bays hydrodynamic model: 2000-2001. Boston: Massachusetts Water Resources Authority. Draft Report. ENQUAD 2004-08. 71pp.

Jiang, M.S. and Zhou M. 2007. User's guide to the water-quality part of the Bays Eutrophication Model (BEM). Boston: MWRA Report 2007-09. 36 pp.

Jiang, M.S. and Zhou, M. 2008. Massachusetts Bay Eutrophication Model: 2005 Simulation. Boston: Massachusetts Water Resources Authority. Report 2008-13. 82pp.

Kropp, R. K., Diaz, R., Hecker, B., Dahlen, D., Boyle, J. D., Abramson, S. L., and Emsbo-Mattingly, S. 2001. 2000 Outfall Benthic Monitoring Report. Boston: Massachusetts Water Resources Authority. ENQUAD 2001-14, 148pp.

Kropp, R. K., Diaz, R., Dahlen, D., Boyle, J. D., and Hunt, C. D. 2002. 2001 Harbor Benthic Monitoring Report. Boston: Massachusetts Water Resources Authority. ENQUAD 2002-19, 74pp.

Libby, P. S., Hunt, C. D, Geyer, W. R., Keller, A. A., Oviatt, C. A., and Turner, J. T. 2000. 1999 Annual Water Column Monitoring Report. Boston: Massachusetts Water Resources Authority. ENQUAD 2000-09, 180pp.

Libby, P. S., Hunt, C. D, McLeod, L. A., Geyer, W. R., Keller, A. A., Borkman, D., Oviatt, C. A., and Turner, J. T. 2001. 2000 Annual Water Column Monitoring Report. Boston: Massachusetts Water Resources Authority. ENQUAD 2001-17, 196pp.

Libby P.S., Mansfield A., Buhl R., Lescarbeau G., Leo W., Keller A.A., Borkman D.G., Turner J.T., and Oviatt C.A. 2006. Combined work/quality assurance project plan (QAPP) for water column monitoring 2006 - 2007, tasks 4, 5, 6, 7, 8, 11. Boston: Massachusetts Water Resources Authority. ENQUAD 2006-03, 119pp.

Libby P.S., Geyer W.R., Keller A.A., Mansfield A.D., Turner J.T., Anderson D.M., Borkman D.G., Rust S., Hyde K., and Oviatt C.A. 2007. Water Column Monitoring in Massachusetts Bay: 1992-2006. Boston: Massachusetts Water Resources Authority. ENQUAD 2007-11, 228pp.

Libby P.S., Borkman D.G., Geyer W.R., Keller A.A., Turner J.T., Mickelson M.J., and Oviatt C.A. 2008. Water Column Monitoring in Massachusetts Bay: 1992-2007. Boston: Massachusetts Water Resources Authority. ENQUAD 2008-16, 170pp.

Lynch, D.R., Naimie, C.E. and Werner, F.E. 1996. Comprehensive coastal circulation model with application to the Gulf of Maine. Cont. Shelf Res., 12: 37-64.

Maciolek, N. J., Diaz, R. J., Dahlen, D., Hecker, B., Gallagher, E. D., Blake, J. A., Williams, I. P., Emsbo-Mattingly, S., Hunt, C., and Keay, K. E. 2003. 2002 Outfall Benthic Monitoring Report. Boston: Massachusetts Water Resources Authority. ENQUAD 2003-13, 166pp.

Menzie-Cura, 1991. Sources and loadings of pollutants to Massachusetts Bays. Boston: Massachusetts Water Resources Authority Report, 1991-01, 266pp.

Taylor D.I. 2004. Harbor-Bay eutrophication-related water chemistry changes after 'offshore transfer'. Boston: Massachusetts Water Resources Authority. Report 2004-06. 83 p.

Tucker, J., Kelsey, J., Giblin, A., and Hopkinson, C. S. 2002. Benthic Metabolism and Nutrient Cycling in Boston Harbor and Massachusetts Bay: Summary of Baseline Data and Observations after One Year of Harbor-to-Bay Diversion of Sewage Effluent. Boston: Massachusetts Water Resources Authority. ENQUAD 2002-13, 83pp.

Tucker J., Kelsey S., Giblin A.E., and Hopkinson Jr. C.S. 2007. 2006 Annual benthic nutrient flux monitoring report. Boston: Massachusetts Water Resources Authority. ENQUAD 2007-07, 65pp.

Tucker J., Kelsey S., Giblin A.E., and Hopkinson Jr. C.S. 2008. 2007 Annual benthic nutrient flux monitoring report. Boston: Massachusetts Water Resources Authority. ENQUAD 2008-14, 59pp.

Turner, J.T., 1994. Planktonic Copepods of Boston Harbor, Massachusetts Bay and Cape-Cod Bay, 1992. Hydrobiologia. 293: 405-413.

Werme, C. and Hunt, C. D. 2003. 2002 Outfall monitoring overview. Boston: Massachusetts Water Resources Authority. ENQUAD 2003-12, 80pp.

Table 2.1 Model variables

No.	Variables	Units
1	Salinity	ppt
2	Phytoplankton winter/spring group	mg C l^{-1}
3	Phytoplankton fall group	mg C l^{-1}
4	Particulate organic phosphorous – refractory component	mg P l^{-1}
5	Particulate organic phosphorous – labile component	mg P l^{-1}
6	Dissolved organic phosphorous – refractory component	mg P l^{-1}
7	Dissolved organic phosphorous – labile component	mg P l^{-1}
8	Total dissolved inorganic phosphorous	mg P l^{-1}
9	Particulate organic nitrogen – refractory component	mg N l^{-1}
10	Particulate organic nitrogen – labile component	mg N l^{-1}
11	Dissolved organic nitrogen – refractory component	mg N l^{-1}
12	Dissolved organic nitrogen – labile component	mg N l^{-1}
13	Total ammonia (ammonia in water and phytoplankton cell)	mg N l^{-1}
14	Nitrite + nitrate	mg N l^{-1}
15	Biogenic silica	mg Si l^{-1}
16	Total silica – (silica in water and phytoplankton cell)	mg Si l^{-1}
17	Particulate organic carbon – refractory component	mg C l^{-1}
18	Particulate organic carbon – labile component	mg C l^{-1}
19	Dissolved organic carbon – refractory component	mg C l^{-1}
20	Dissolved organic carbon – labile component	mg C l^{-1}
21	Dissolved organic carbon – reactive component	mg C l^{-1}
22	Dissolved organic carbon – algal exudate	mg C l^{-1}
23	O2* - aqueous oxygen	mg O_2 l^{-1}
24	Dissolved oxygen	mg O_2 l^{-1}
25	Total active metal (TAM)	mmol l^{-1}
26	Phytoplankton summer group	mg C l^{-1}

Table 2.2 Model parameters for nitrogen cycle

Notation	Description	Values
Winter/spring group growth, carbon to nitrogen ratios and carbon to chlorophyll ratios		
T_{opt1}	Optimal growth temperature for winter/spring phytoplankton	8 ºC
β_{11}	Temperature exponential coefficient on growth rate for T<Topt1	0.004 (ºC)$^{-2}$
β_{21}	Temperature exponential coefficient on growth rate for T>Topt1	0.006 (ºC)$^{-2}$
G_{pre1}	Gross photosynthetic rate	2.5 day^{-1}
G_{pr01}	Nutrient-saturated gross photosynthetic rate per unit light intensity	0.28 m2(mol quanta)$^{-1}$
k_{N1}	Half saturation constant for nitrogen uptake	0.01 mg N l^{-1}
k_{RB1}	Basal respiration rate	0.03 day^{-1}
k_{RG1}	Growth-rate-dependent respiration coefficient	0.28
k_{grz01}	Mortality rate due to grazing	0.1 day^{-1}
θ_{grz1}	Temperature dependent coefficient for grazing	1.1
f_{sc1}	Fraction of C allocated to structural purposes	0.1
W_{CChl1}	Nutrient-saturated carbon to chlorophyll ratio	40 mgC (mgChl a)$^{-1}$
Q_{F1}	Quotient of nutrient-limited N:C ratio	0.85
W_{CN1}	Nutrient-saturated carbon to nitrogen ratio	5.0 mgC (mgN)$^{-1}$
Summer group growth, carbon to nitrogen ratios and carbon to chlorophyll ratios		
T_{opt2}	Optimal growth temperature	18 ºC
β_{12}	Temperature exponential coefficient on growth rate for T<Topt2	0.004 (ºC)$^{-2}$
β_{22}	Temperature exponential coefficient on growth rate for T>Topt2	0.006 (ºC)$^{-2}$
G_{pre2}	Gross photosynthetic rate	3.0 day^{-1}
G_{pr02}	Nutrient-saturated gross photosynthetic rate per unit light intensity	0.28 m^2(mol quanta)$^{-1}$
k_{N2}	Half saturation constant for nitrogen uptake	0.01 mg N l^{-1}
k_{RB2}	Basal respiration rate	0.036 day^{-1}
k_{RG2}	Growth-rate-dependent respiration coefficient	0.28
k_{grz02}	Mortality rate due to grazing	0.1 day^{-1}
θ_{grz2}	Temperature dependent coefficient for grazing	1.1
f_{sc2}	Fraction of C allocated to structural purposes	0.1
W_{CChl2}	Carbon to chlorophyll ratio	65 mgC (mgChl a)$^{-1}$
Q_{F2}	Quotient of nutrient-limited N:C ratio	0.85
W_{CN2}	Nutrient-saturated carbon to nitrogen ratio	5.67 mgC (mgN)$^{-1}$
Fall group growth, carbon to nitrogen ratios and carbon to chlorophyll ratios		
T_{opt3}	Optimal growth temperature	14 ºC
β_{13}	Temperature exponential coefficient on growth rate for T<Topt3	0.004 (ºC)$^{-2}$
β_{23}	Temperature exponential coefficient on growth rate for T>Topt3	0.006 (ºC)$^{-2}$
G_{pre3}	Gross photosynthetic rate	2.5 day^{-1}
G_{pr03}	Nutrient-saturated gross photosynthetic rate per unit light intensity	0.28 m2(mol quanta)$^{-1}$
k_{N3}	Half saturation constant for nitrogen uptake	0.005 mg N l^{-1}
k_{RB3}	Basal respiration rate	0.03 day^{-1}
k_{RG3}	Growth-rate-dependent respiration coefficient	0.28

k_{grz03}	Mortality rate due to grazing	0.1 day^{-1}
θ_{grz3}	Temperature dependent coefficient for grazing	1.1
f_{sc3}	Fraction of C allocated to structural purposes	0.1
W_{CChl3}	Carbon to chlorophyll ratio	15 mgC $(mgChl\ a)^{-1}$
Q_{F3}	Quotient of nutrient-limited N:C ratio	0.85
W_{CN3}	Nutrient-saturated carbon to nitrogen ratio	5.67 mgC $(mgN)^{-1}$
Light attenuation		
k_{base}	Background light attenuation coefficient (2-D parameter)	0.16~0.6 m^{-1}
k_c	Chlorophyll self-shading coefficient	0.017 $m2(mg\ chl)^{-1}$
Nitrogen regeneration, nitrification and denitrification		
k_{mp}	Half saturation constant for nitrogen regeneration	0.05 mgC l^{-1}
k_{RPON}	Hydrolysis rate of RPON to RDON at 20ºC	0.008 day^{-1}
θ_{RPON}	Temperature coefficient for RPON hydrolysis	1.08
k_{LPON}	Hydrolysis rate of LPON to LDON at 20ºC	0.05 day^{-1}
θ_{LPON}	Temperature coefficient for LPON hydrolysis	1.08
k_{RDON}	Mineralization rate for RDON at 20ºC	0.008 day^{-1}
θ_{RDON}	Temperature coefficient for LDON mineralization	1.08
k_{RDON}	Mineralization rate for RDON at 20ºC	0.05 day^{-1}
θ_{RDON}	Temperature coefficient for LDON mineralization	1.08
k_{Nit}	Nitrification rate at 20ºC	0.1 day^{-1}
θ_{Nit}	Temperature coefficient for nitrification	1.08
$k_{Nit\ DO}$	Half saturation constant of oxygen for nitrification	1.0 $mgO_2\ l^{-1}$
k_{Denit}	Denitrification rate at 20ºC	0.05 day^{-1}
θ_{Denit}	Temperature coefficient for denitrification	1.045
$k_{Denit\ DO}$	Half saturation constant of oxygen for denitrification	0.1 $mgO^2\ l^{-1}$
Fraction of respired and grazed phytoplankton into organic pool		
f_{RPON}	Fraction of RPON from respiration and grazing	0.15
f_{LPON}	Fraction of LPON from respiration and grazing	0.325
f_{RDON}	Fraction of RDON from respiration and grazing	0.15
f_{LDON}	Fraction of LDON from respiration and grazing	0.175
f_{nh3}	Fraction of ammonia from respiration and grazing	0.2
Exudation of phytoplankton primary productivity into dissolved organic carbon		
F_{ExDOC}	Exudation fraction of primary productivity to DOC	0.1
Phytoplankton settling		
V_{b1}	Base algal settling rate for winter/spring group at 20ºC	0.5 m day^{-1}
V_{N1}	Nutrient stressed algal settling rate for winter/spring group at 20ºC	1.0 m day^{-1}
V_{b2}	Base algal settling rate for summer group at 20ºC	0.3 m day^{-1}
V_{N2}	Nutrient stressed algal settling rate for summer group at 20ºC	0.7 m day^{-1}
V_{b3}	Base algal settling rate for fall group at 20ºC	0.3 m day^{-1}

V_{N3}	Nutrient stressed algal settling rate for fall group at 20ºC	1.0 m day^{-1}
θ_{sp}	Temperature correction for phytoplankton settling	1.027
Settling of particulate organic nitrogen		
V_{PON}	Settling rate for PON at 20ºC	1.0 m day^{-1}
θ_{PON}	Temperature correction for PON settling	1.027

Table 2.3 Data-model conversion for the MWRA sewage treatment plant and CSO effluents.

Model			Conversion	Data	
Variable	Definition	Units	Function	Variable	Units
Flow	Sewage flow	l day^{-1}	3.785mflow	mflow	gallon d^{-1}
TOC	Total organic C	mg C d^{-1}	0.7CBOD+18	CBOD	mg O d^{-1}
RPOC	Refractory POC	mg C d^{-1}	9	CBOD	mg O d^{-1}
LPOC	Labile POC	mg C d^{-1}	0.198CBOD	CBOD	mg O d^{-1}
RDOC	Refractory DOC	mg C d^{-1}	9	CBOD	mg O d^{-1}
LDOC	Labile DOC	mg C d^{-1}	0.132CBOD	CBOD	mg O d^{-1}
REDOC	Reactive DOC	mg C d^{-1}	0.37CBOD	CBOD	mg O d^{-1}
TON	Total organic N	mg N d^{-1}	(TKN-NH4)/1000	TKN	ug N d^{-1}
RPON	Refractory PON	mg N d^{-1}	0.4(TKN-NH4)/1000	TKN	ug N d^{-1}
LPON	Labile PON	mg N d^{-1}	0.4(TKN-NH4)/1000	TKN	ug N d^{-1}
RDON	Refractory DON	mg N d^{-1}	0.1(TKN-NH4)/1000	TKN	ug N d^{-1}
LDON	Labile DON	mg N d^{-1}	0.1(TKN-NH4)/1000	TKN	ug N d^{-1}
TOP	Total organic P	mg P d^{-1}	(TP-PO4)/1000	TP	ug P d^{-1}
RPOP	Refractory DOP	mg P d^{-1}	0.3(TP-PO4)/1000	TP	ug P d^{-1}
LPOP	Labile DOP	mg P d^{-1}	0.55(TP-PO4)/1000	TP	ug P d^{-1}
RDOP	Refractory DOP	mg P d^{-1}	0.05(TP-PO4)/1000	TP	ug P d^{-1}
LDOP	Labile DOP	mg P d^{-1}	0.1(TP-PO4)/1000	TP	ug P d^{-1}

Table 2.4 Partition coefficients of chlorophyll to phytoplankton groups at the open boundary.

	Winter-spring group	Summer group	Fall group
January-April	1.0	0	0
May	0.5	0.5	0
June-July	0	1.0	0
August	0	0.5	0.5
September-November	0	0	1.0
December	0.5	0	0.5

Table 2.5 Partition coefficients for organic matter.

		Labile	Refractory	Reactive	Exudate
Nitrogen	PON	0.5	0.5		
	DON	0.5	0.5		
Phosphorus	POP	0.647	0.353		
	DOP	0.66	0.33		
Carbon	POC	0.4	0.6	-	-
	DOC	0.2	0.7	0.05	0.05

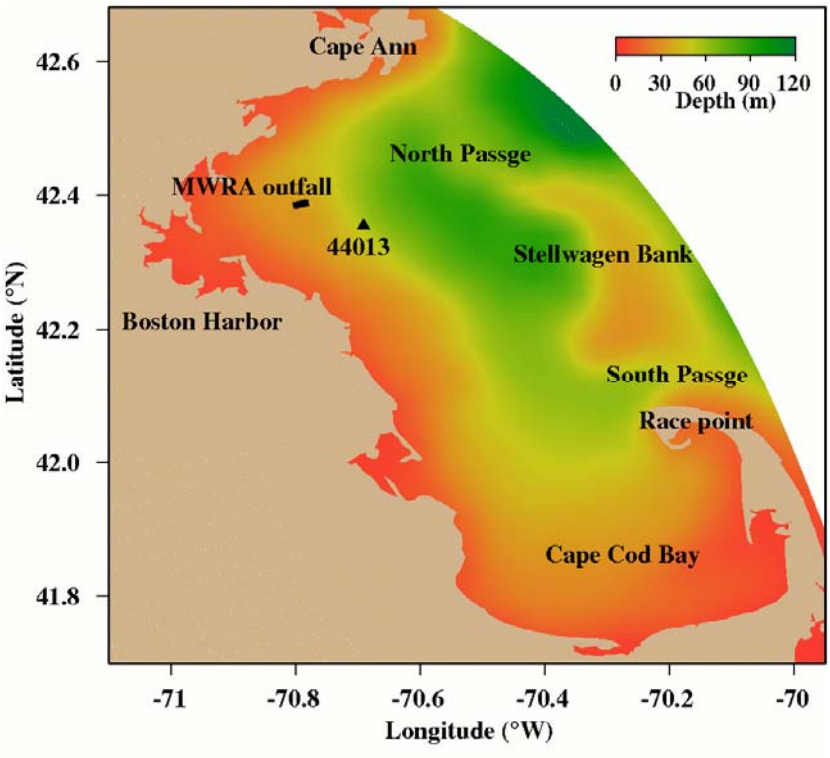

Figure 1.1 The Massachusetts Bay system (MBS) and location of the MWRA outfall and the NOAA 44013 Buoy.

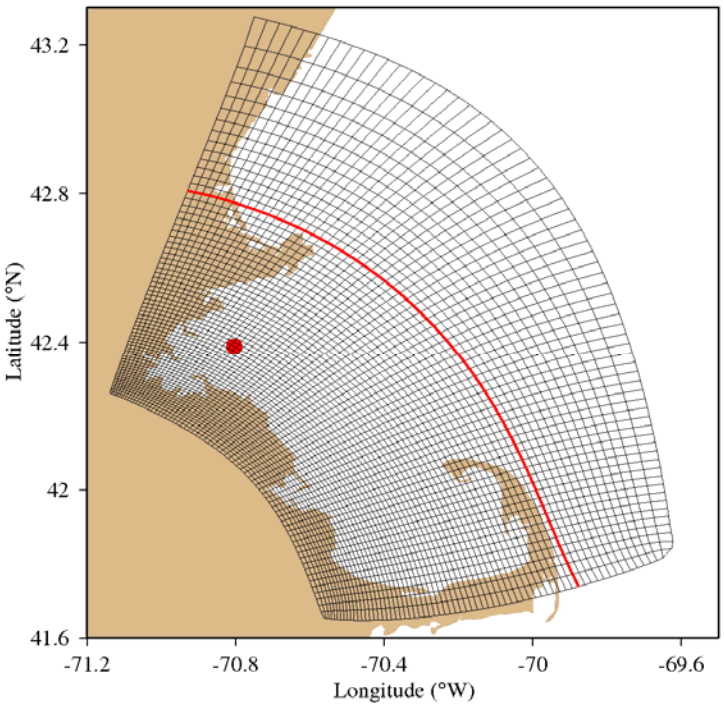

Figure 2.1 Model domain and grid of ECOMsi (larger domain) and RCA (smaller domain) in the Mass Bay system. Red dot represents the MWRA outfall and the thick red line indicates the boundary of the RCA domain

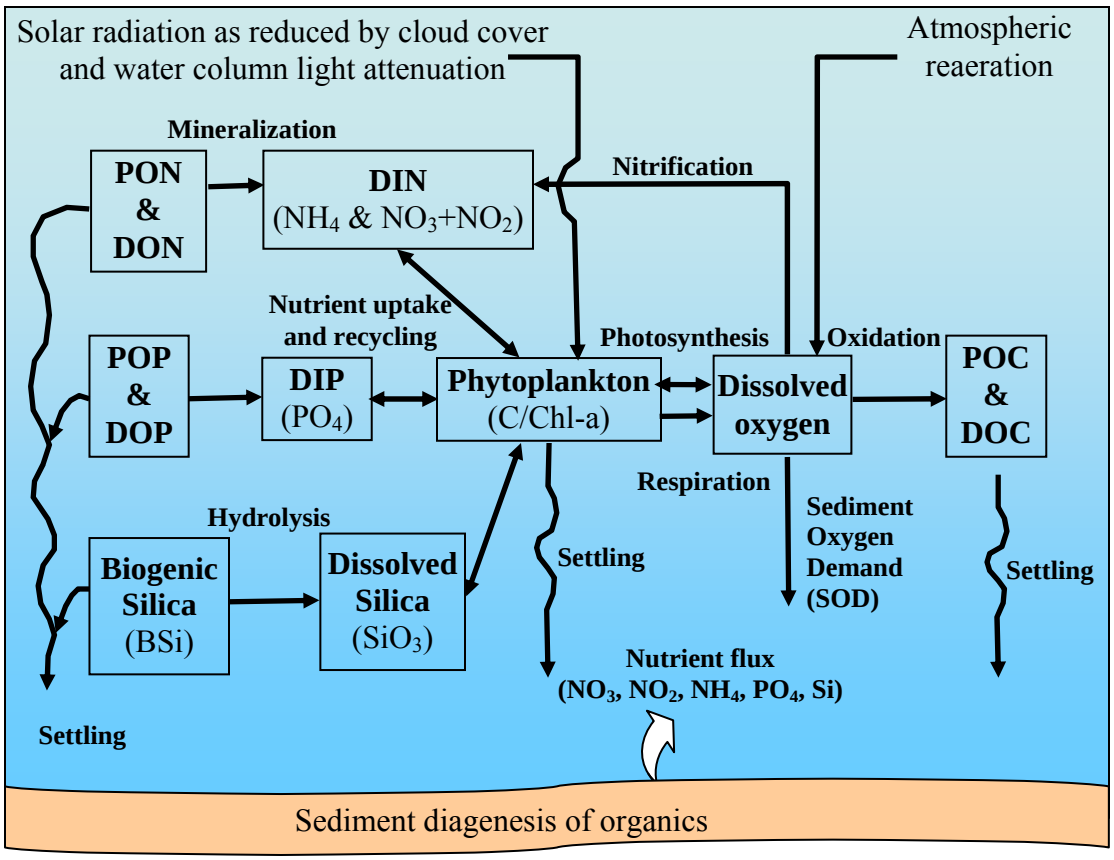

Figure 2.2 The RCA water quality model (reproduced from HydroQual, 2004).

RCA Nitrogen Cycle

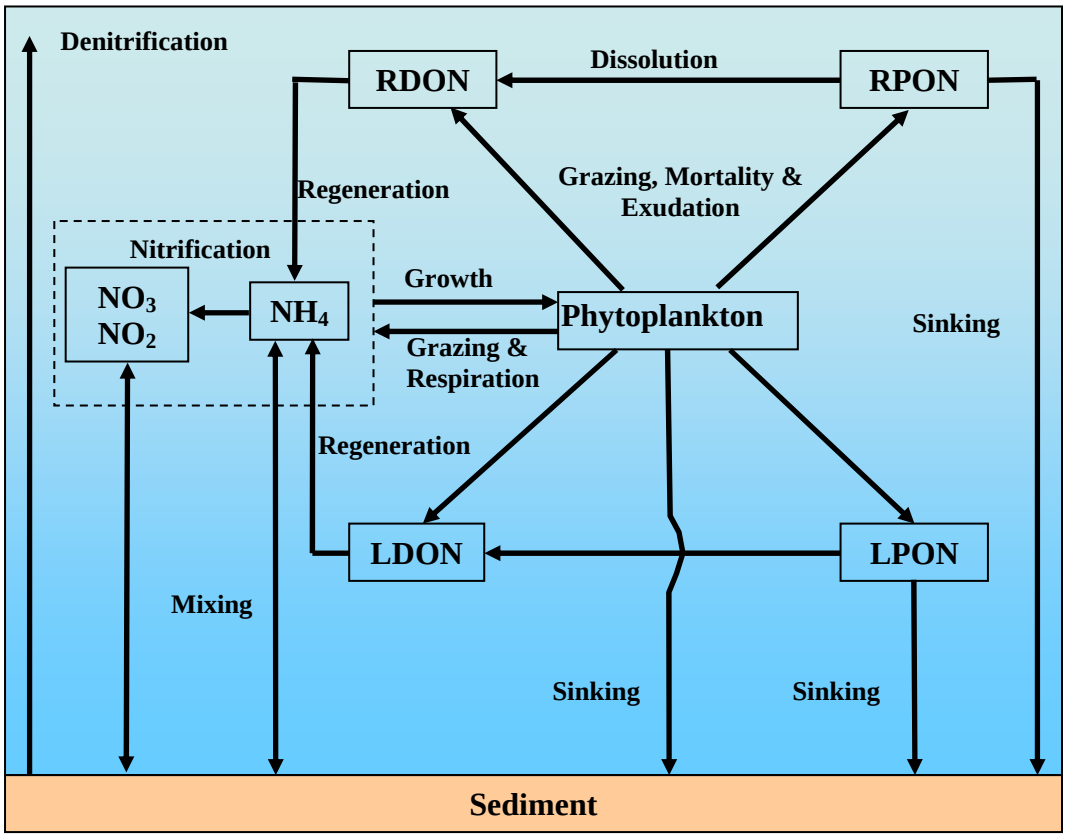

RCA: Row-Column Advanced Ecological Systems Operating Program
RDON: Refractory Dissolved Organic Nitrogen
RPON: Refractory Particulate Organic Nitrogen
LDON: Labile Dissolved Organic Nitrogen
LPON: Labile Particulate Organic Nitrogen

Figure 2.3 Nitrogen dynamics in the BEM (reproduced from Jiang and Zhou, 2007).

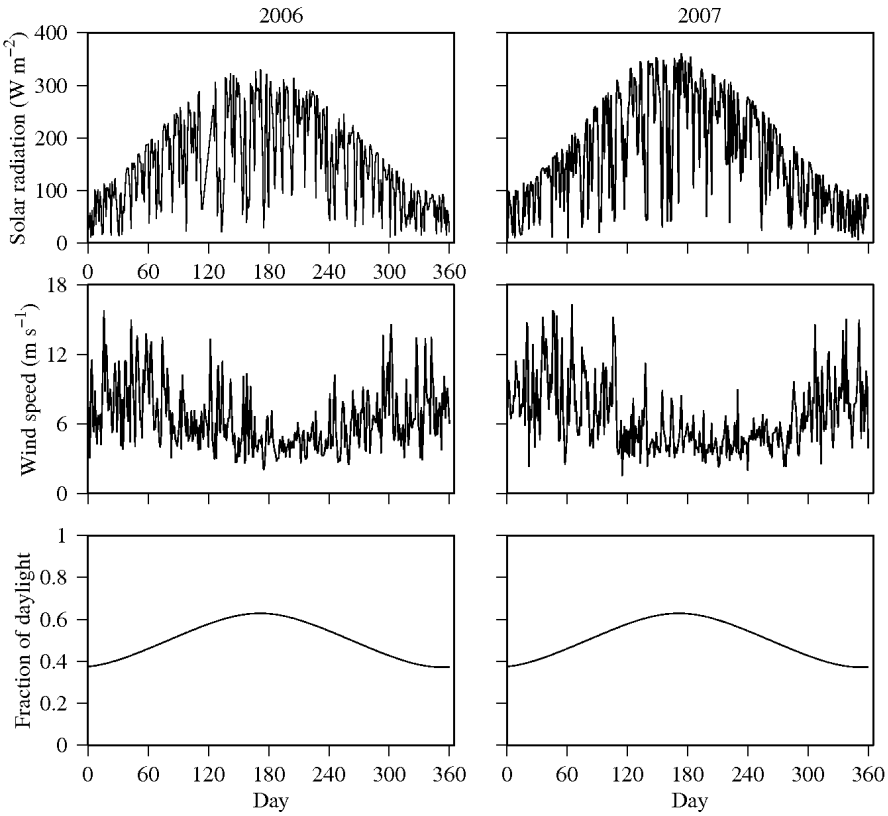

Figure 2.4 Daily averaged pyranometer solar radiation, wind speed, and fraction of daylight in 2006 and 2007.

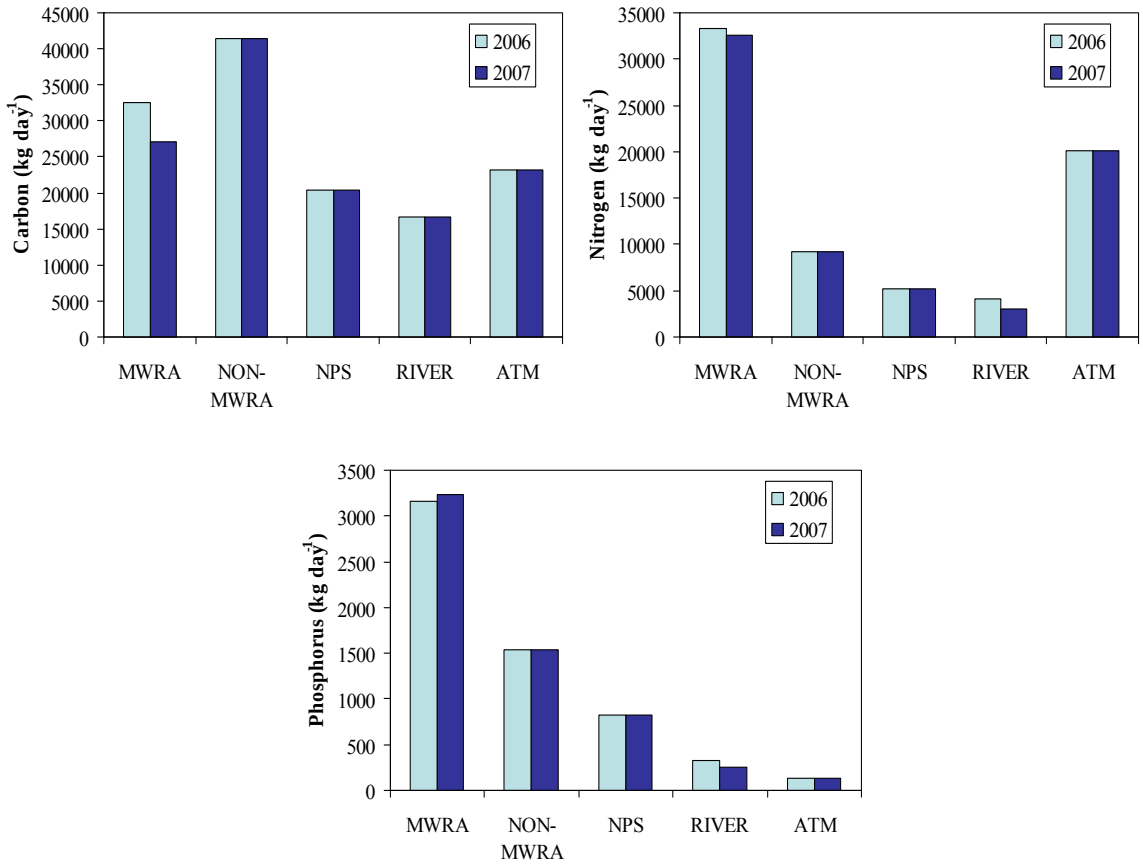

Figure 2.5 Mean daily loadings of carbon, nitrogen and phosphorus from different anthropogenic sources. MWRA: MWRA outfall; NON-MWRA: Non MWRA point sources; NPS: Non-point sources; River: River loadings; ATM: Atmospheric input.

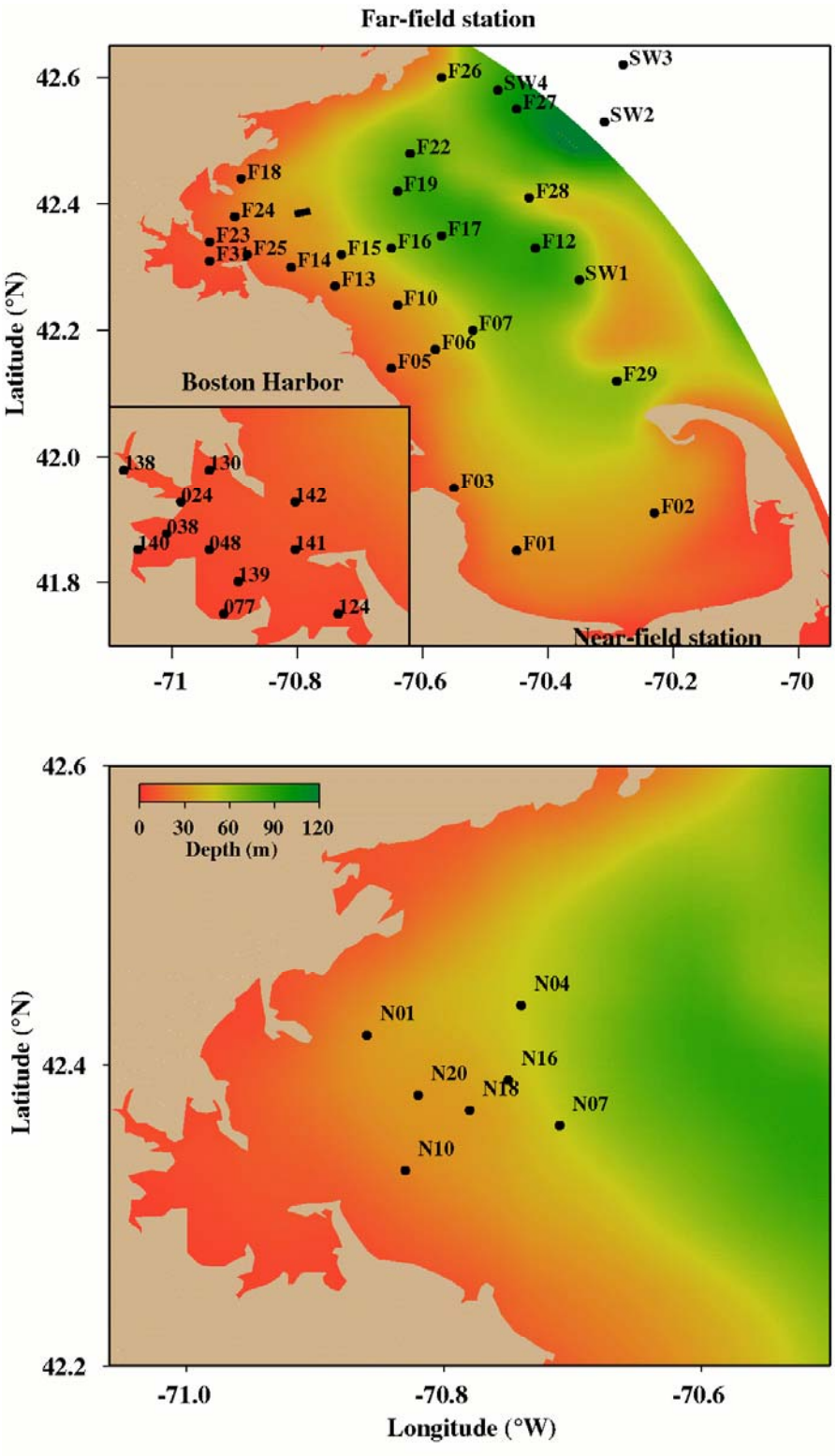

Figure 2.6 Far-field (upper panel) and near-field (lower panel) MWRA monitoring stations. The bold line represents the location of the MWRA outfall. Stations in Boston Harbor were monitored by the Boston Harbor Water Quality Monitoring Program.

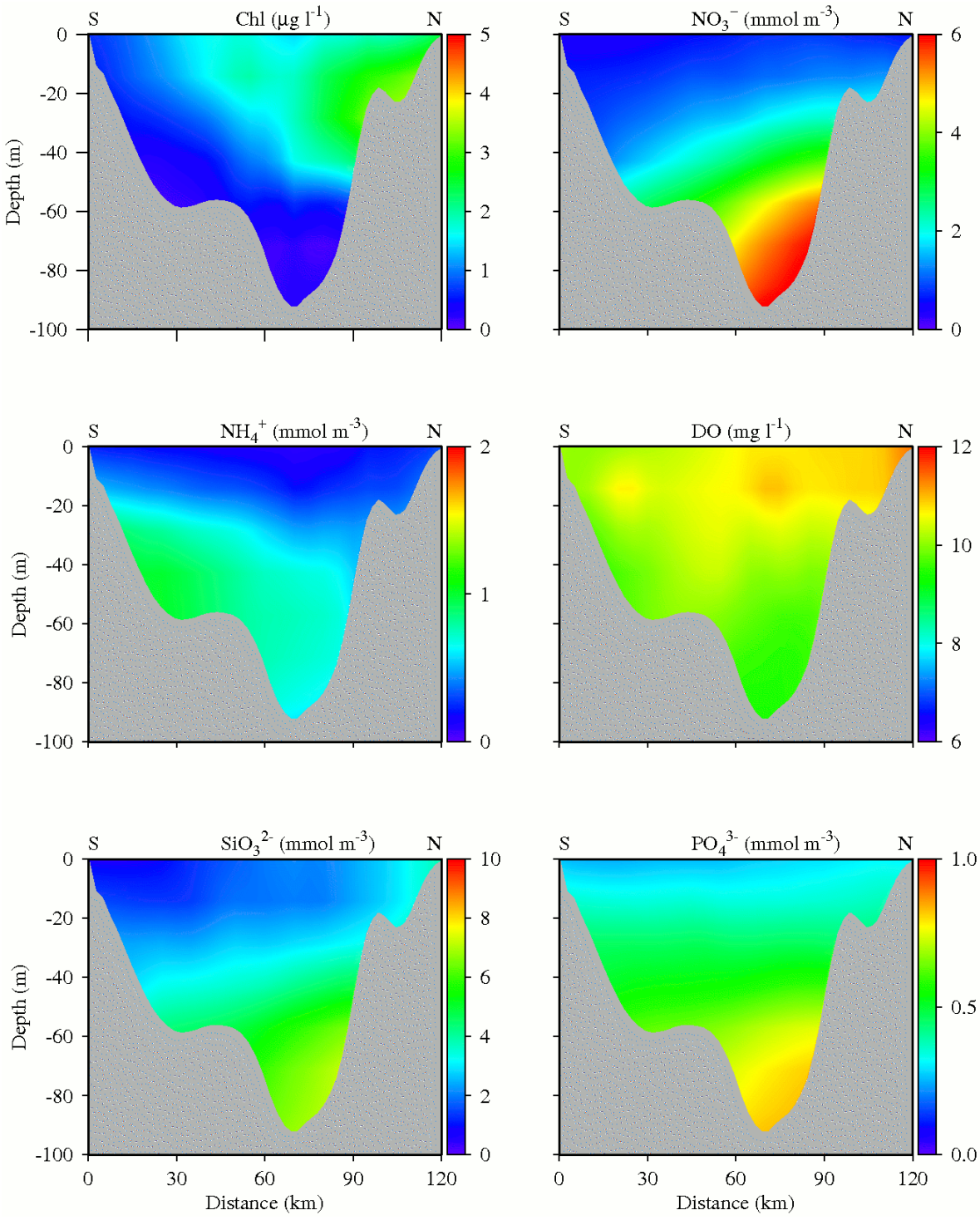

Figure 2.7 Transect of open boundary conditions from Cape Cod (south S) to Cape Ann (north N) of chlorophyll, nutrients and DO in April 2006.

.

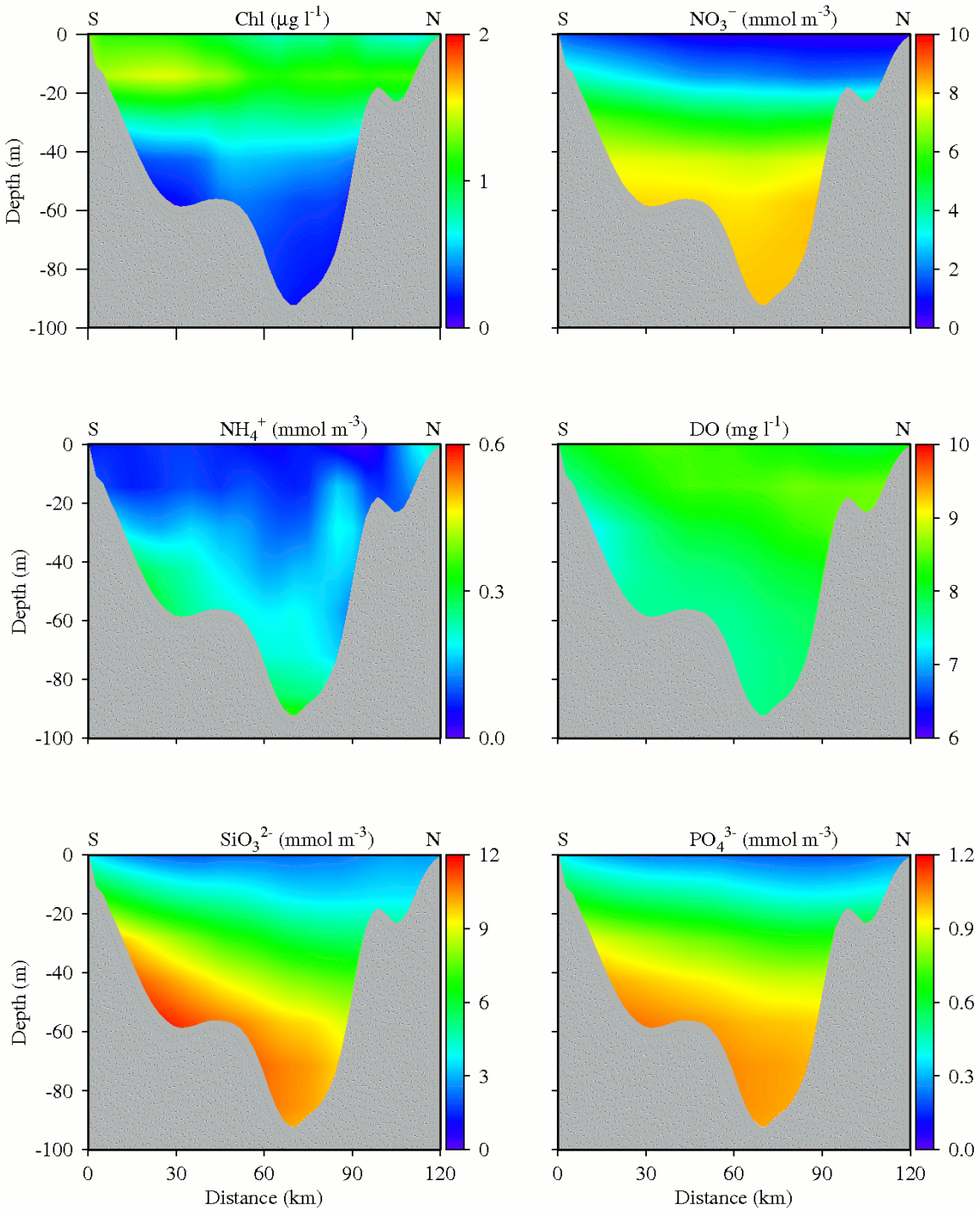

Figure 2.8 Transect of open boundary conditions from Cape Cod (south S) to Cape Ann (north N) of chlorophyll, nutrients and DO in August 2006.

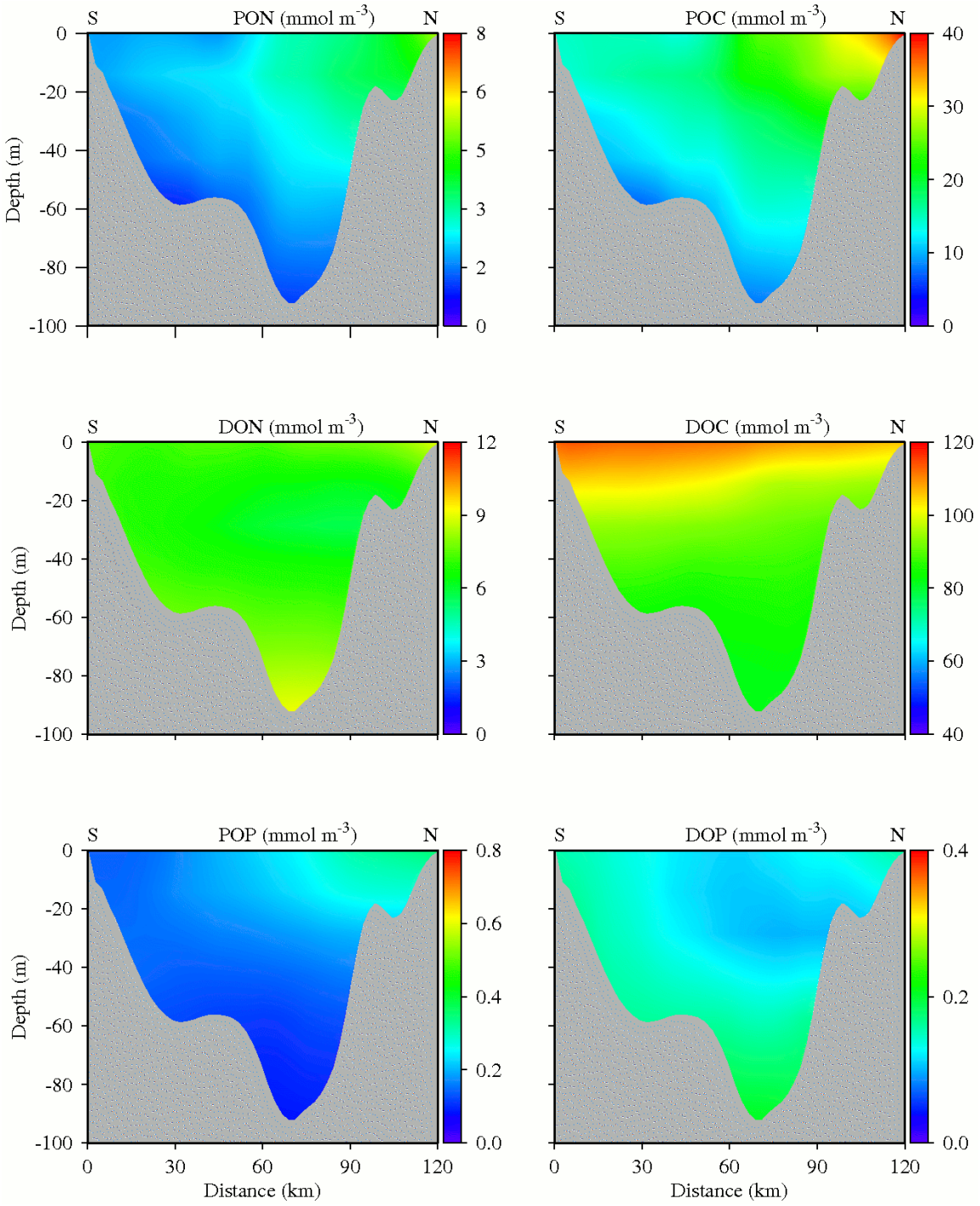

Figure 2.9 Transect of open boundary conditions from Cape Cod (south S) to Cape Ann (north N) of organic nutrients in April 2006.

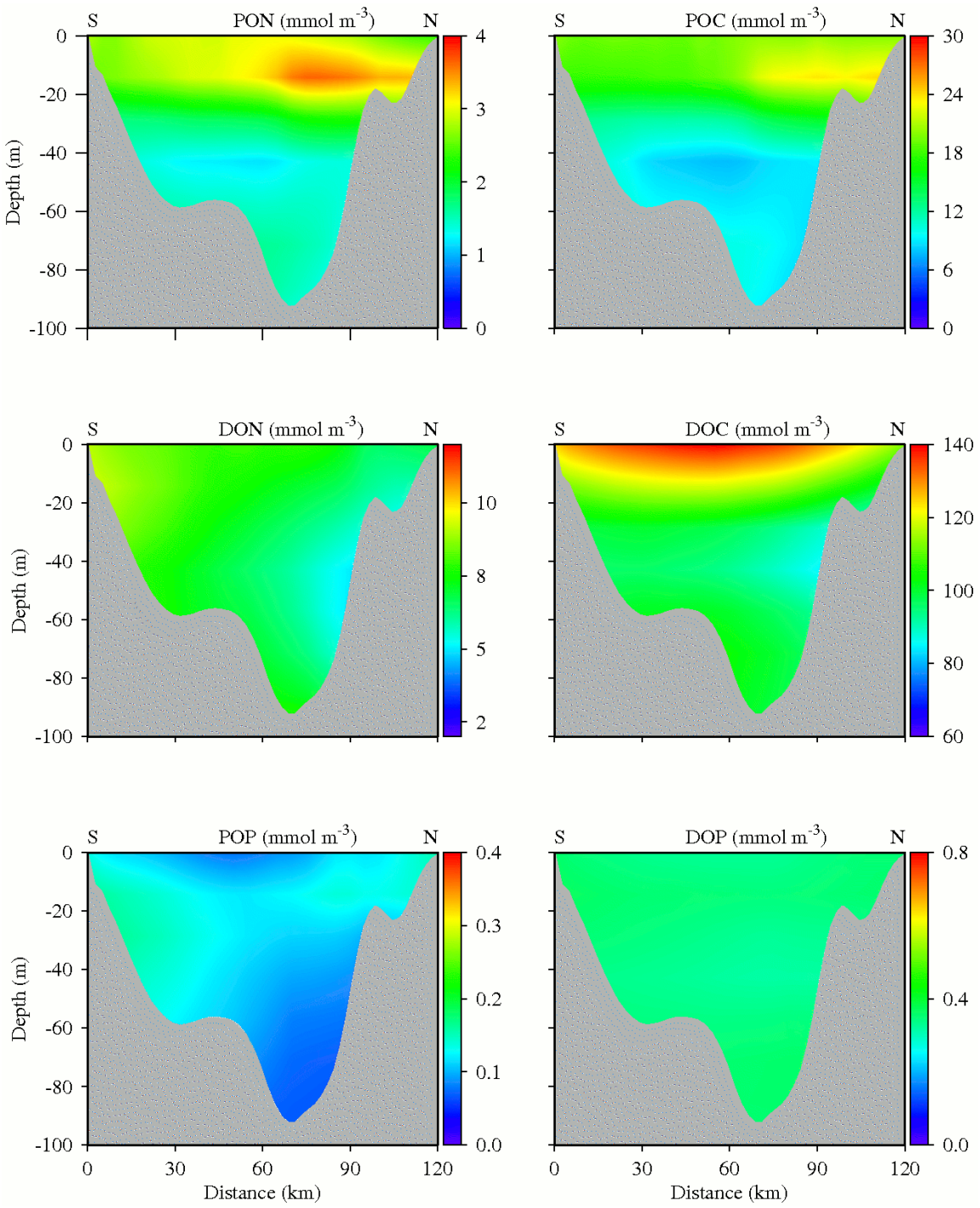

Figure 2.10 Transect of open boundary conditions from Cape Cod (south S) to Cape Ann (north N) of organic nutrients in August 2006.

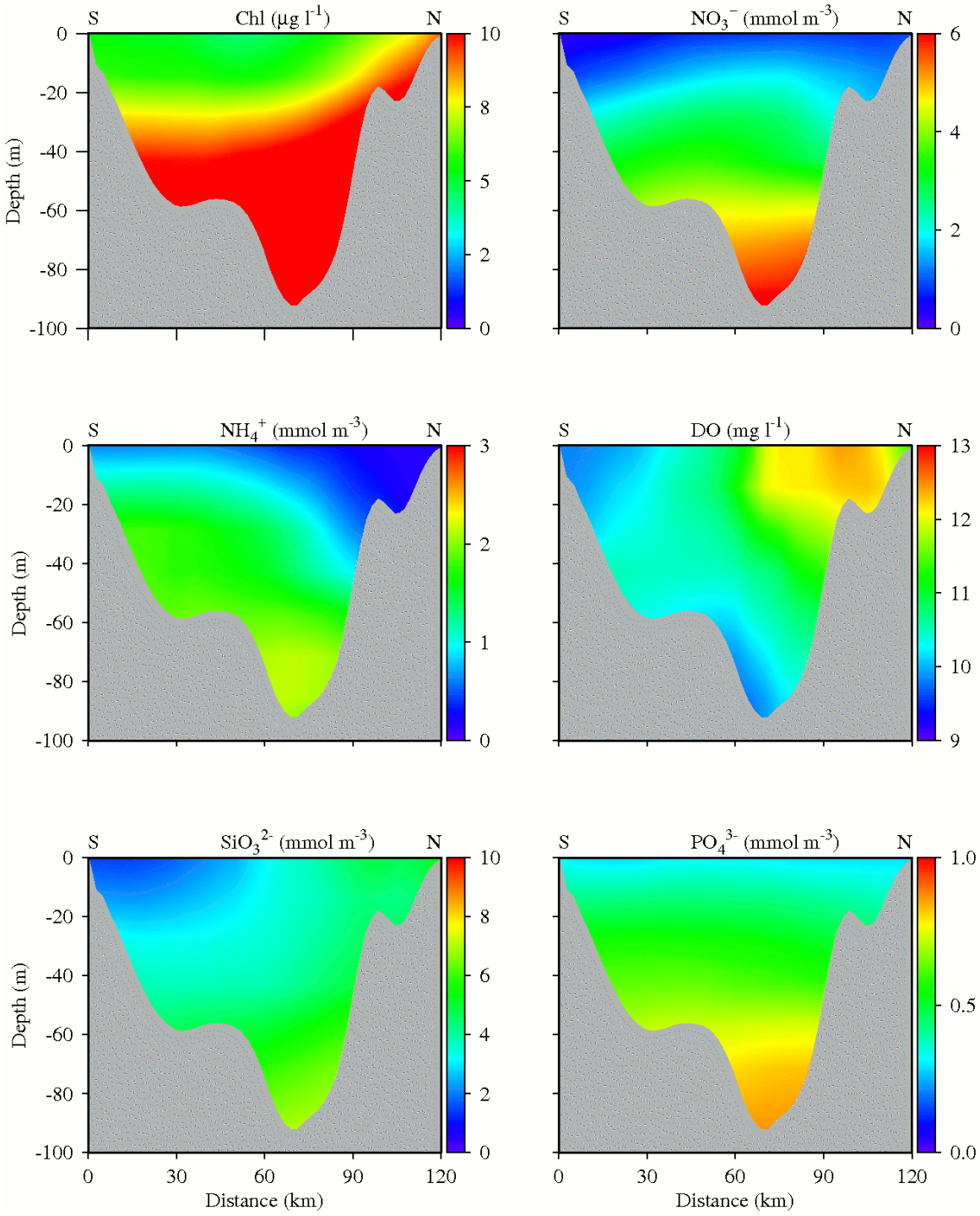

Figure 2.11 Transect of open boundary conditions from Cape Cod (south S) to Cape Ann (north N) of chlorophyll, nutrients and DO in April 2007.

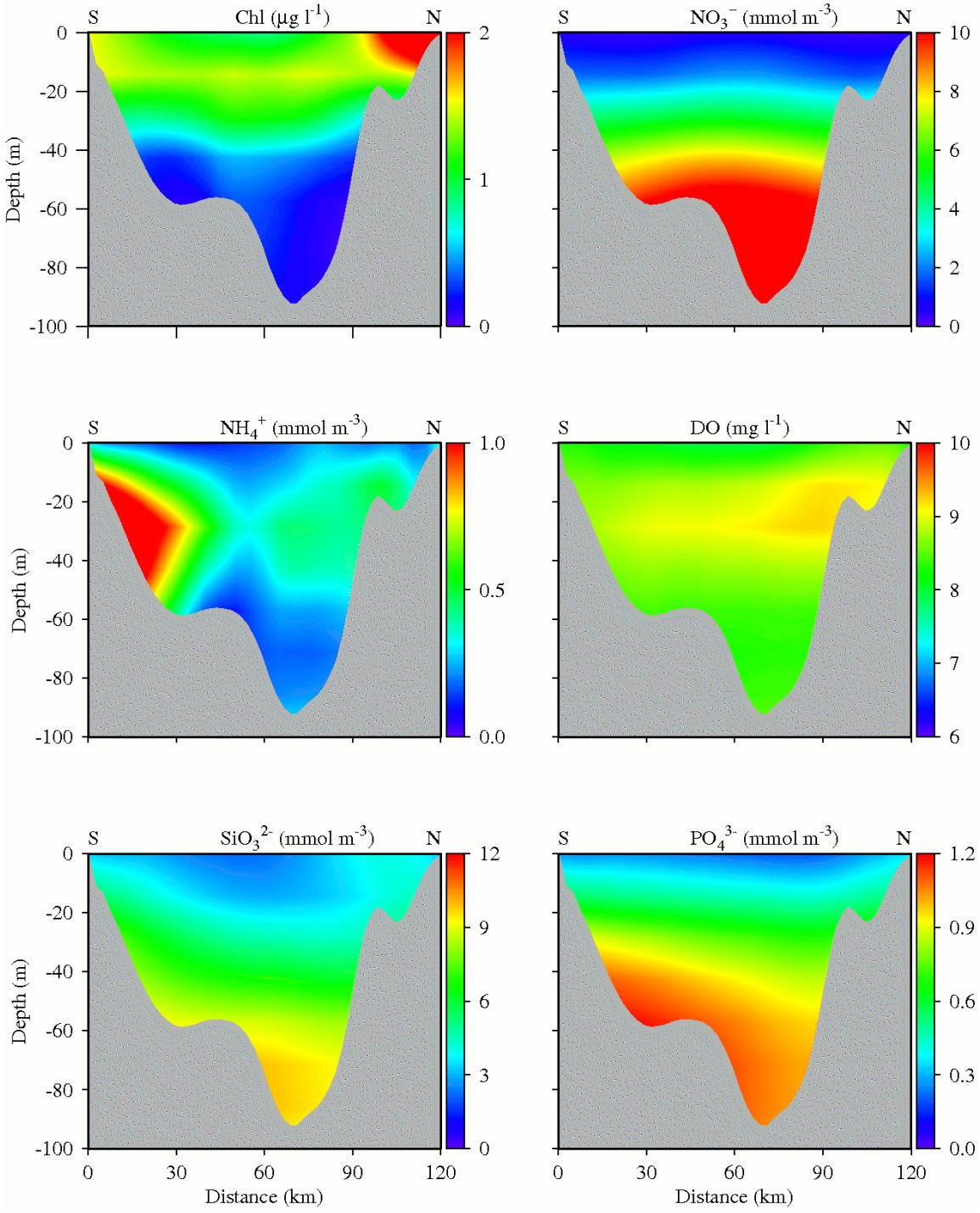

Figure 2.12 Transect of open boundary conditions from Cape Cod (south S) to Cape Ann (north N) of chlorophyll, nutrients and DO in August 2007.

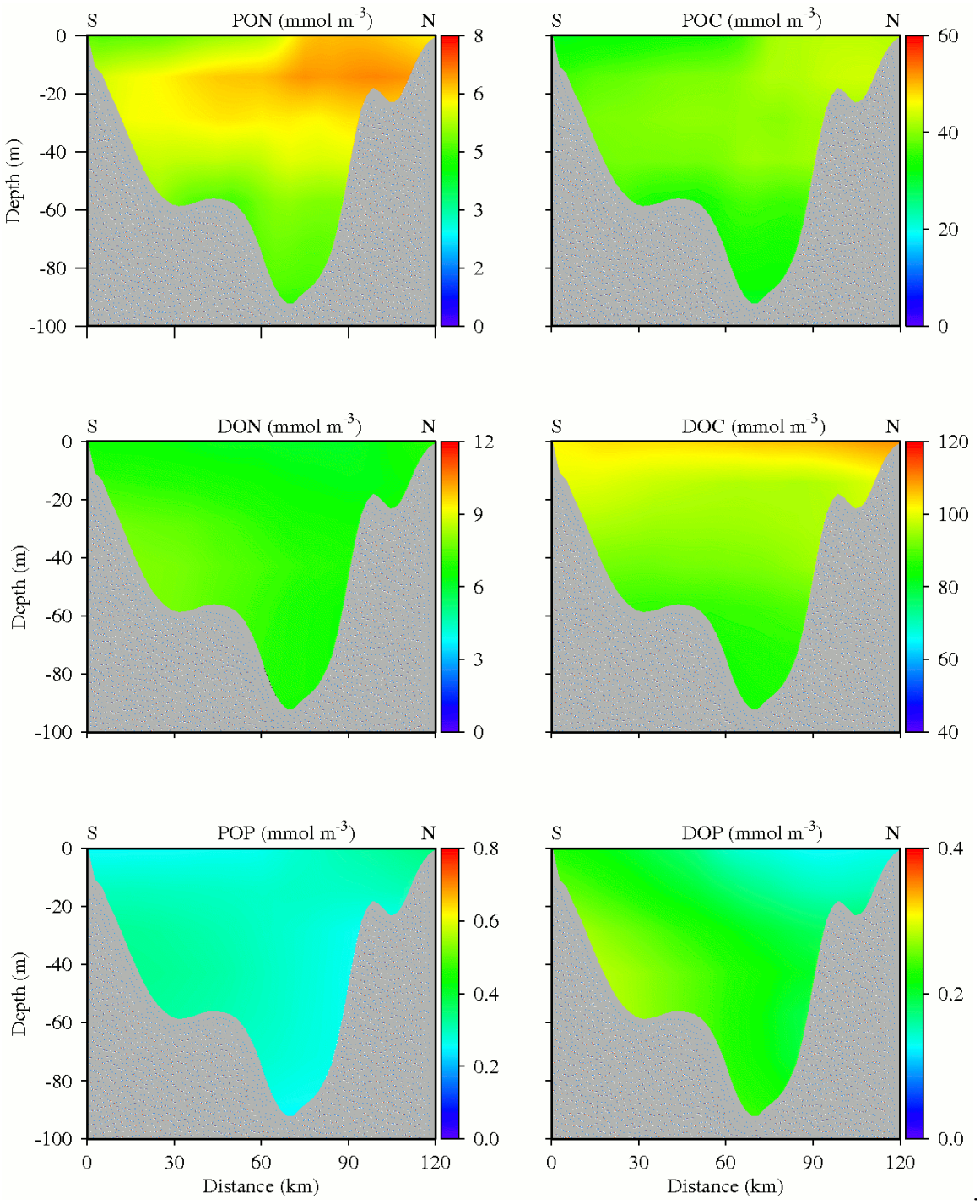

Figure 2.13 Transect of open boundary conditions from Cape Cod (south S) to Cape Ann (north N) of organic nutrients in April 2007.

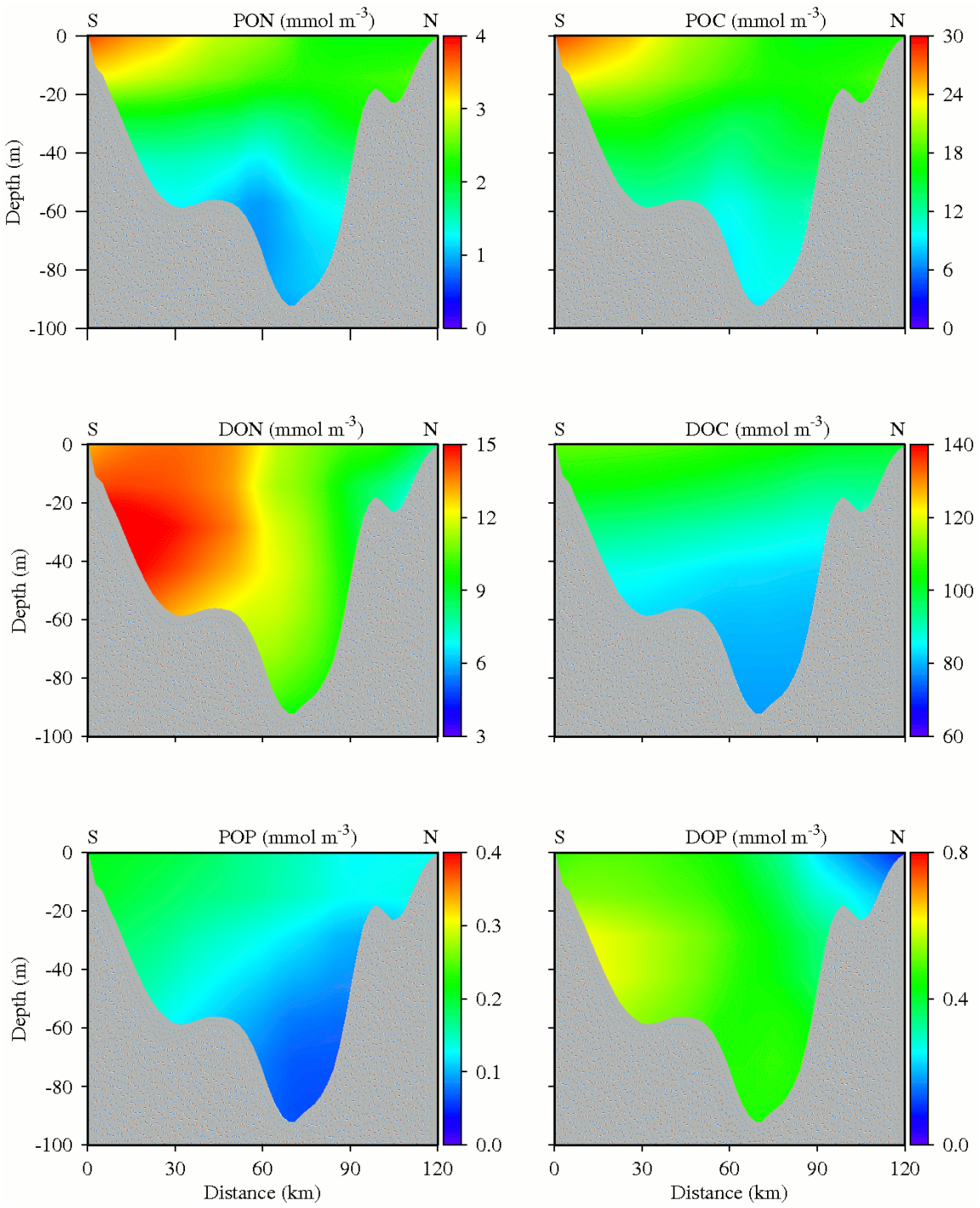

Figure 2.14 Transect of open boundary conditions from Cape Cod (south S) to Cape Ann (north N) of organic nutrients in August 2007.

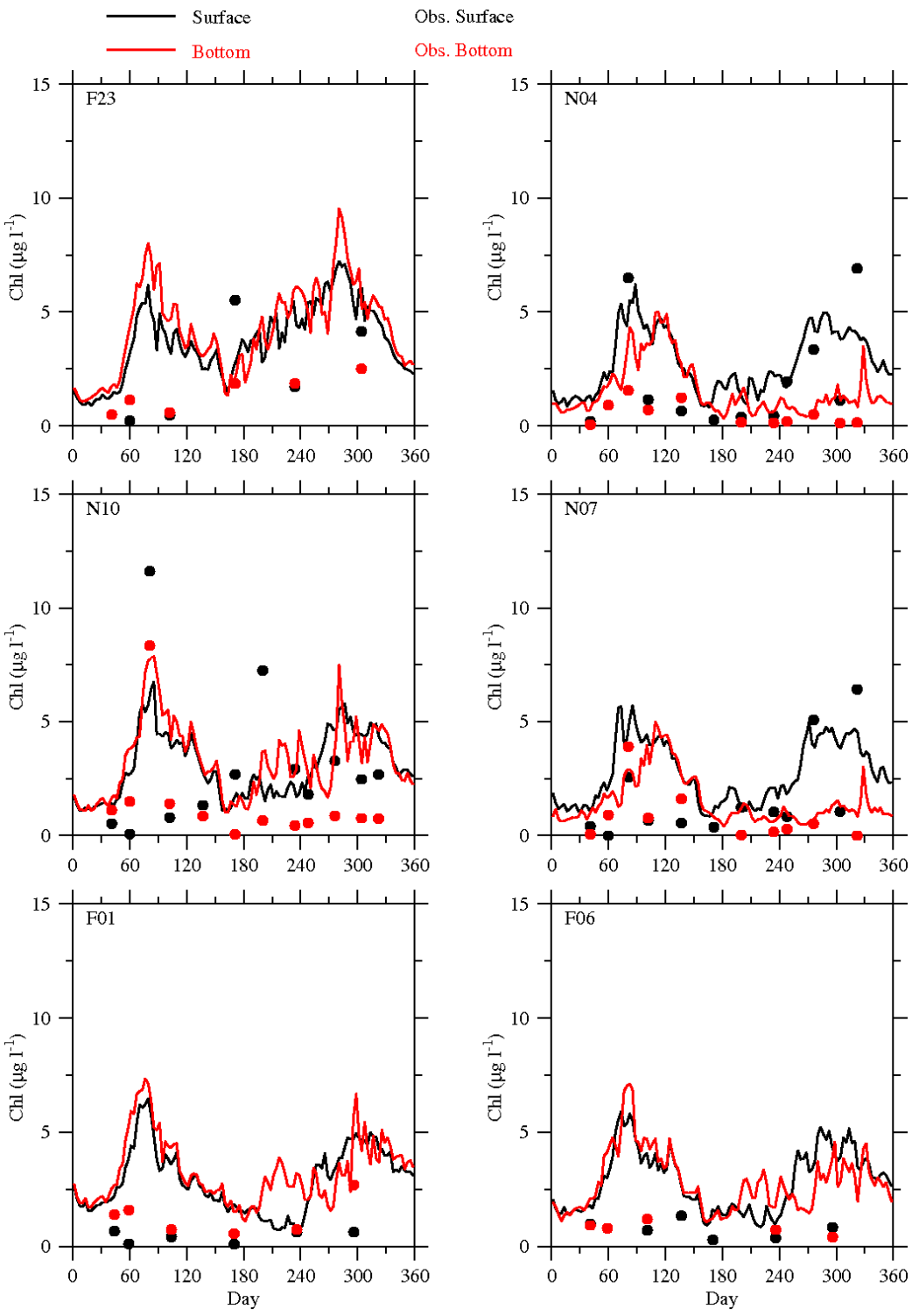

Figure 3.1 Comparison of observed (dots) and modeled (lines) time-series data of chlorophyll at the MWRA monitoring stations in 2006.

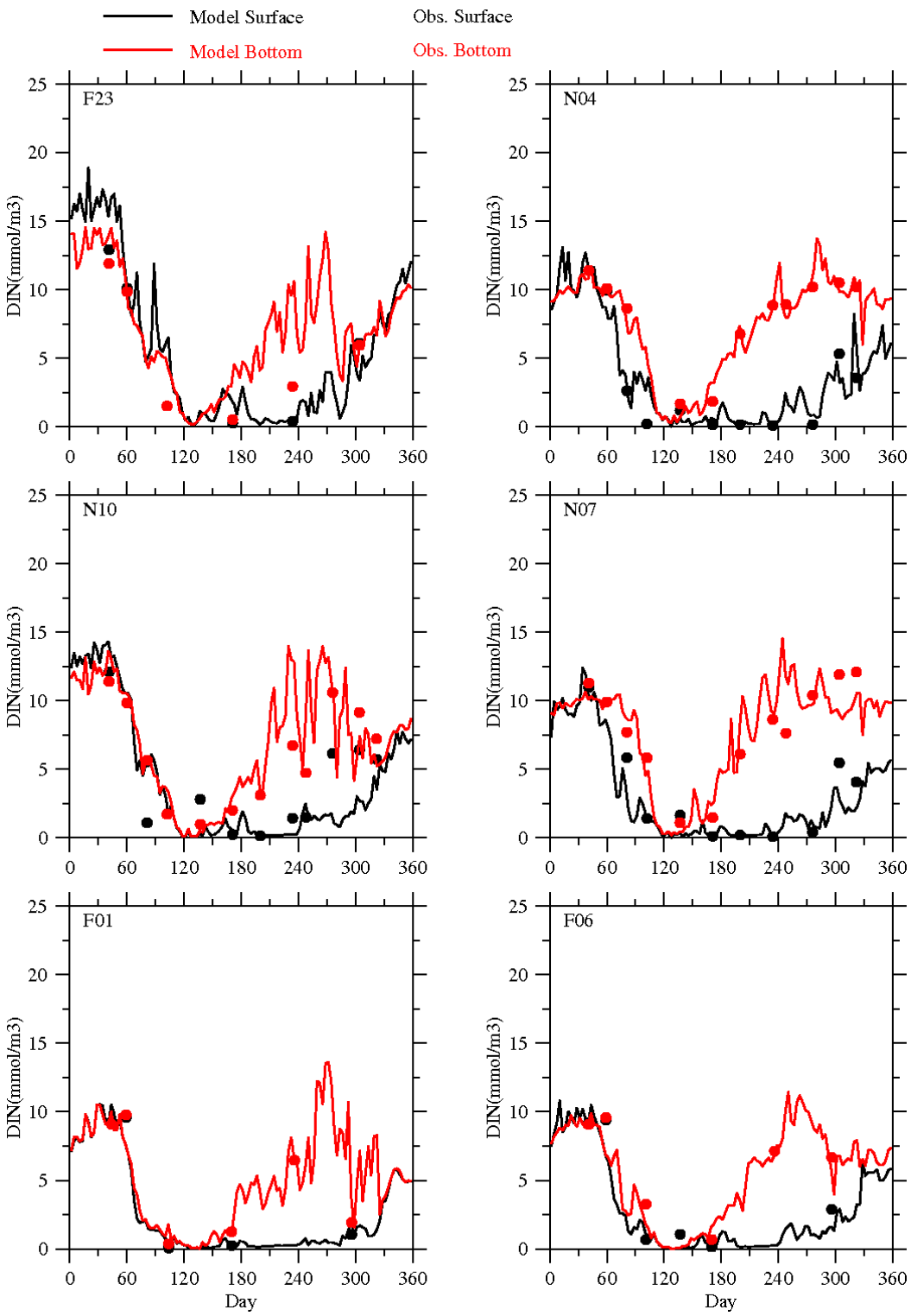

Figure 3.2 Comparison of observed (dots) and modeled (lines) time-series data of DIN at the MWRA monitoring stations in 2006.

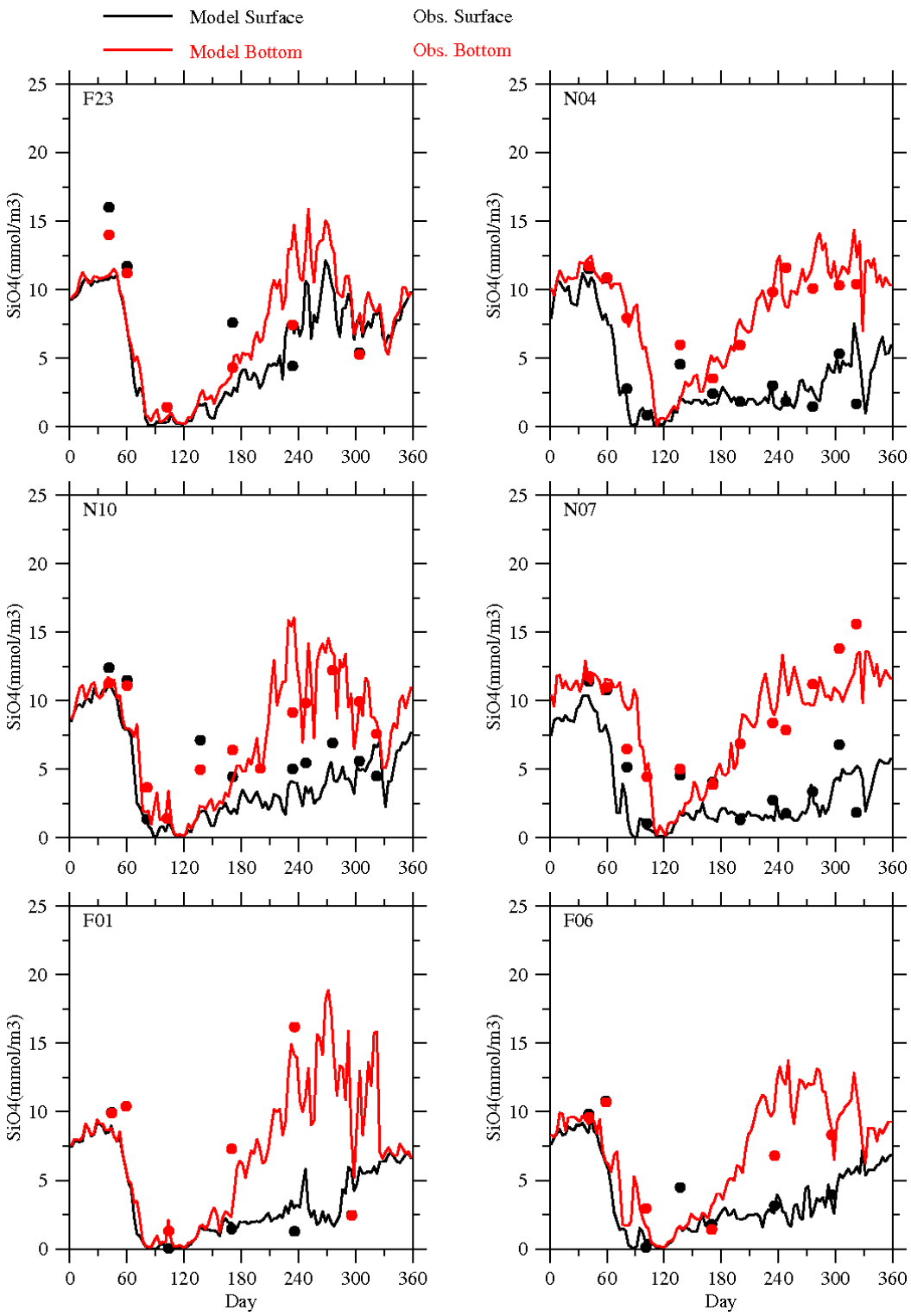

Figure 3.3 Comparison of observed (dots) and modeled (lines) time-series data of silicate at the MWRA monitoring stations in 2006.

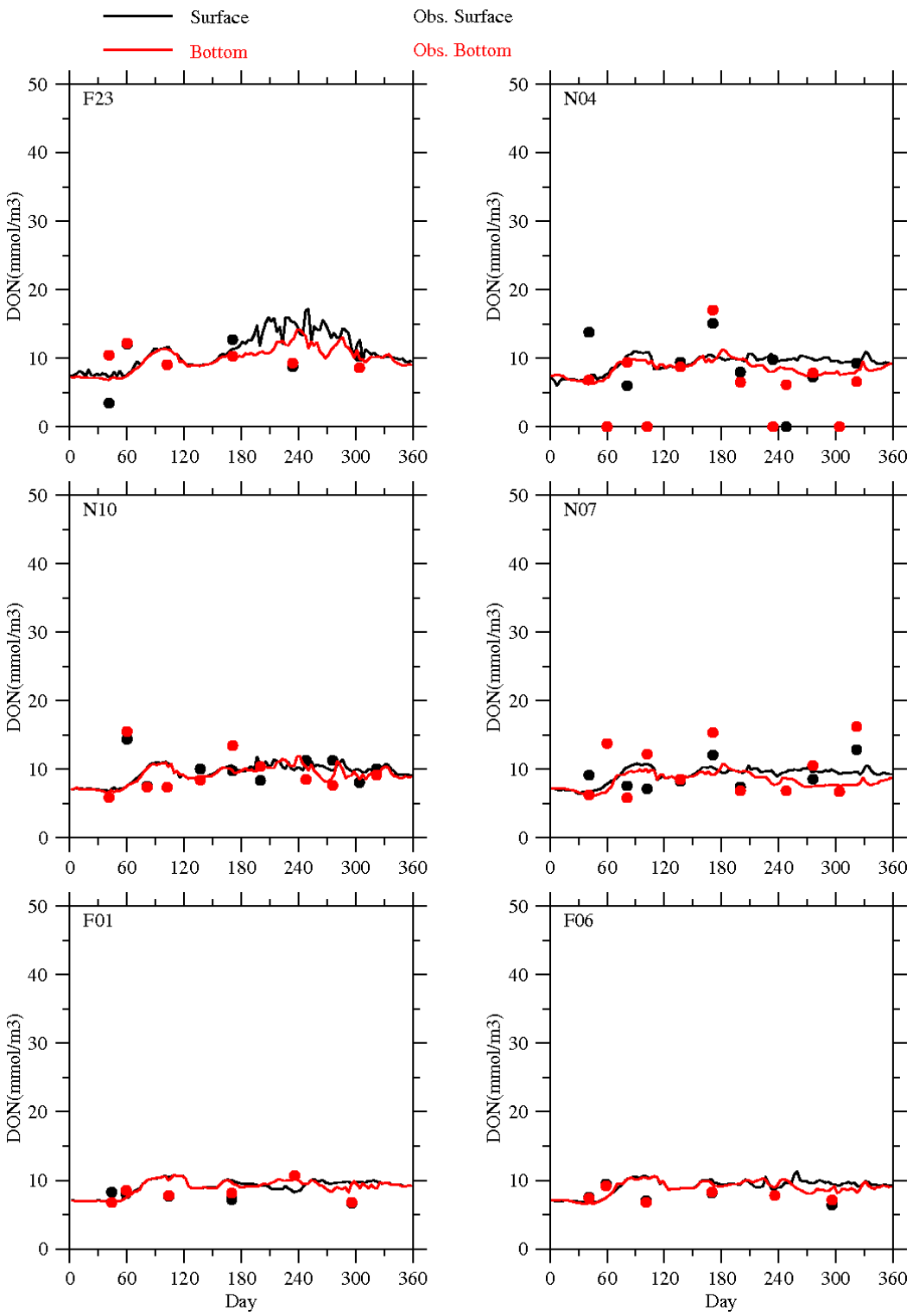

Figure 3.4 Comparison of observed (dots) and modeled (lines) time-series data of DON at the MWRA monitoring stations in 2006.

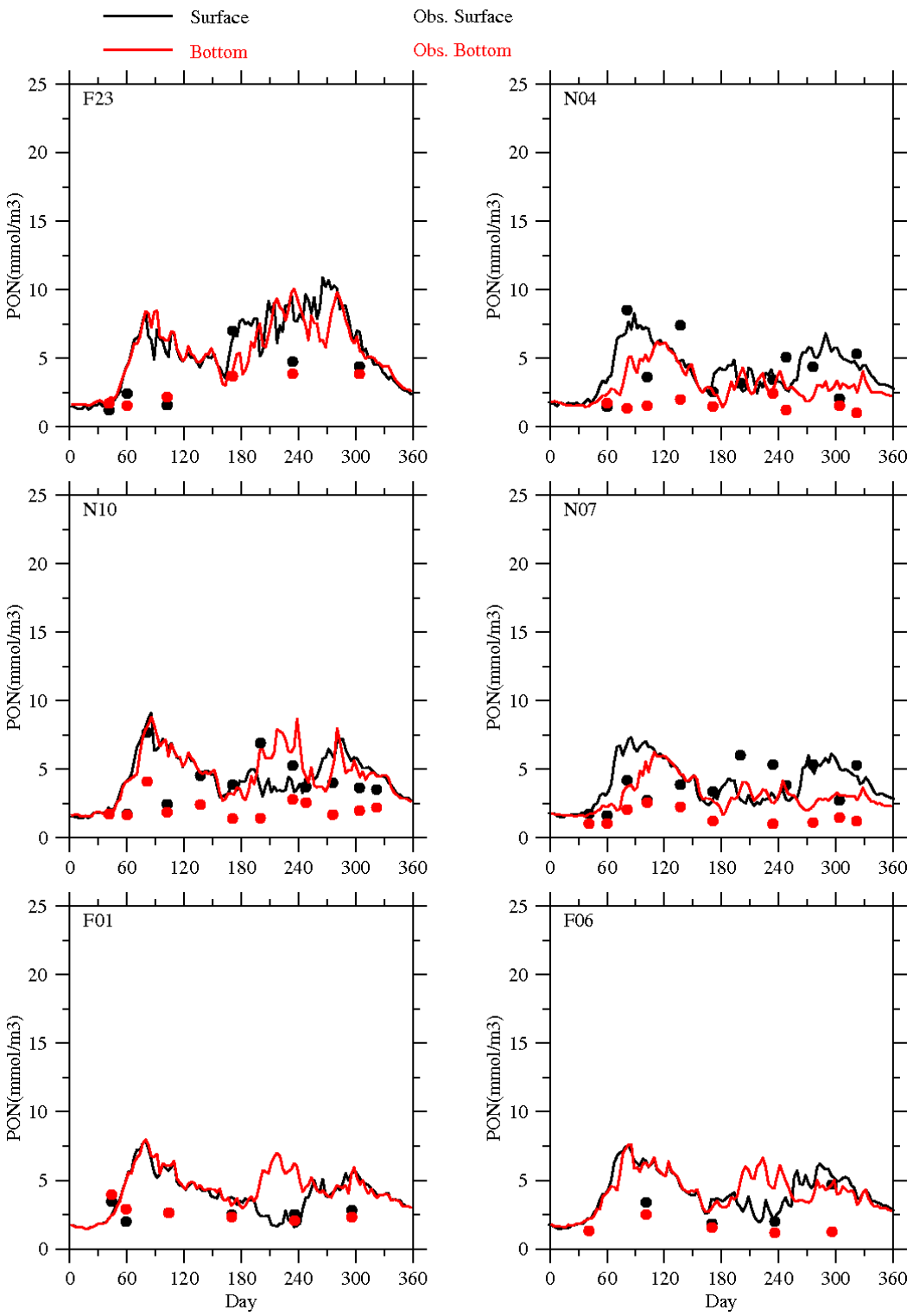

Figure 3.5 Comparison of observed (dots) and modeled (lines) time-series data of PON at the MWRA monitoring stations in 2006.

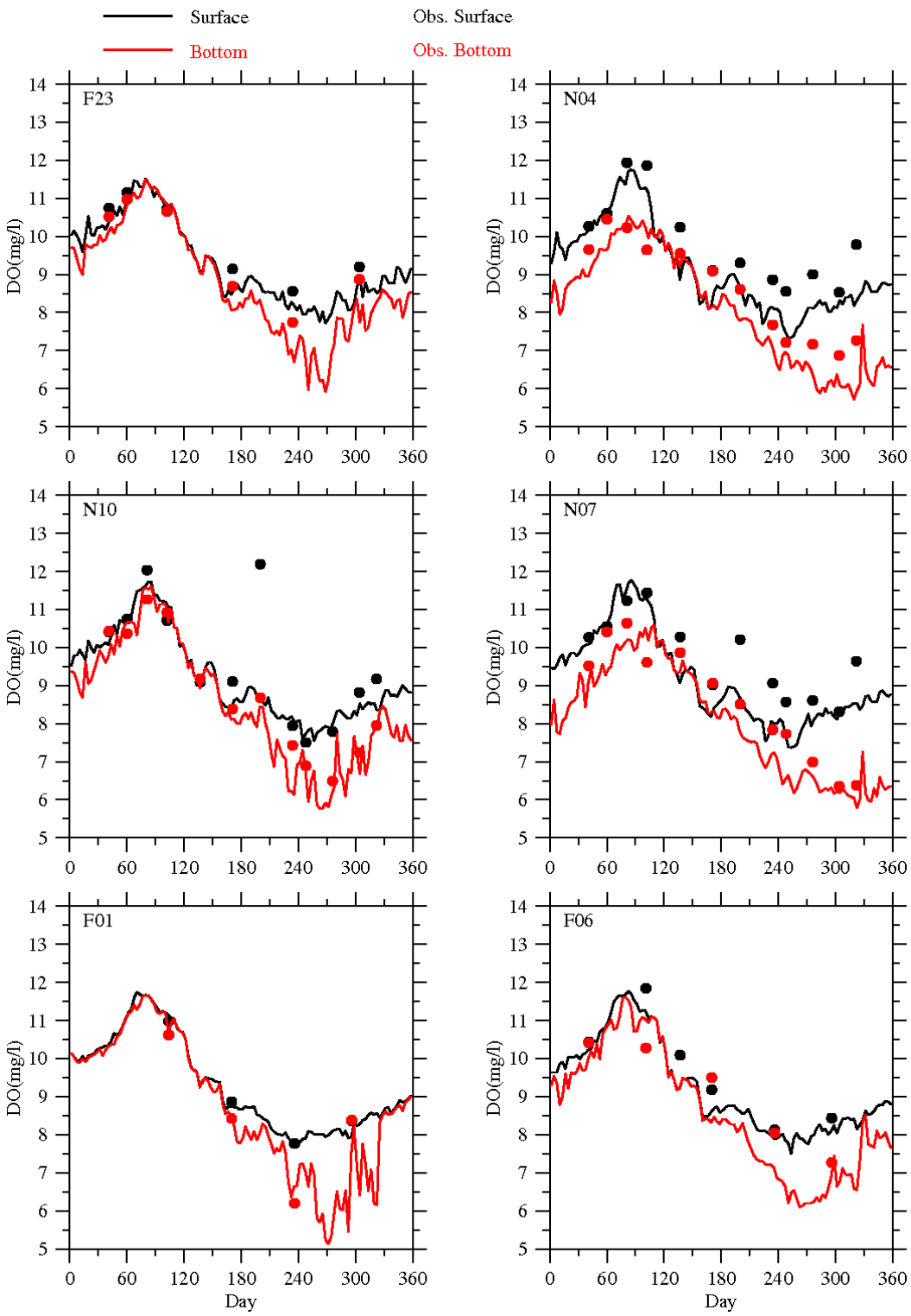

Figure 3.6 Comparison of observed (dots) and modeled (lines) time-series data of DO at the MWRA monitoring stations in 2006.

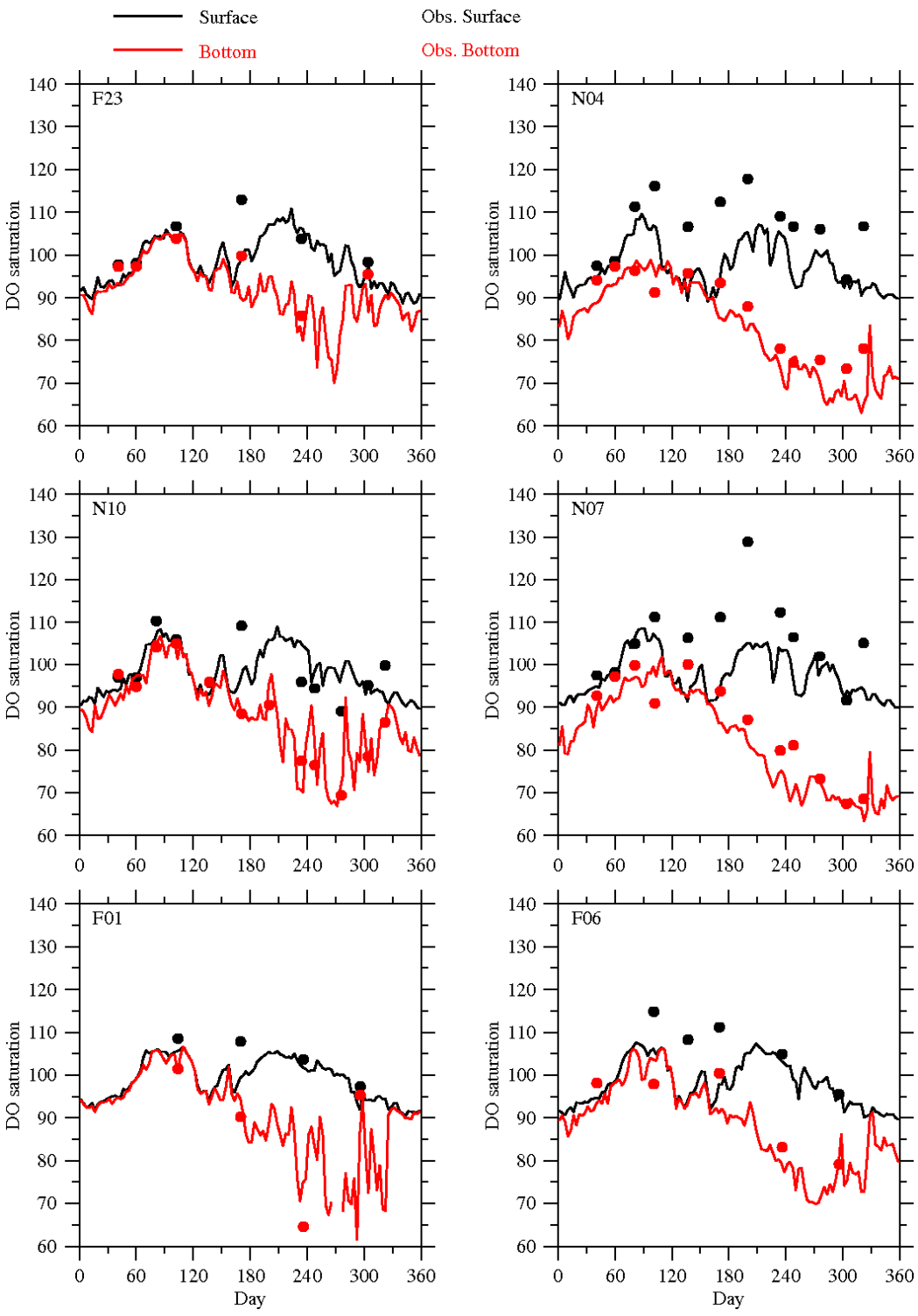

Figure 3.7 Comparison of observed (dots) and modeled (lines) time-series data of DO saturation at the MWRA monitoring stations in 2006.

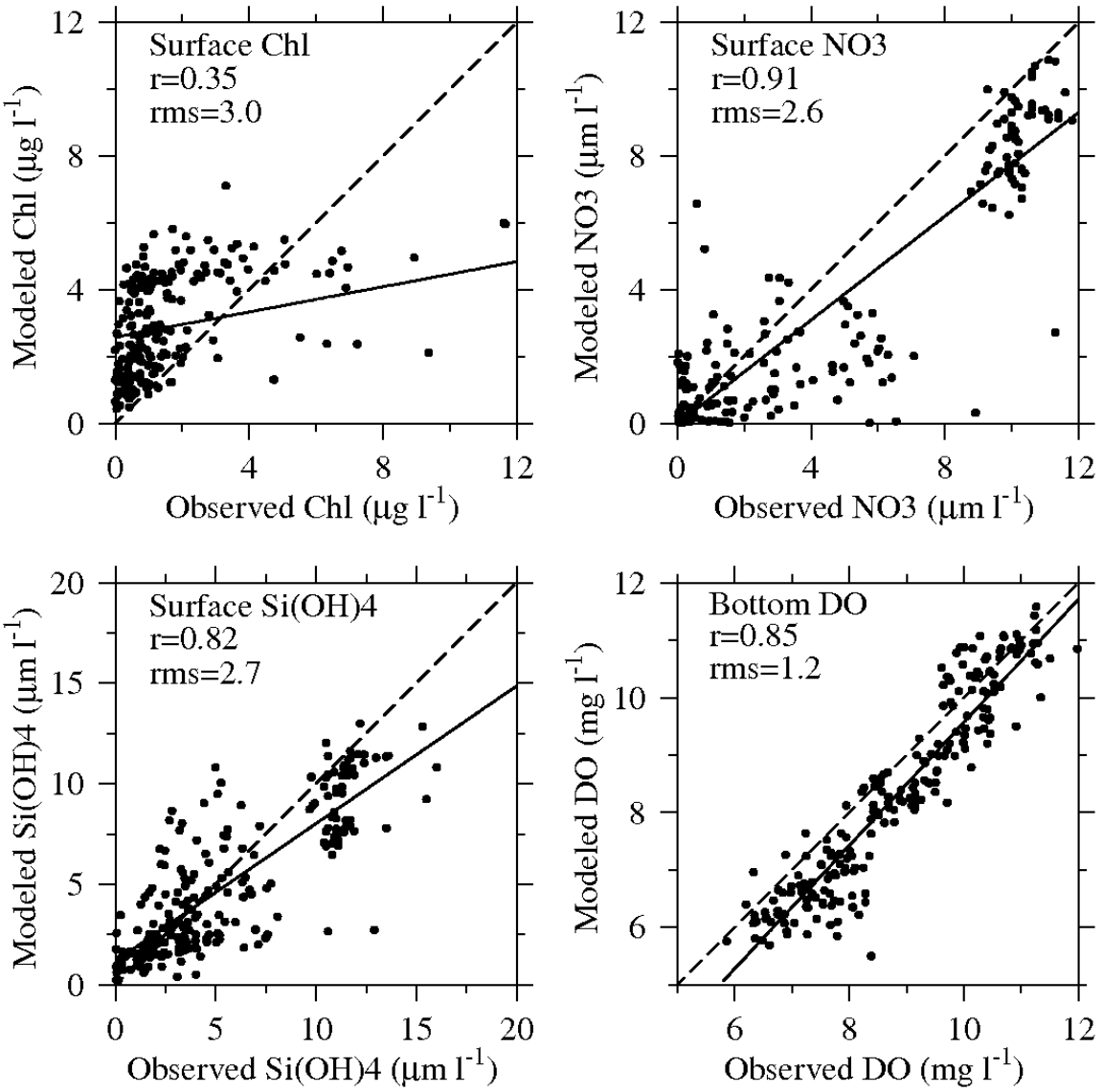

Figure 3.8 Overall correlation and regression (solid lines) between observed (abscissa) and modeled (ordinate) results of key parameters in 2006: Chlorophyll, NO_3^-, $Si(OH)_4$ in surface waters and DO in the bottom layer. The dashed lines indicate a 1:1 relationship between observed and modeled results.

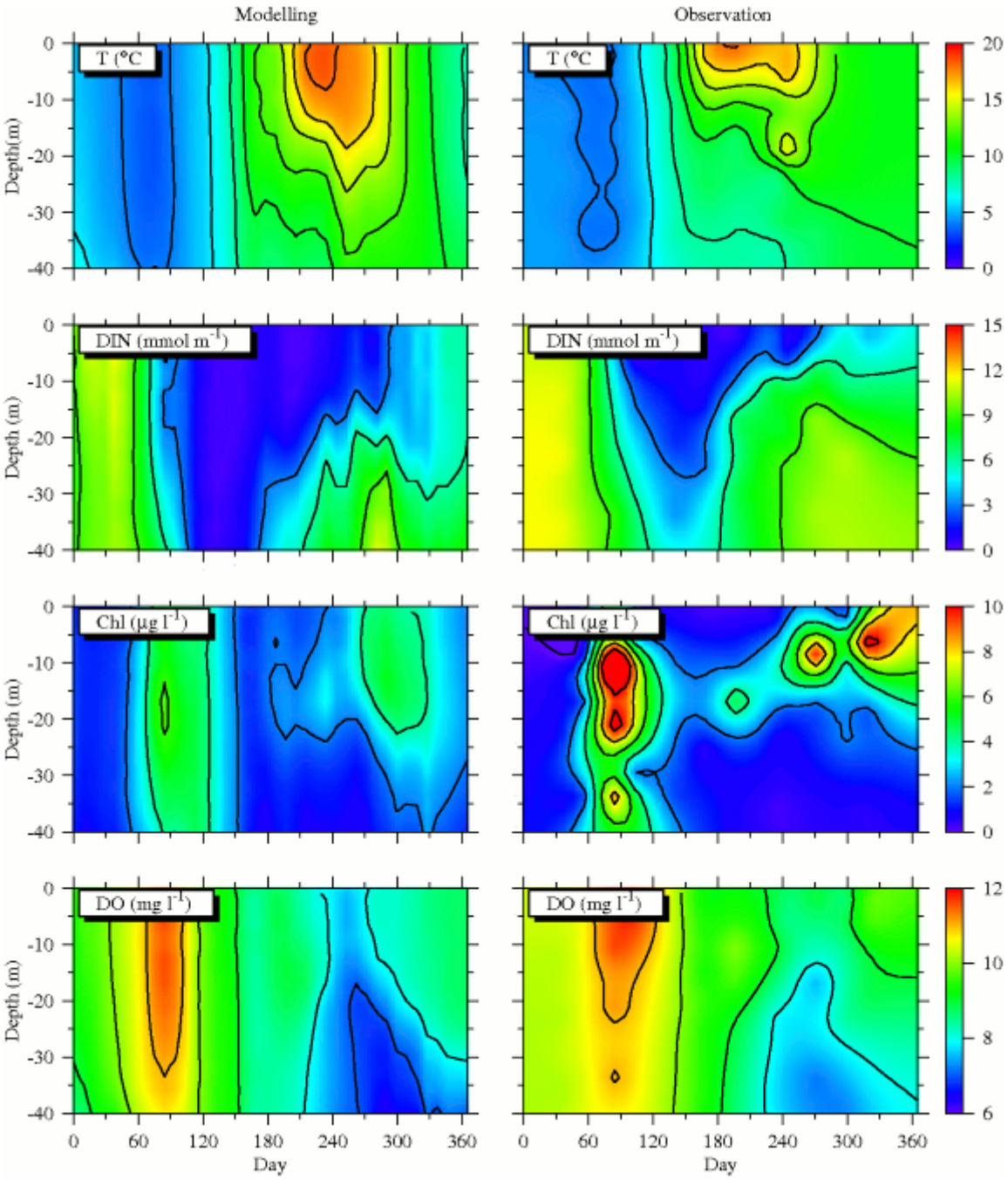

Figure 3.9 Time-series data of modeled (left panels) and observed (right panels) key parameters (T, DIN, Chl and DO) in the water column at the near-field station N04 in 2006.

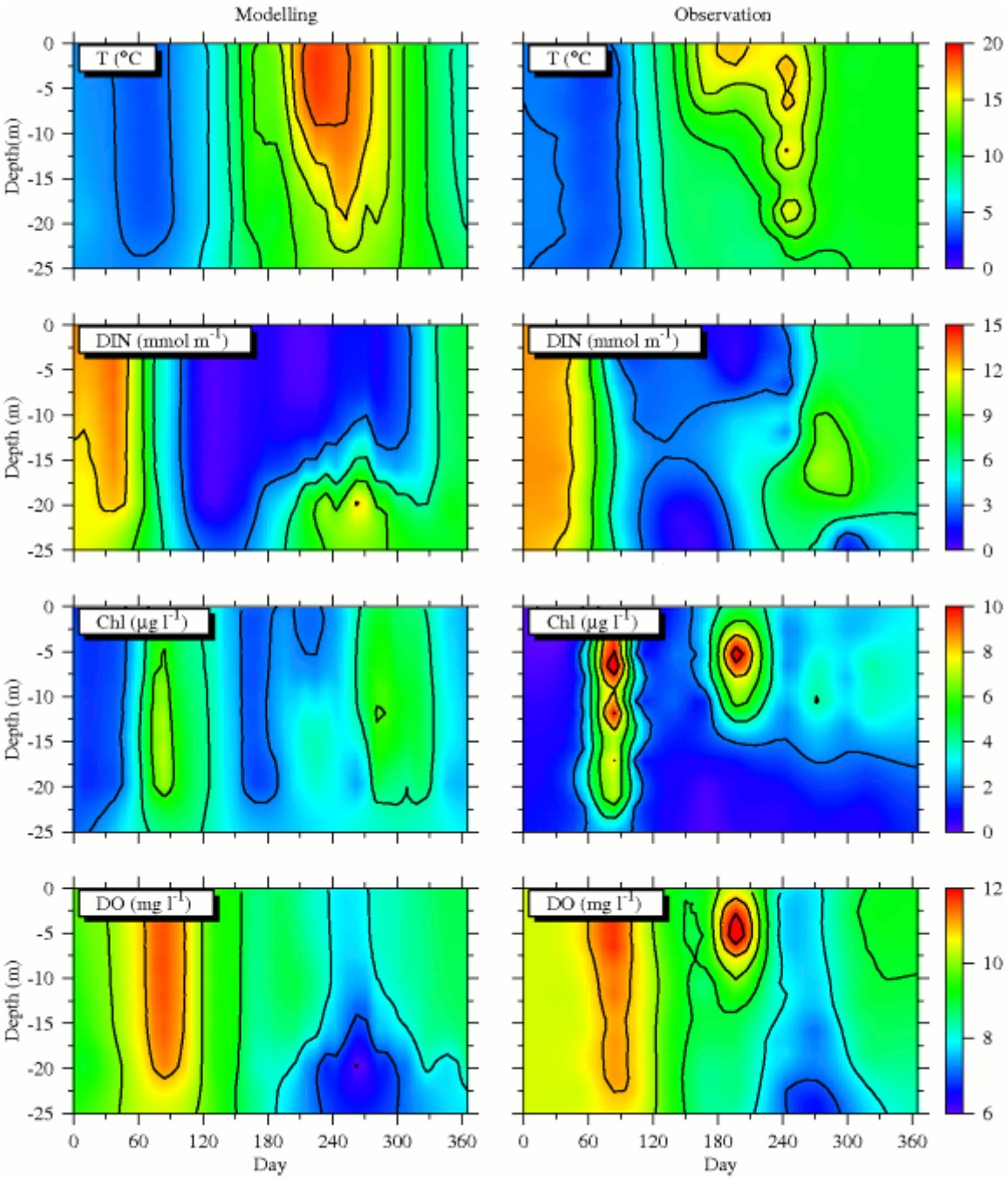

Figure 3.10 Time-series data of modeled (left panels) and observed (right panels) key parameters (T, DIN, Chl and DO) in the water column at the near-field station N10 in 2006.

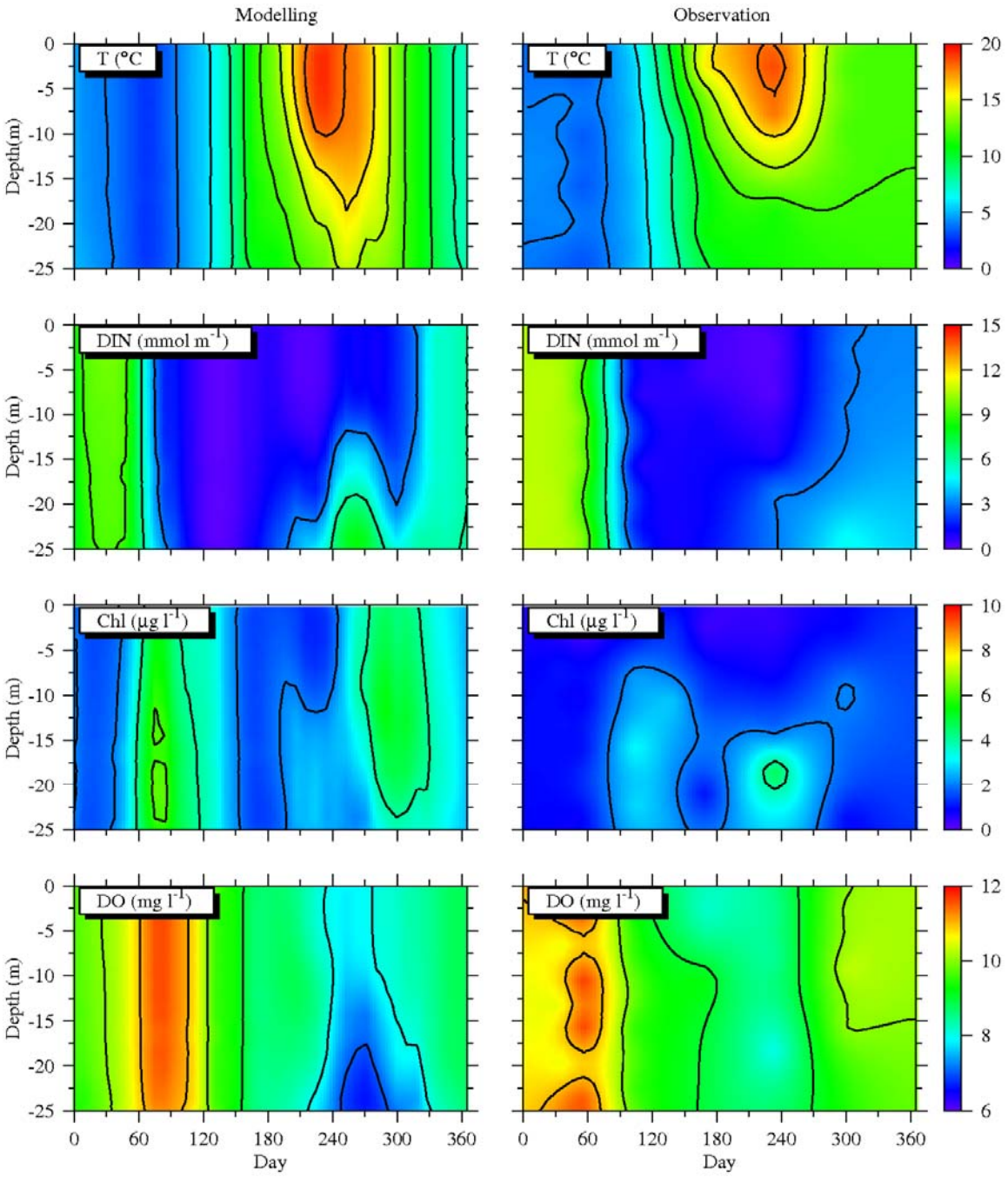

Figure 3.11 Time-series data of modeled (left panels) and observed (right panels) key parameters (T, DIN, Chl and DO) in the water column at the far-field station F06 in 2006.

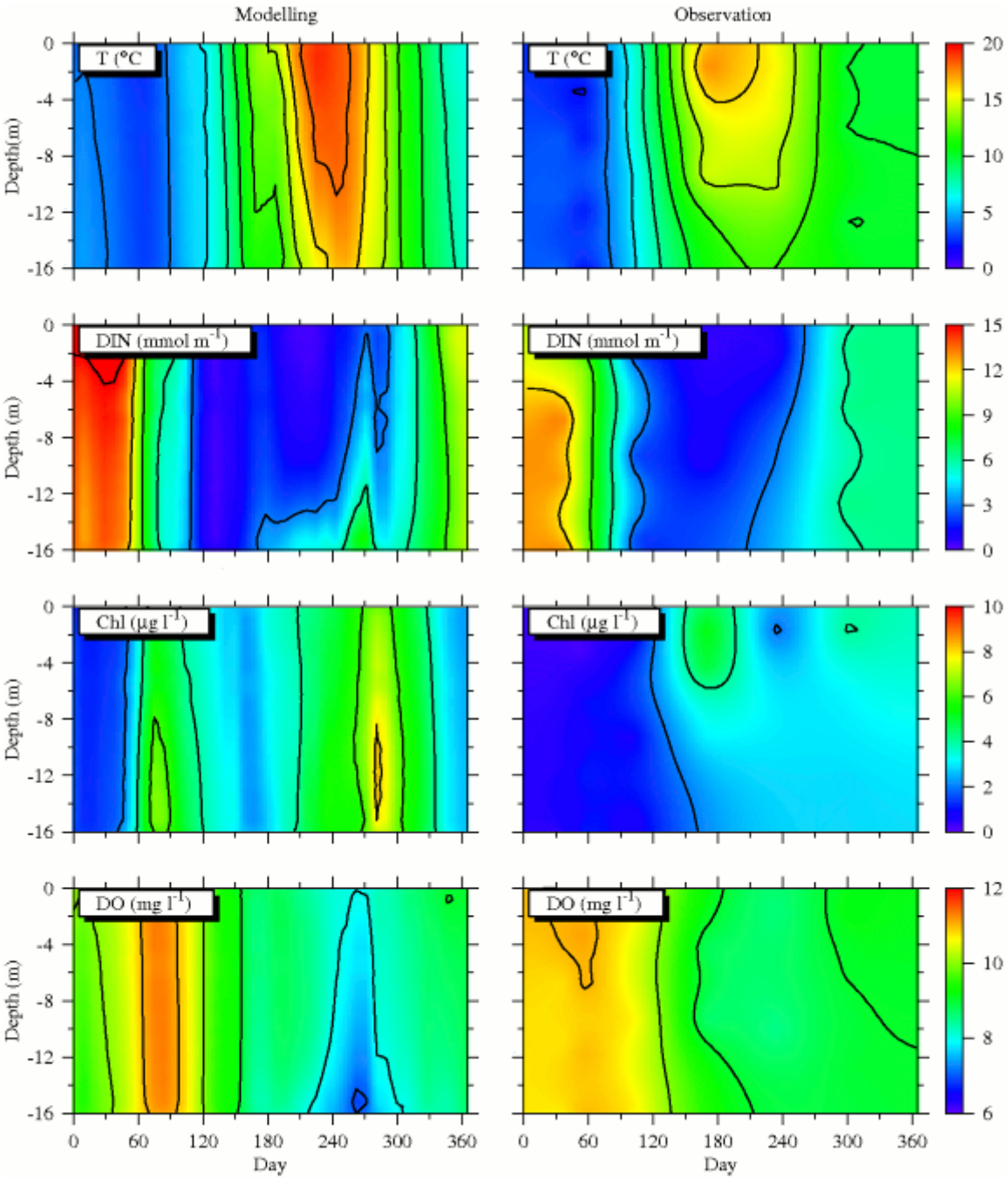

Figure 3.12 Time-series data of modeled (left panels) and observed (right panels) key parameters (T, DIN, Chl and DO) in the water column at the far-field station F23 in 2006.

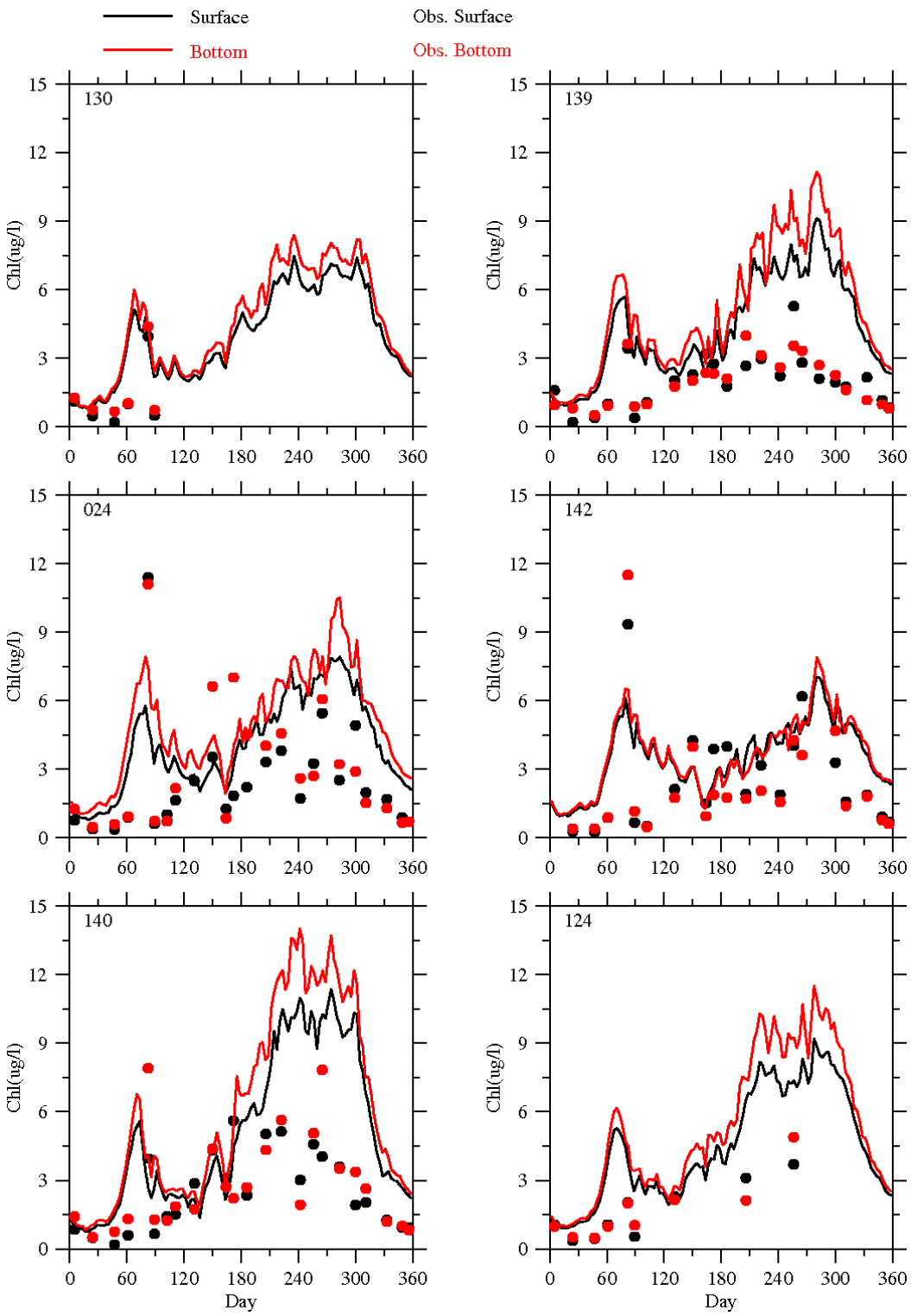

Figure 3.13 Comparison of observed (dots) and modeled (lines) time-series data of chlorophyll at the Boston Harbor monitoring stations in 2006.

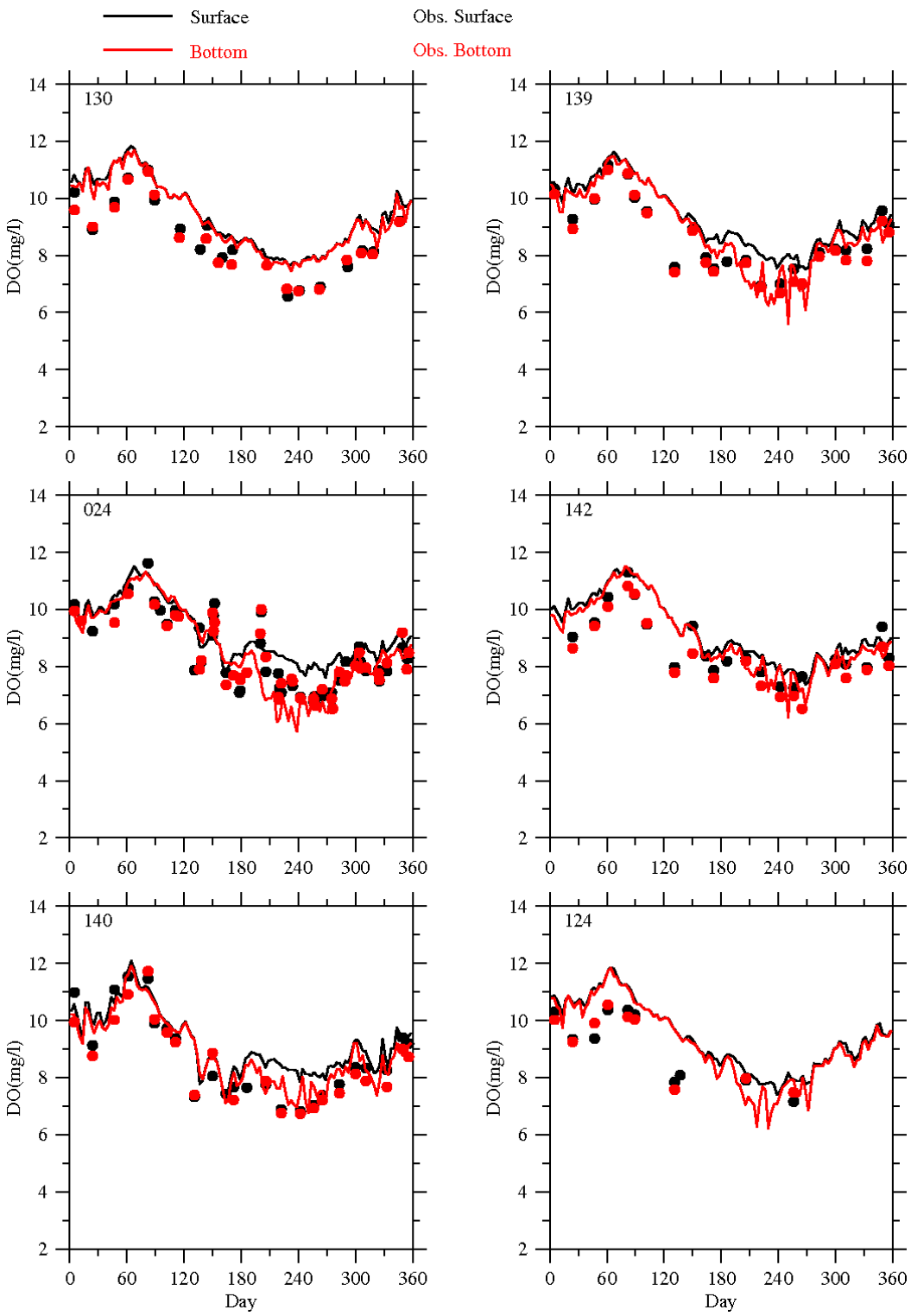

Figure 3.14 Comparison of observed (dots) and modeled (lines) time-series data of DO at the Boston Harbor monitoring stations in 2006.

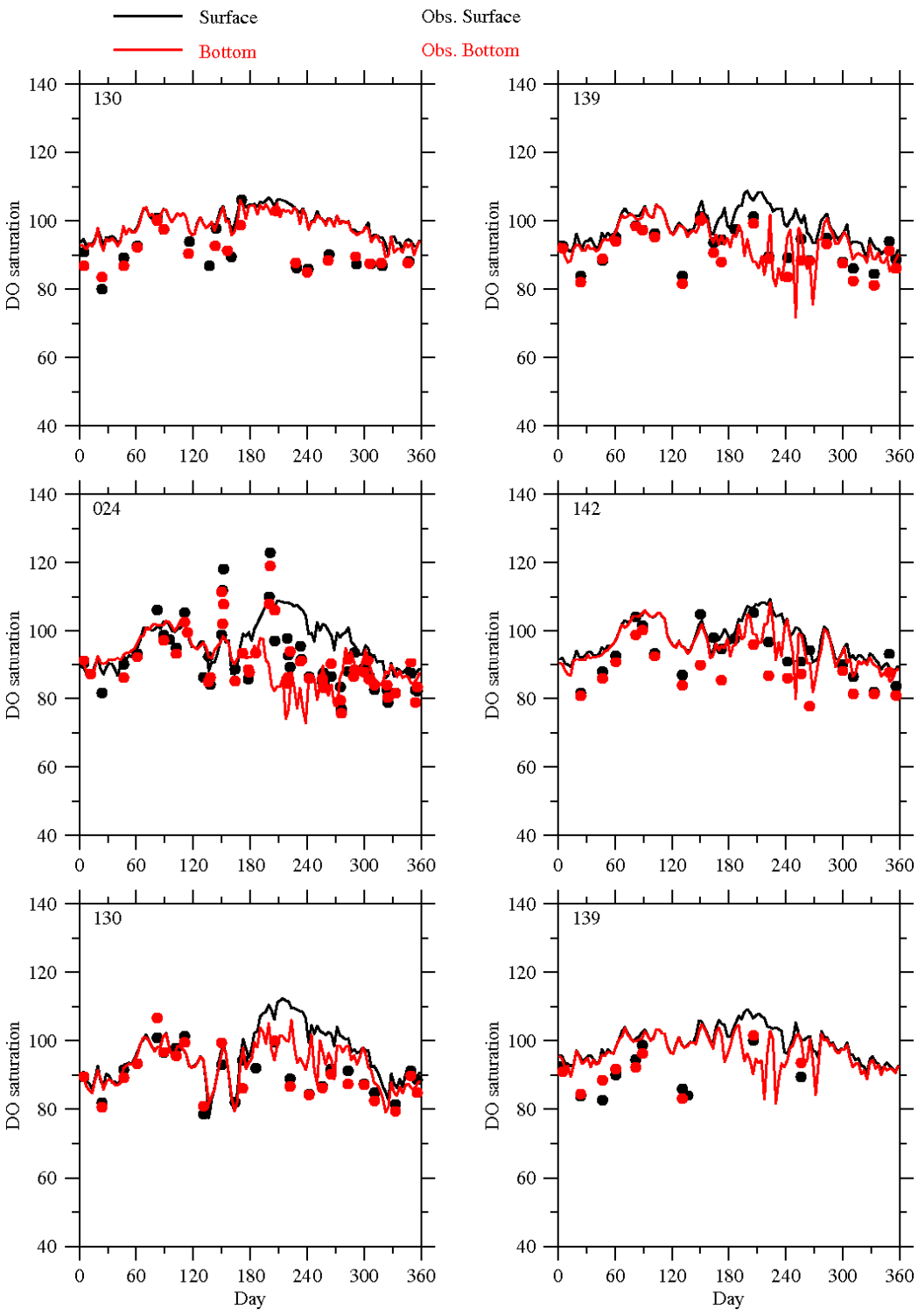

Figure 3.15 Comparison of observed (dots) and modeled (lines) time-series data of DO saturation at the Boston Harbor monitoring stations in 2006.

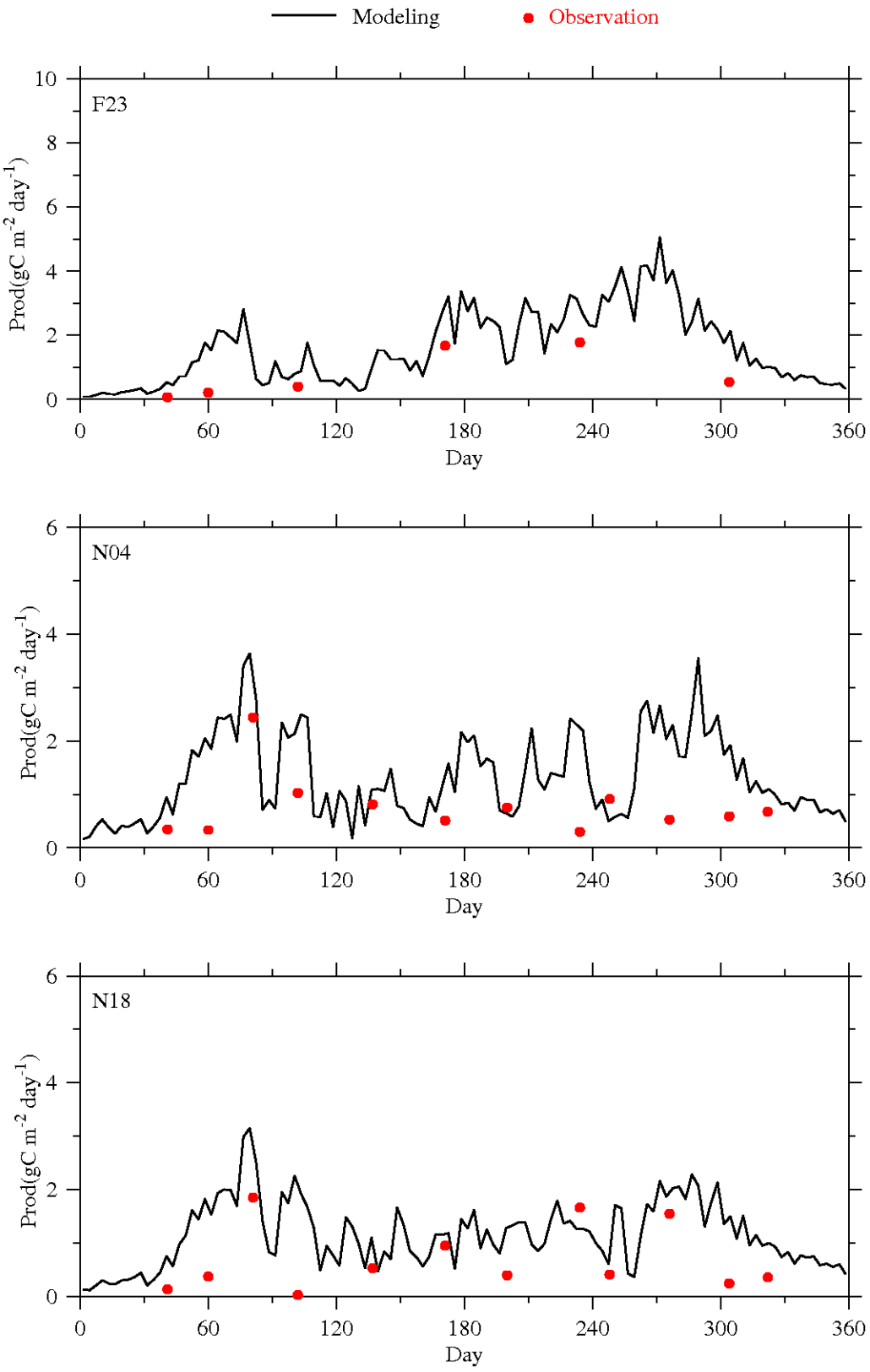

Figure 3.16 Comparison of observed (dots) and modeled (lines) time-series data of integrated primary production at MWRA monitoring stations in 2006.

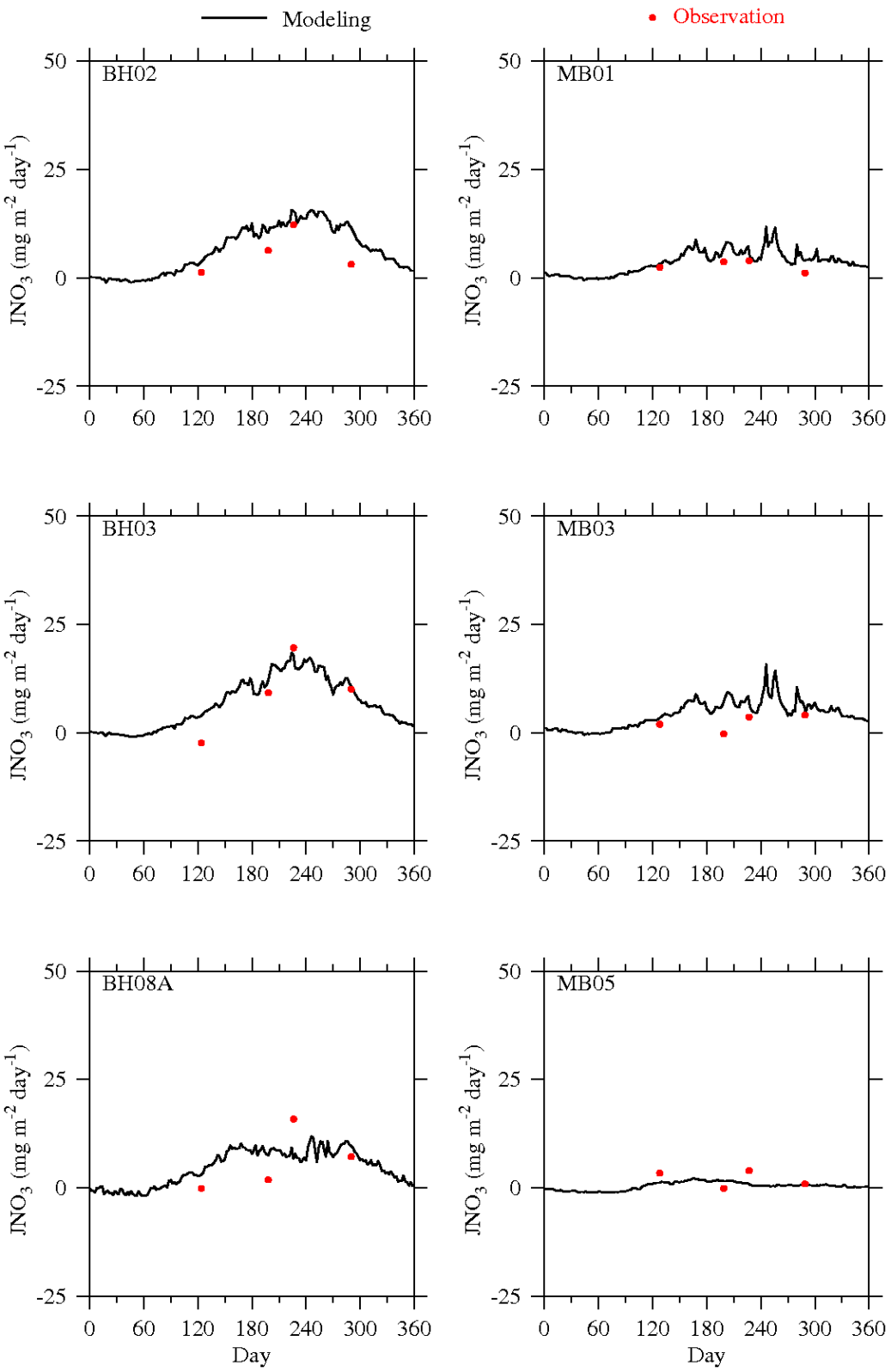

Figure 3.17 Comparison of observed (dots) and modeled (lines) time-series data of sediment NO_3^- flux at monitoring stations in 2006.

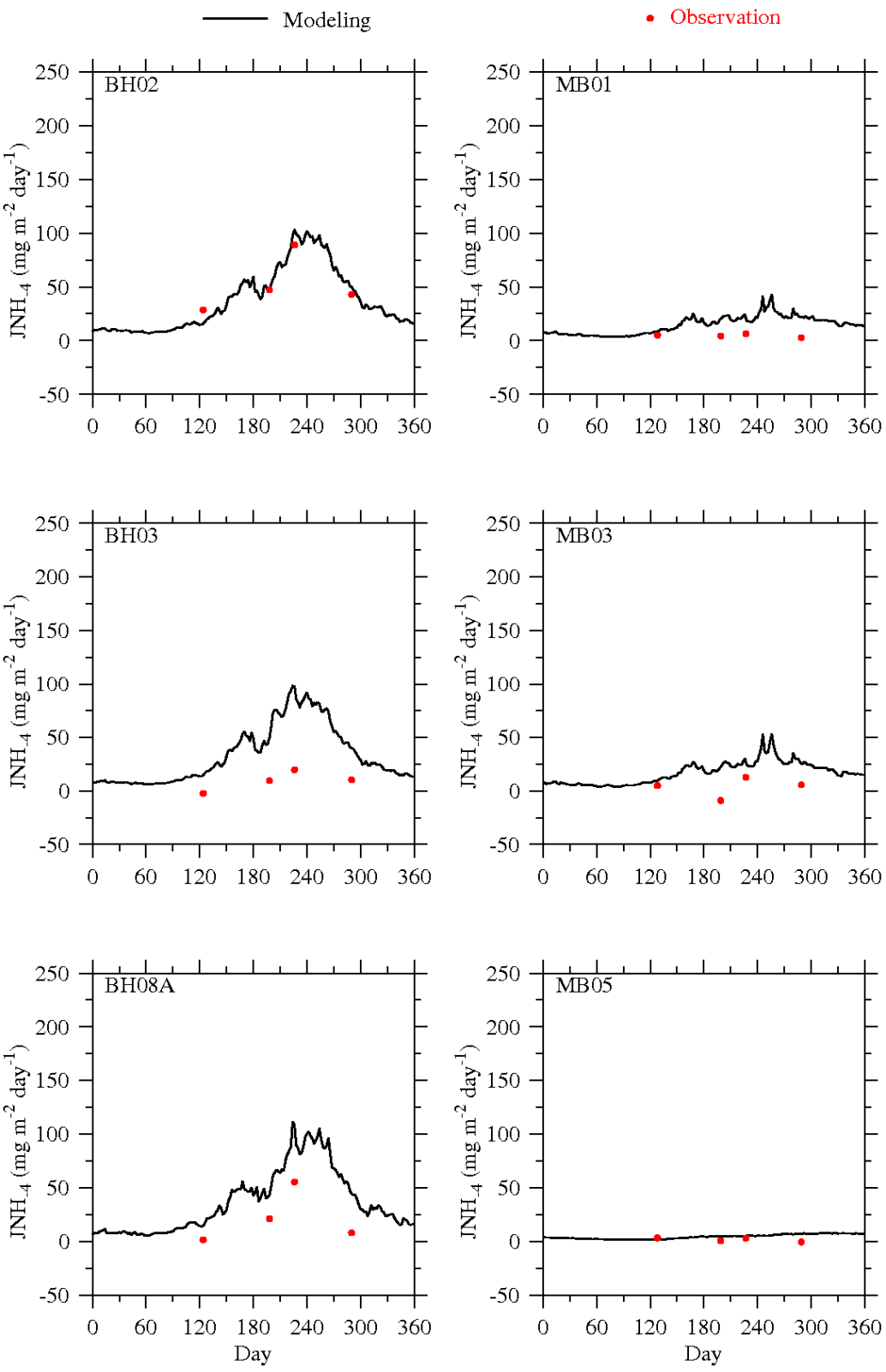

Figure 3.18 Comparison of observed (dots) and modeled (lines) time-series data of sediment NH_4^+ flux at monitoring stations in 2006.

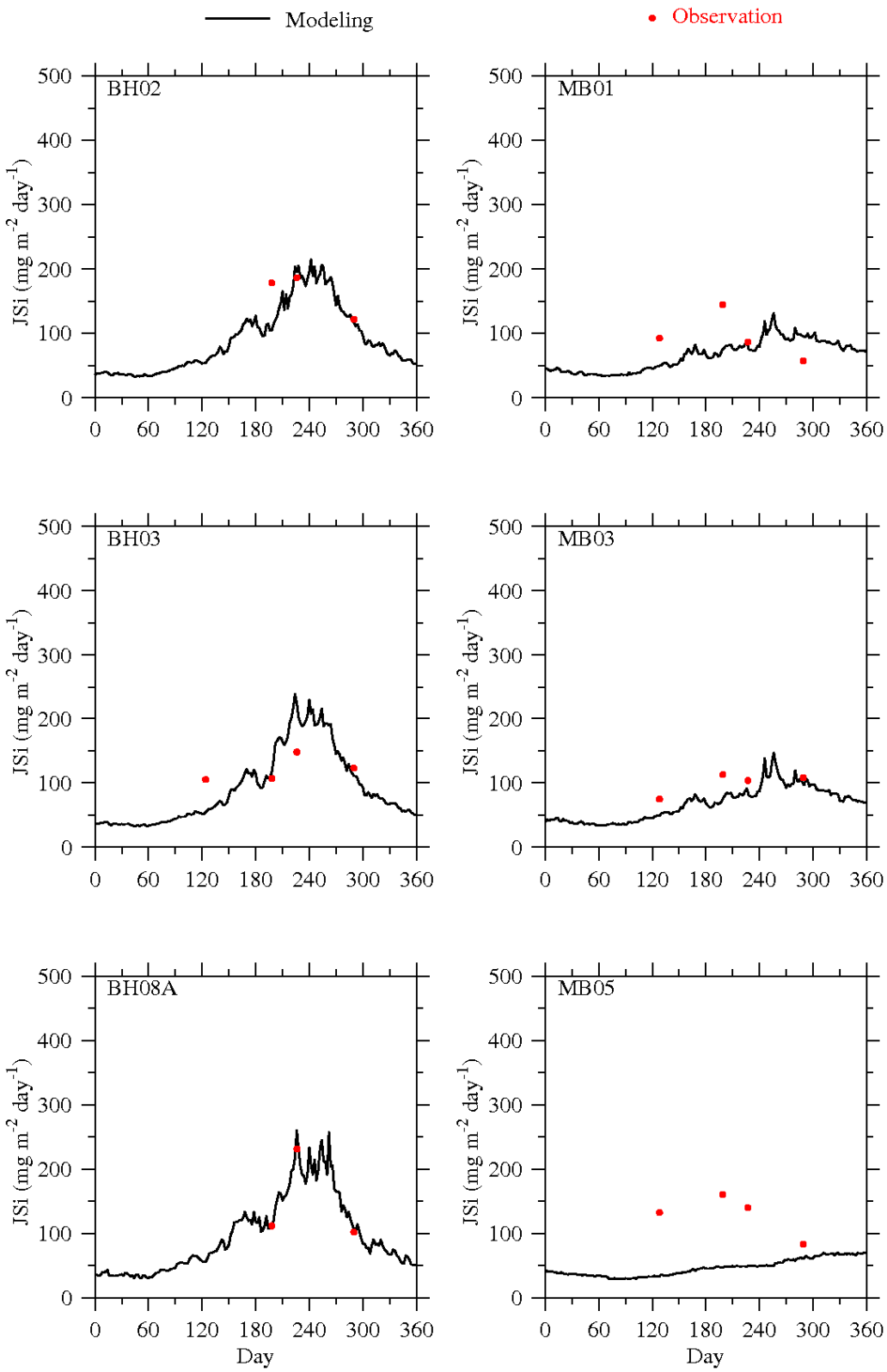

Figure 3.19 Comparison of observed (dots) and modeled (lines) time-series data of sediment $Si(OH)_4$ flux at monitoring stations in 2006.

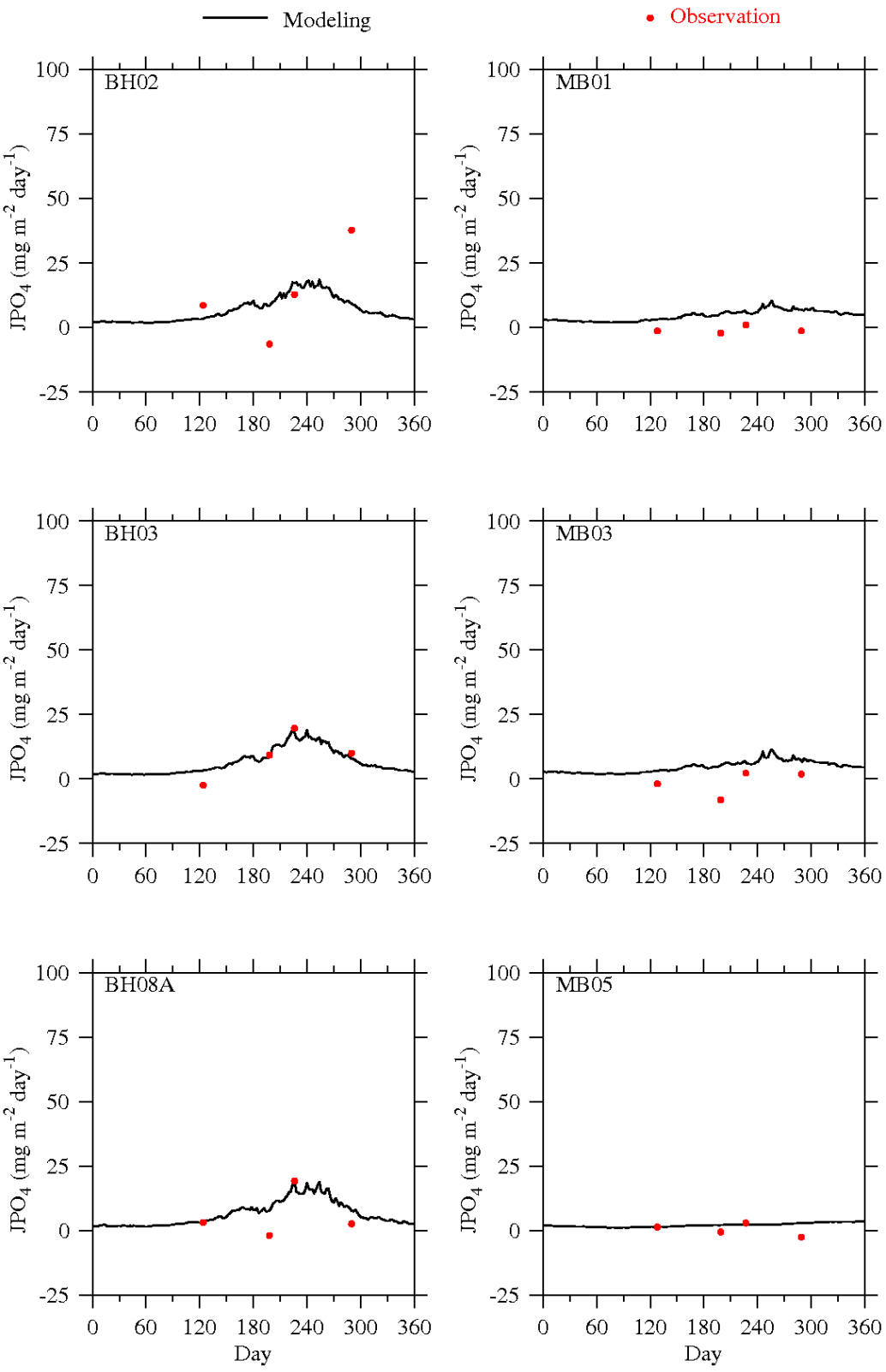

Figure 3.20 Comparison of observed (dots) and modeled (lines) time-series data of sediment PO_4^{3-} flux at monitoring stations in 2006.

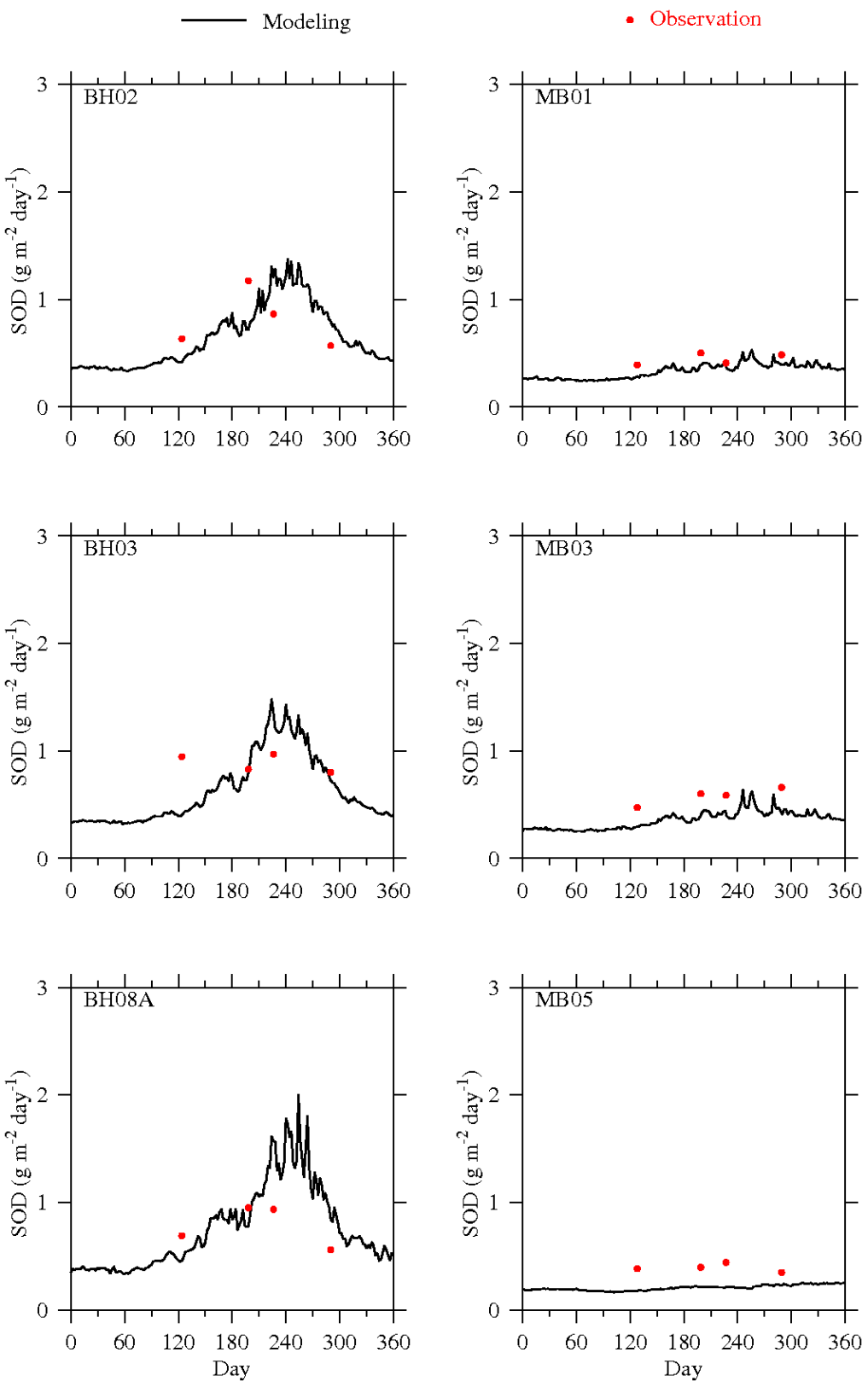

Figure 3.21 Comparison of observed (dots) and modeled (lines) time-series data of SOD at monitoring stations in 2006.

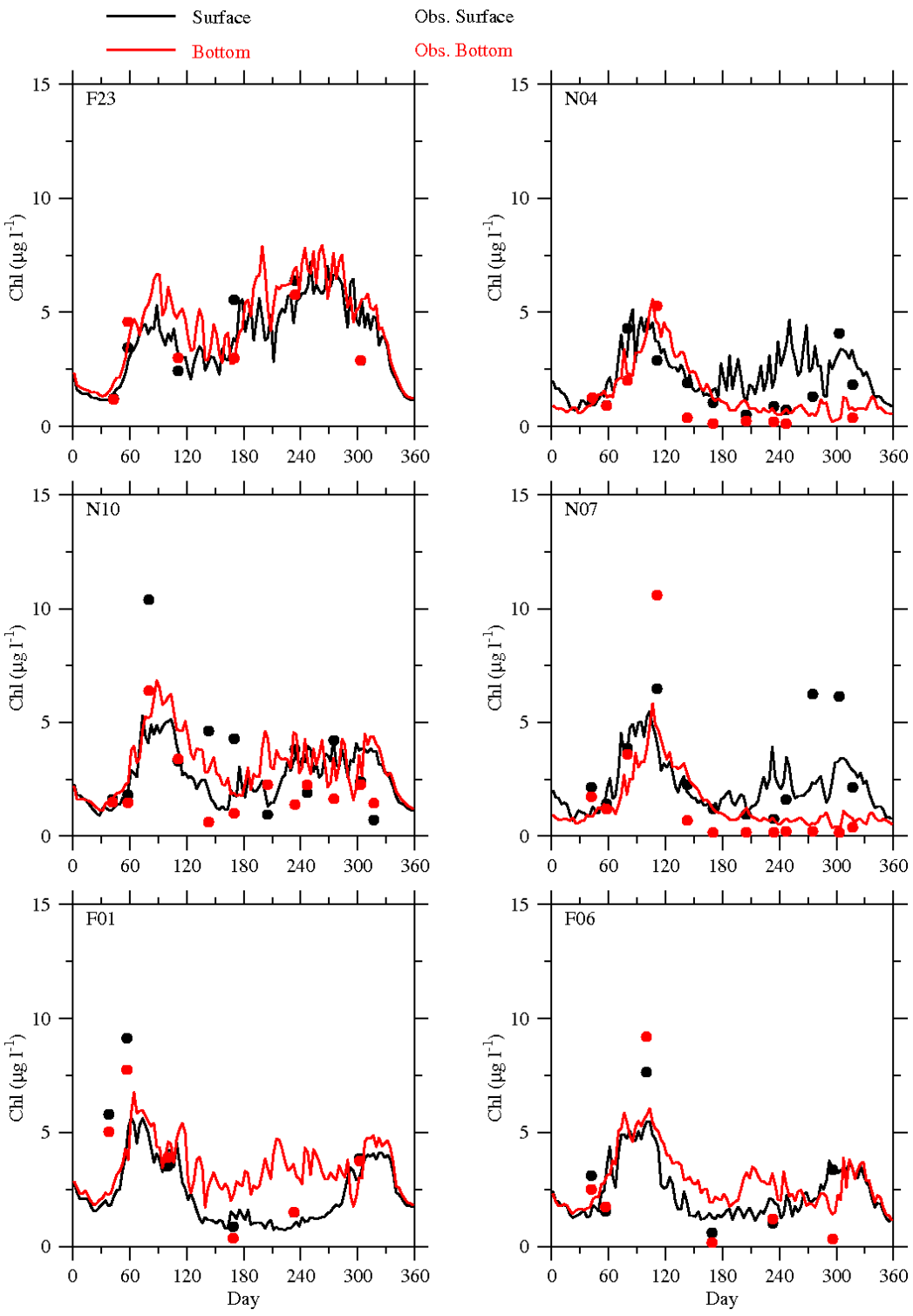

Figure 3.22 Comparison of observed (dots) and modeled (lines) time-series data of chlorophyll at the MWRA monitoring stations in 2007.

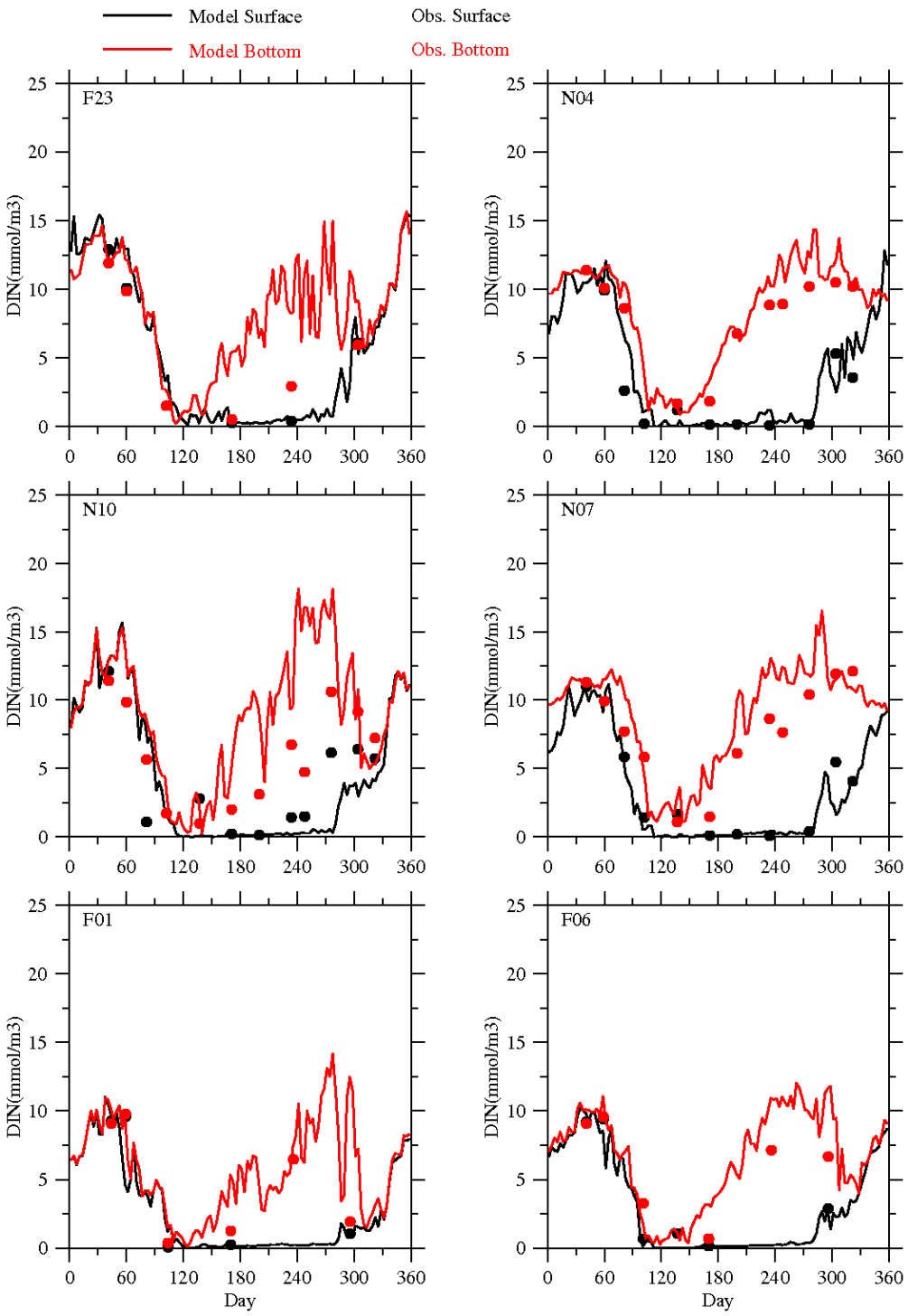

Figure 3.23 Comparison of observed (dots) and modeled (lines) time-series data of DIN at the MWRA monitoring stations in 2007.

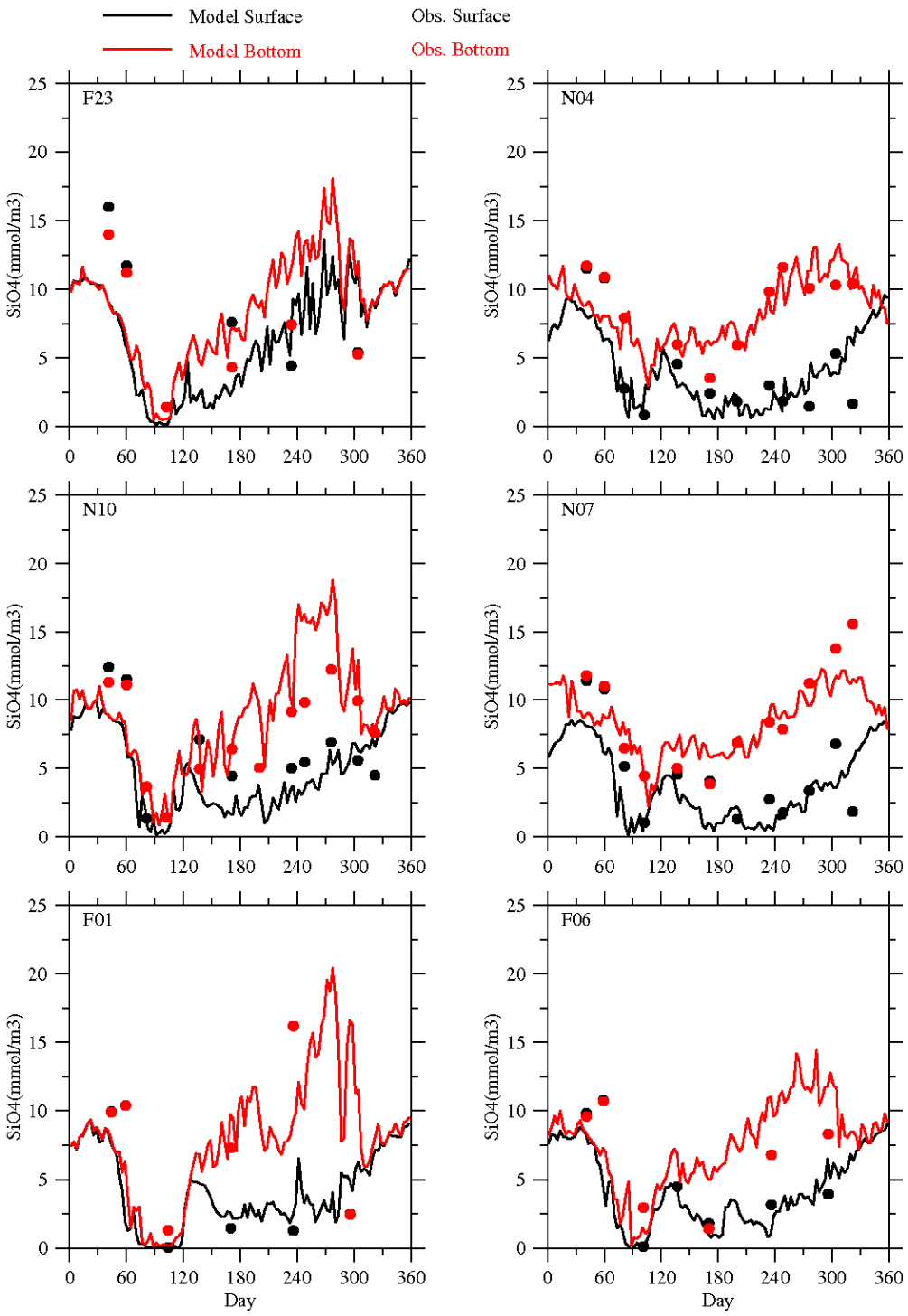

Figure 3.24 Comparison of observed (dots) and modeled (lines) time-series data of silicate at the MWRA monitoring stations in 2007.

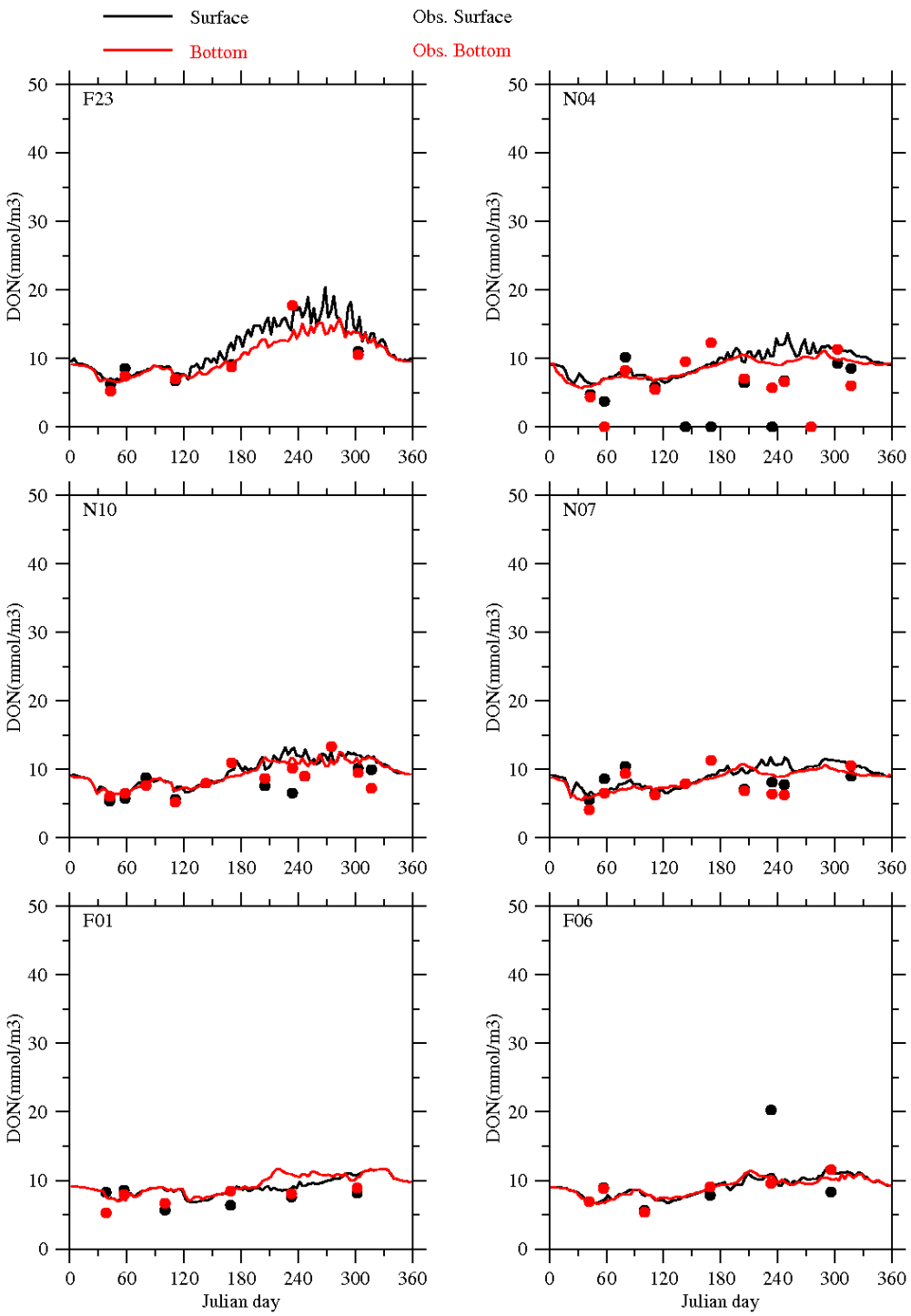

Figure 3.25 Comparison of observed (dots) and modeled (lines) time-series data of DON at the MWRA monitoring stations in 2007.

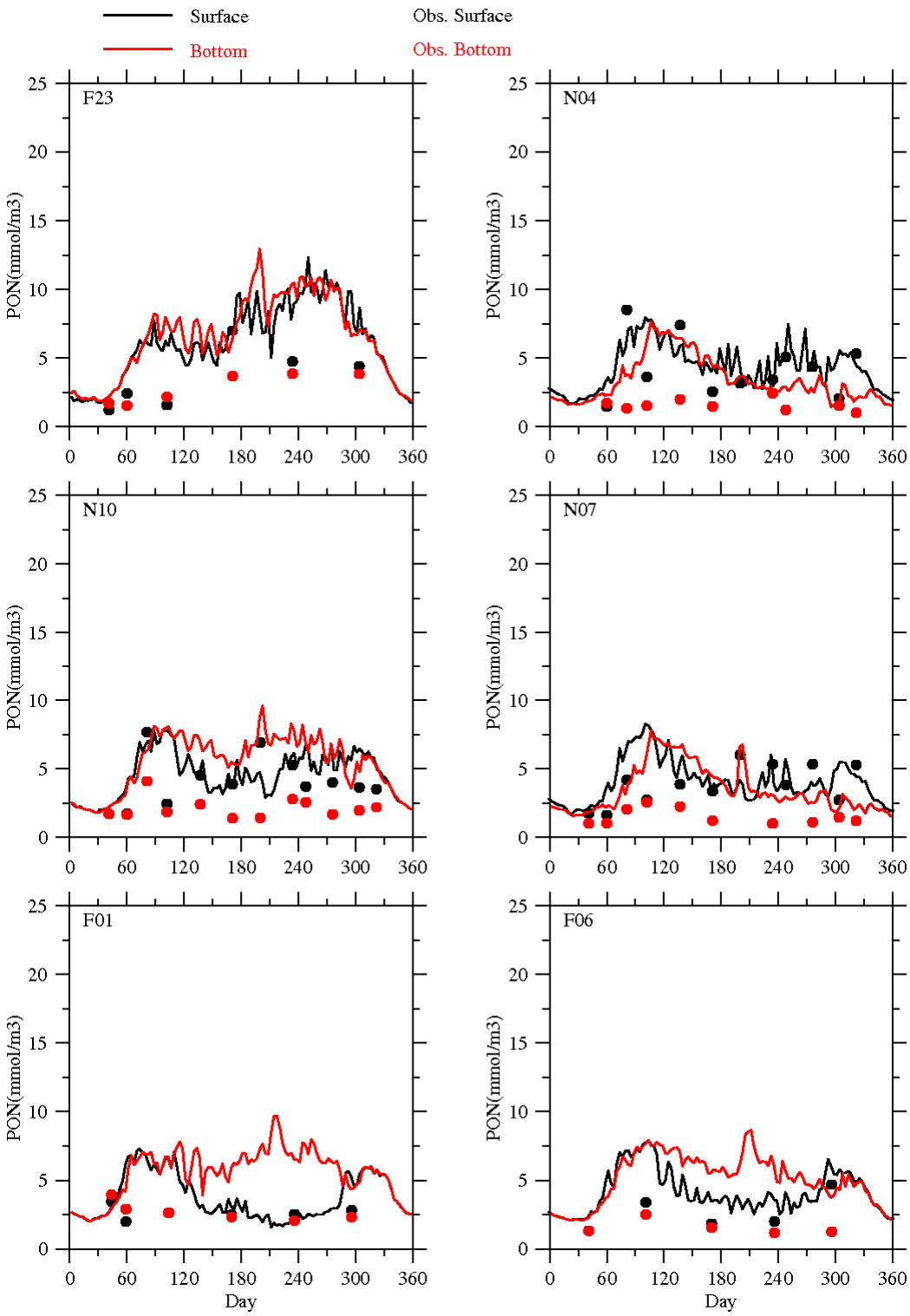

Figure 3.26 Comparison of observed (dots) and modeled (lines) time-series data of PON at the MWRA monitoring stations in 2007.

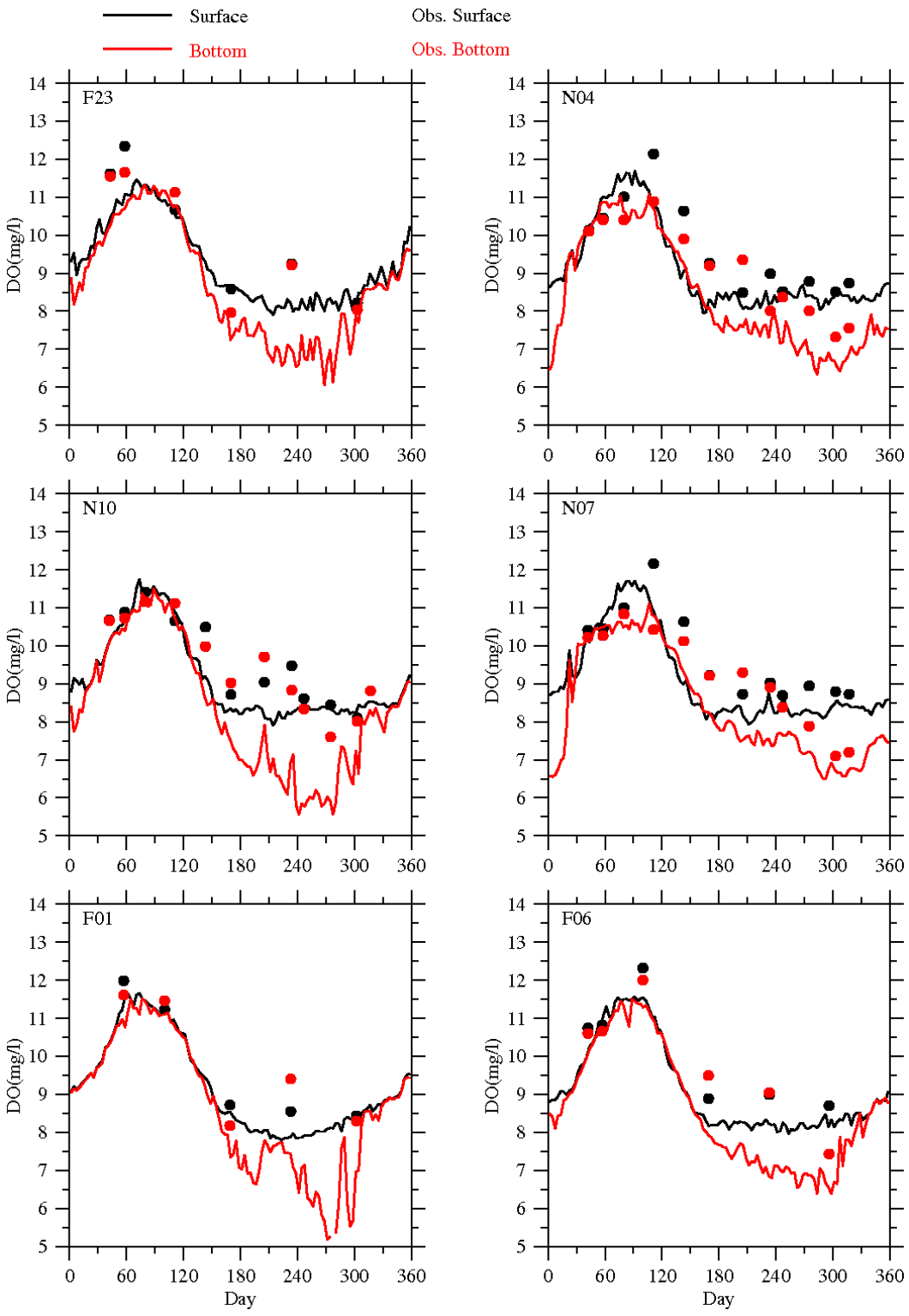

Figure 3.27 Comparison of observed (dots) and modeled (lines) time-series data of DO at the MWRA monitoring stations in 2007.

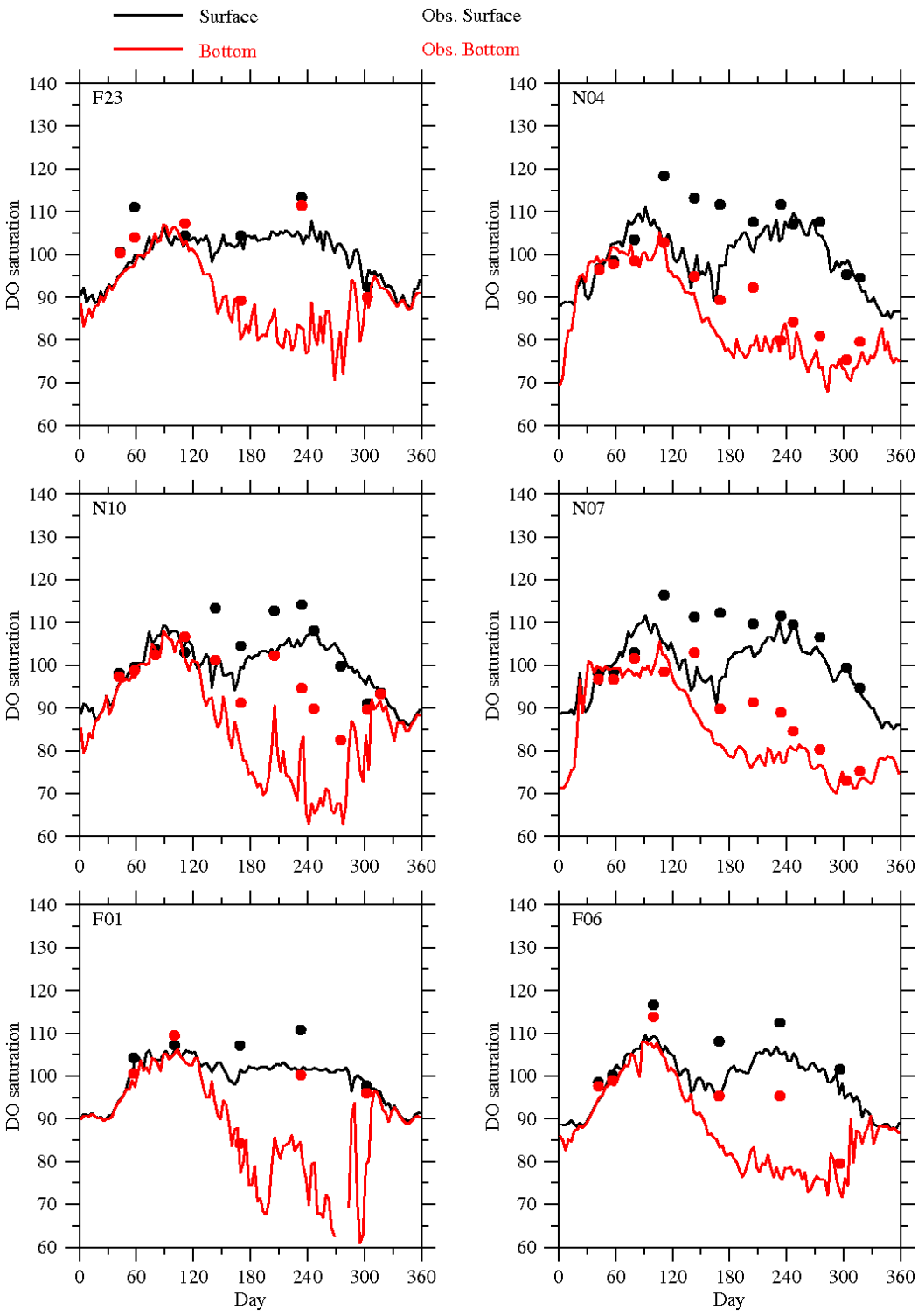

Figure 3.28 Comparison of observed (dots) and modeled (lines) time-series data of DO saturation at the MWRA monitoring stations in 2007.

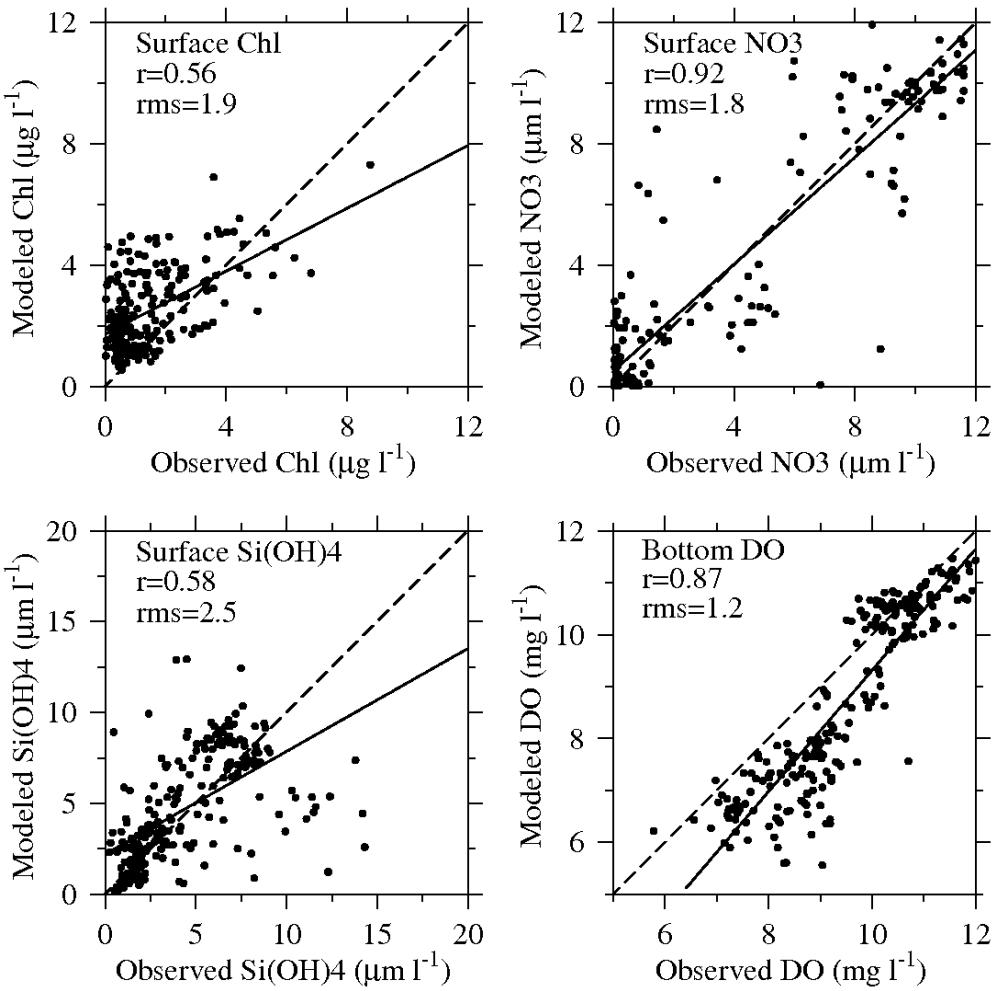

Figure 3.29 Overall correlation and regression (solid lines) between observed (abscissa) and modeled (ordinate) results of key parameters in 2007: Chlorophyll, NO_3^-, $Si(OH)_4$ in surface waters and DO in the bottom layer. The dashed lines indicate a 1:1 relationship between observed and modeled results.

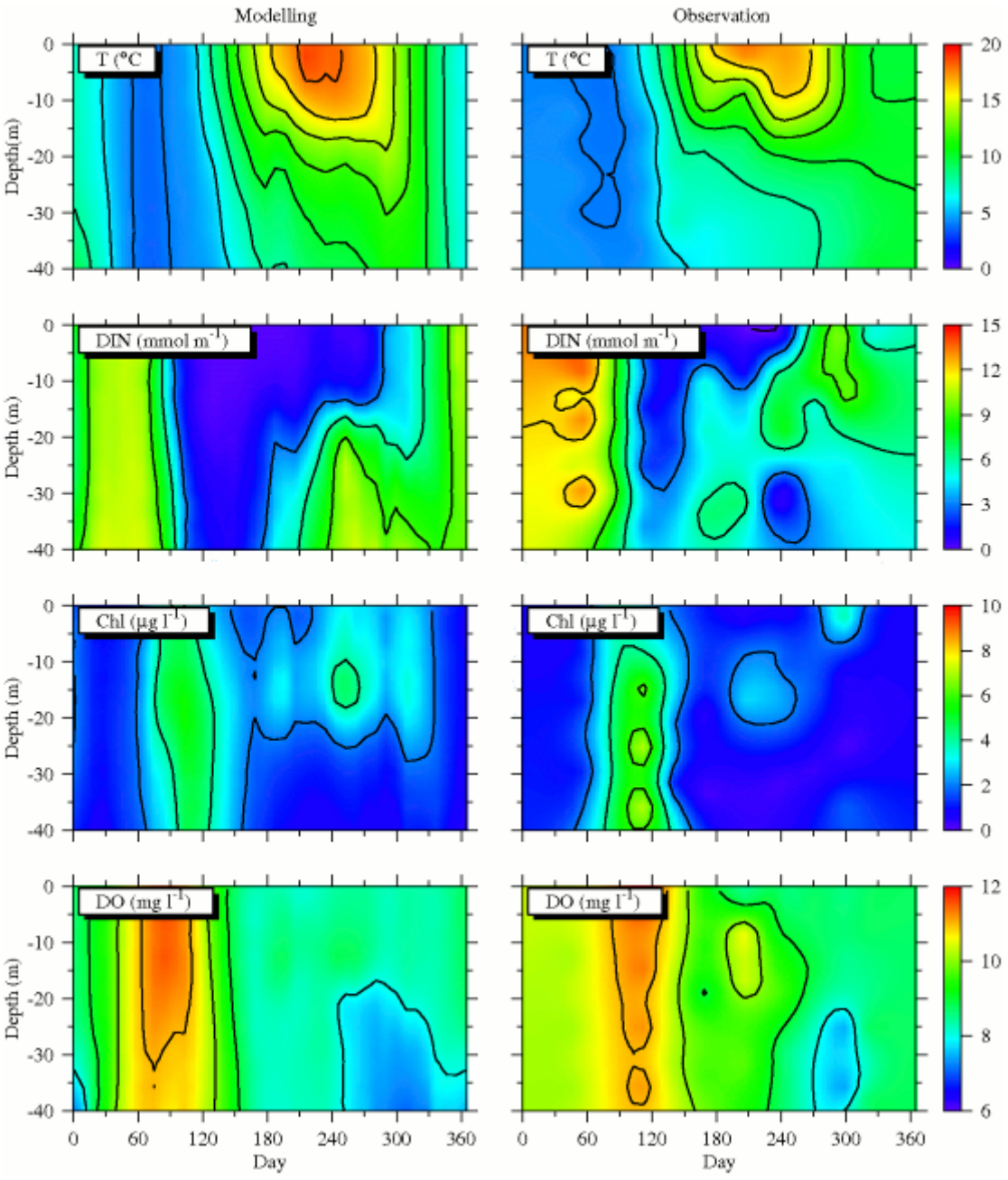

Figure 3.30 Time-series data of modeled (left panels) and observed (right panels) key parameters (T, DIN, Chl and DO) in the water column at the near-field station N04 in 2007.

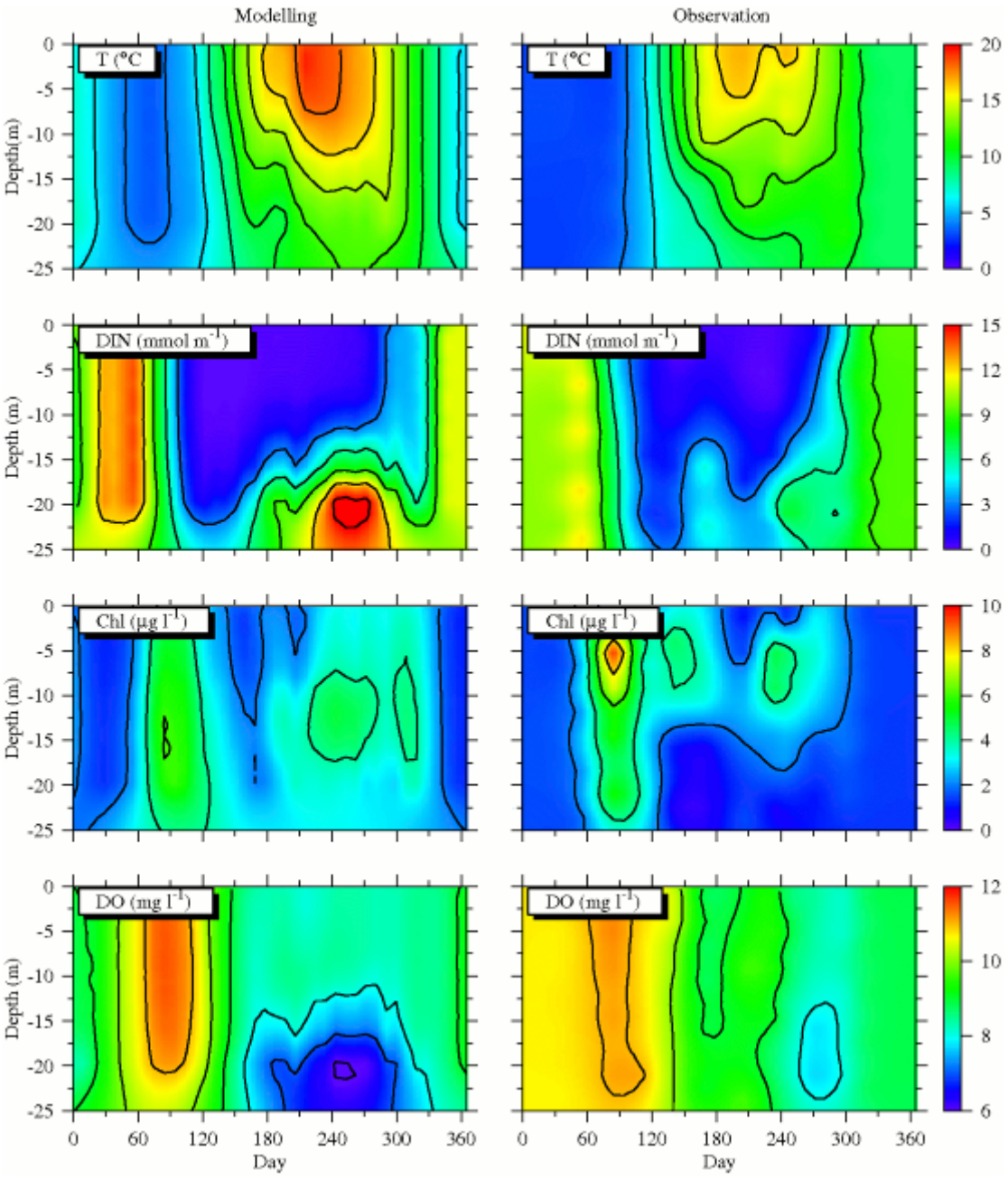

Figure 3.31 Time-series data of modeled (left panels) and observed (right panels) key parameters (T, DIN, Chl and DO) in the water column at the near-field station N10 in 2007.

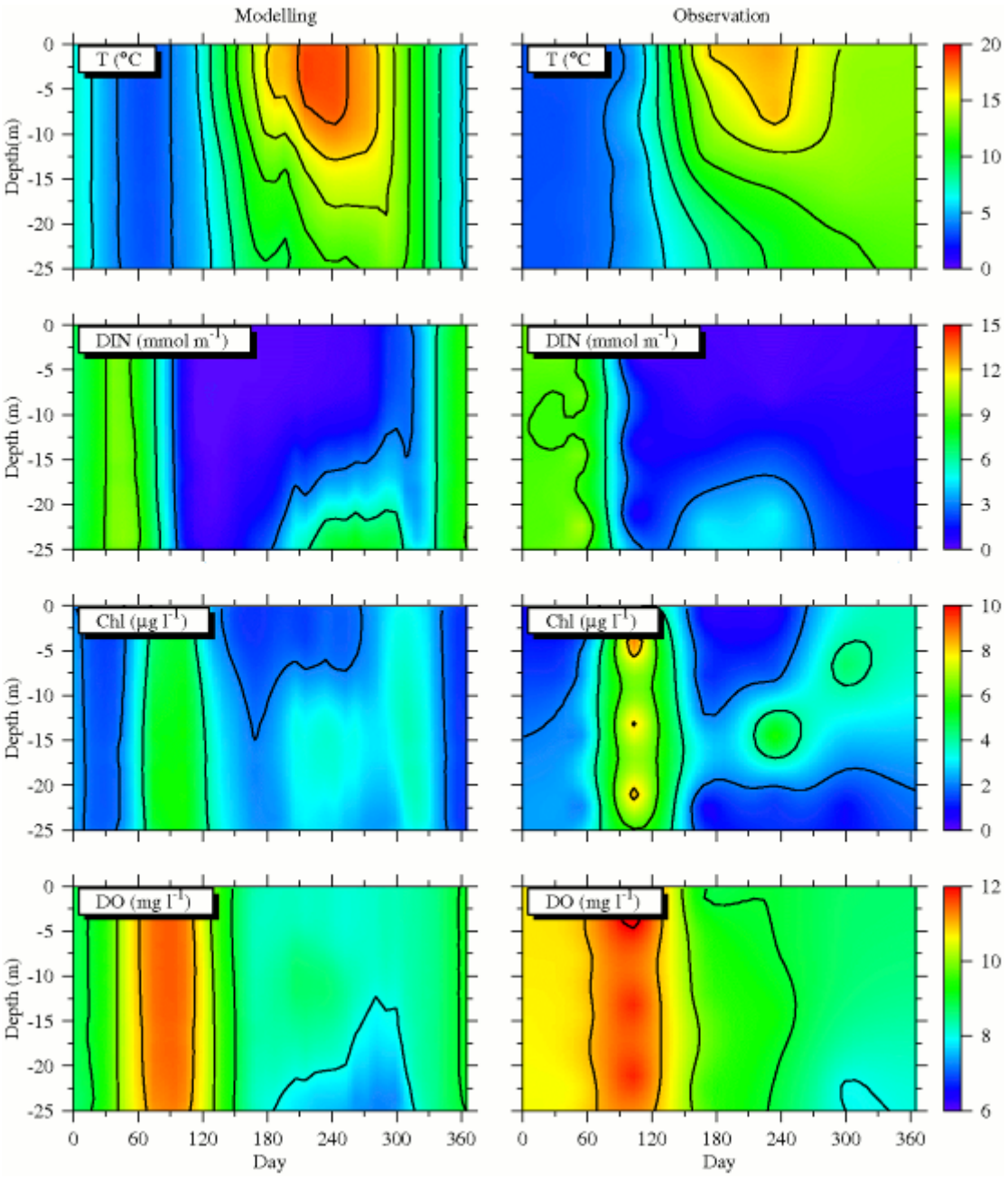

Figure 3.32 Time-series data of modeled (left panels) and observed (right panels) key parameters (T, DIN, Chl and DO) in the water column at the farfield station F06 in 2007.

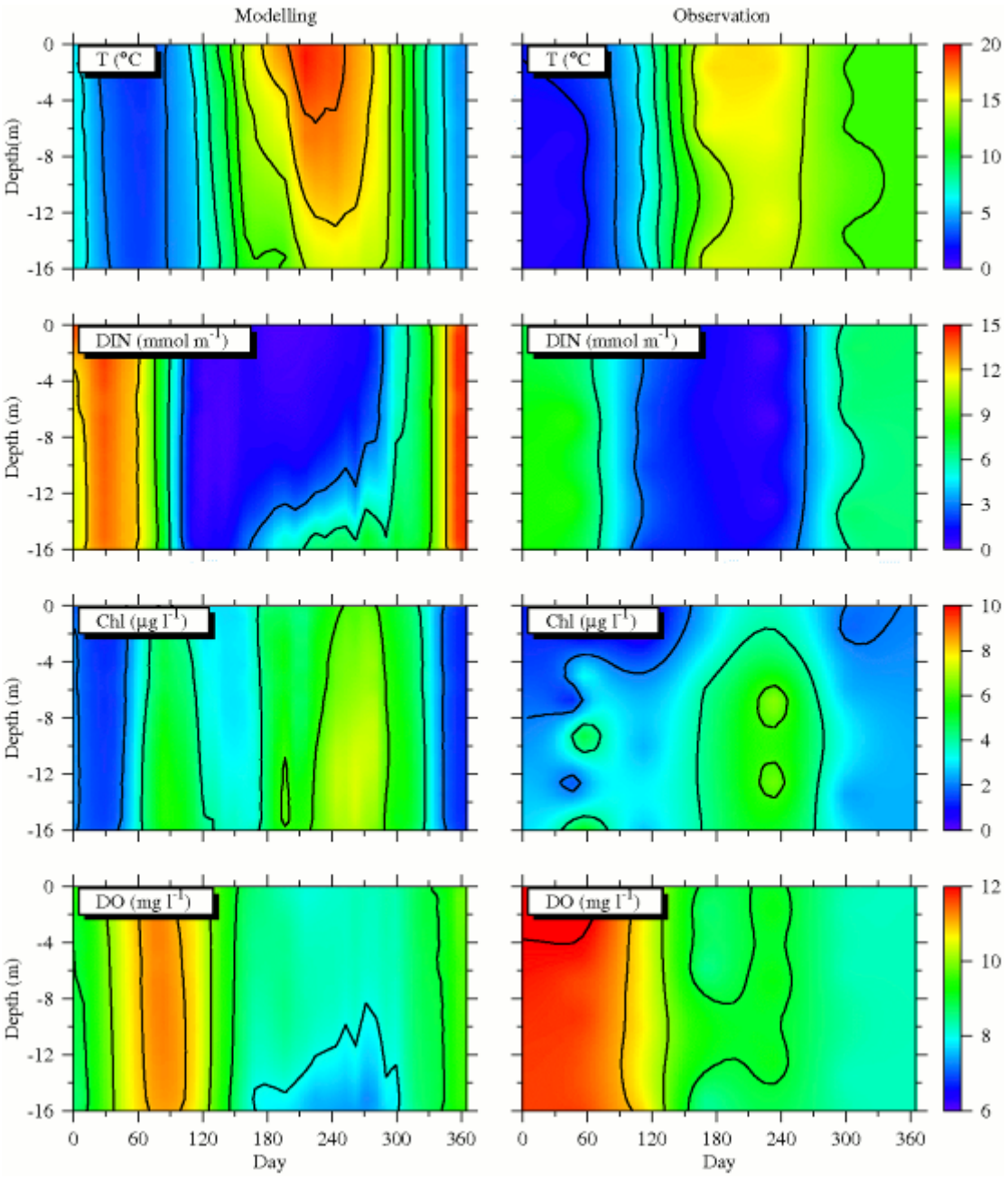

Figure 3.33 Time-series data of modeled (left panels) and observed (right panels) key parameters (T, DIN, Chl and DO) in the water column at the farfield station F23 in 2007.

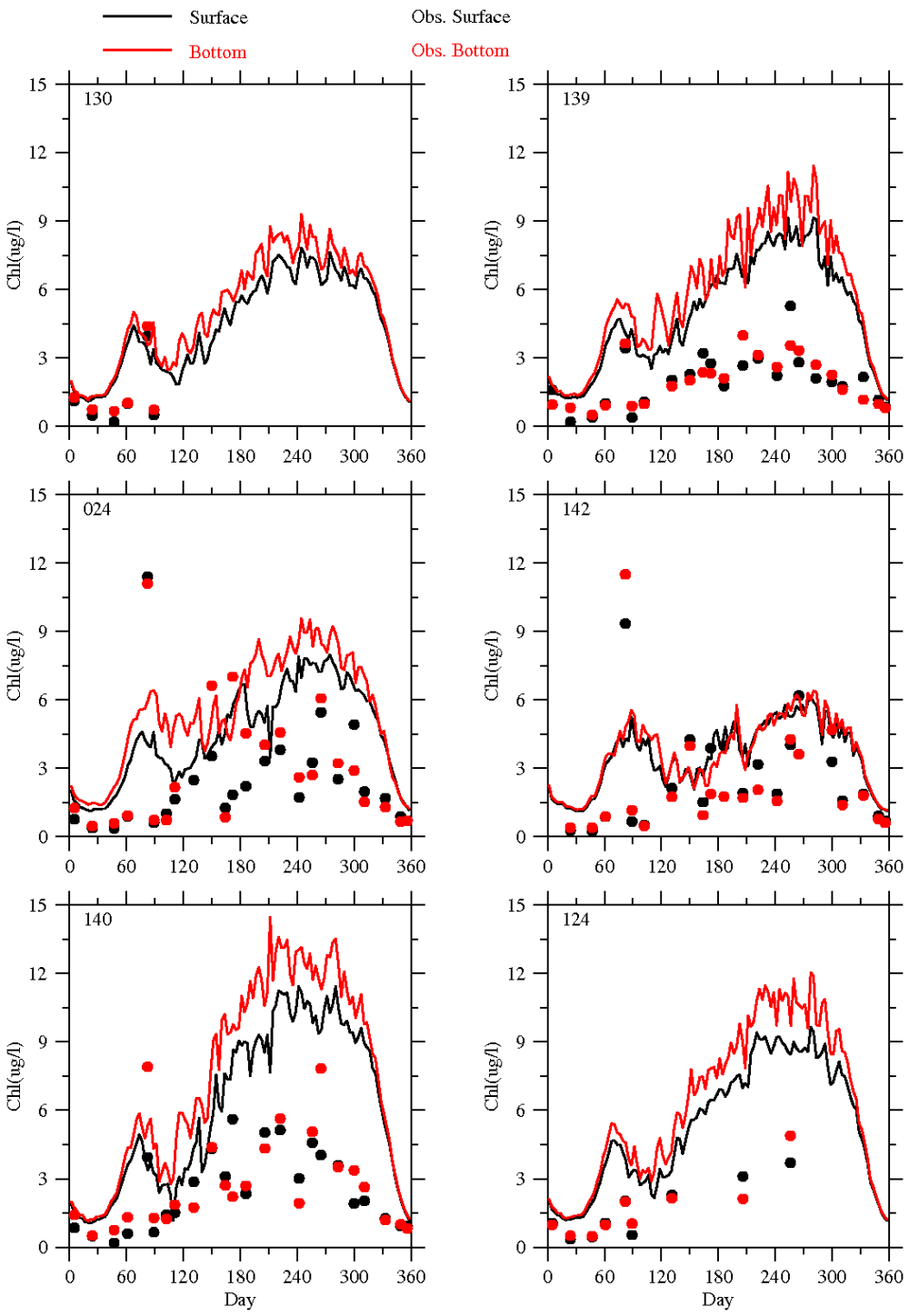

Figure 3.34 Comparison of observed (dots) and modeled (lines) time-series data of chlorophyll at the Boston Harbor monitoring stations in 2007.

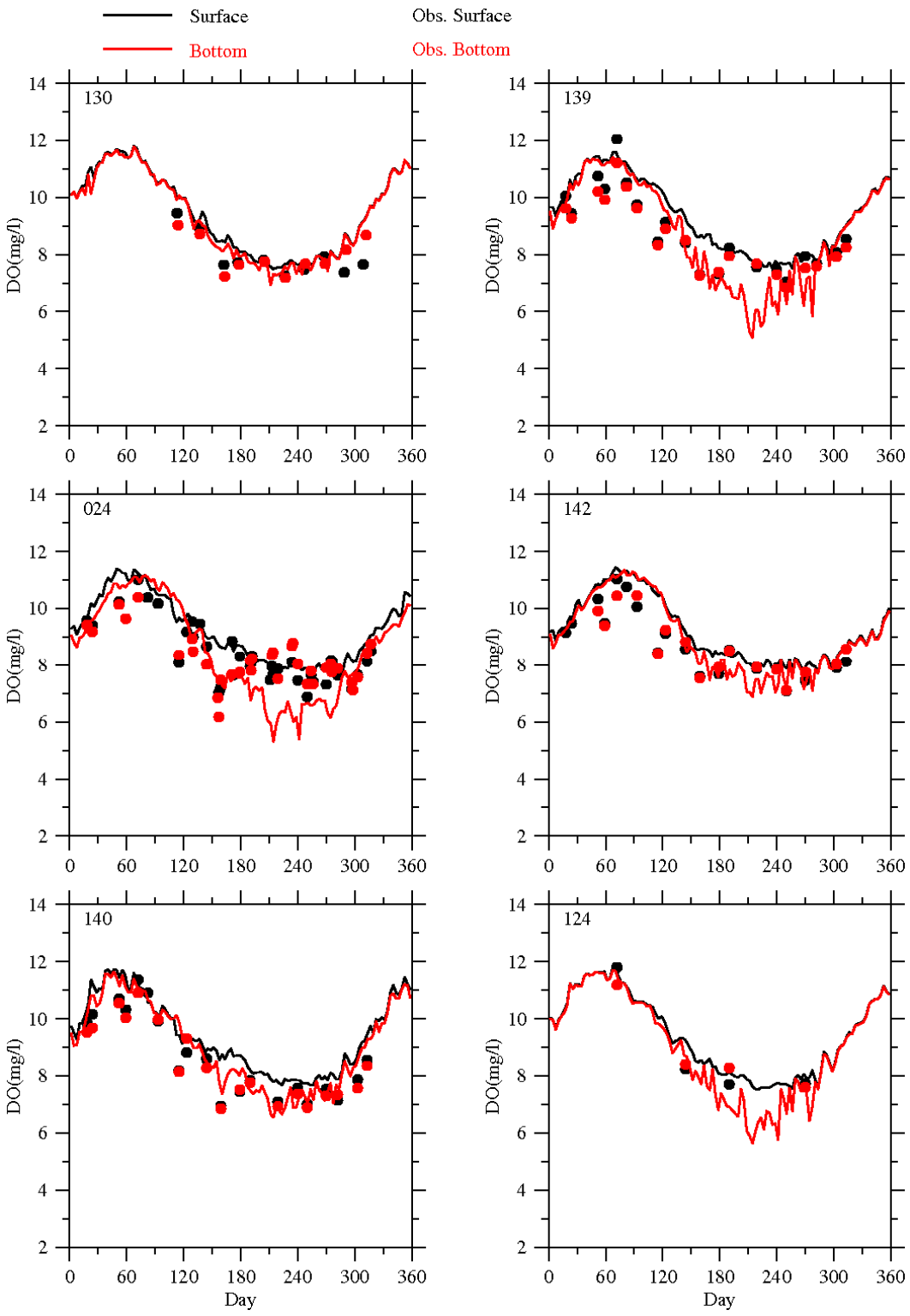

Figure 3.35 Comparison of observed (dots) and modeled (lines) time-series data of DO at the Boston Harbor monitoring stations in 2007.

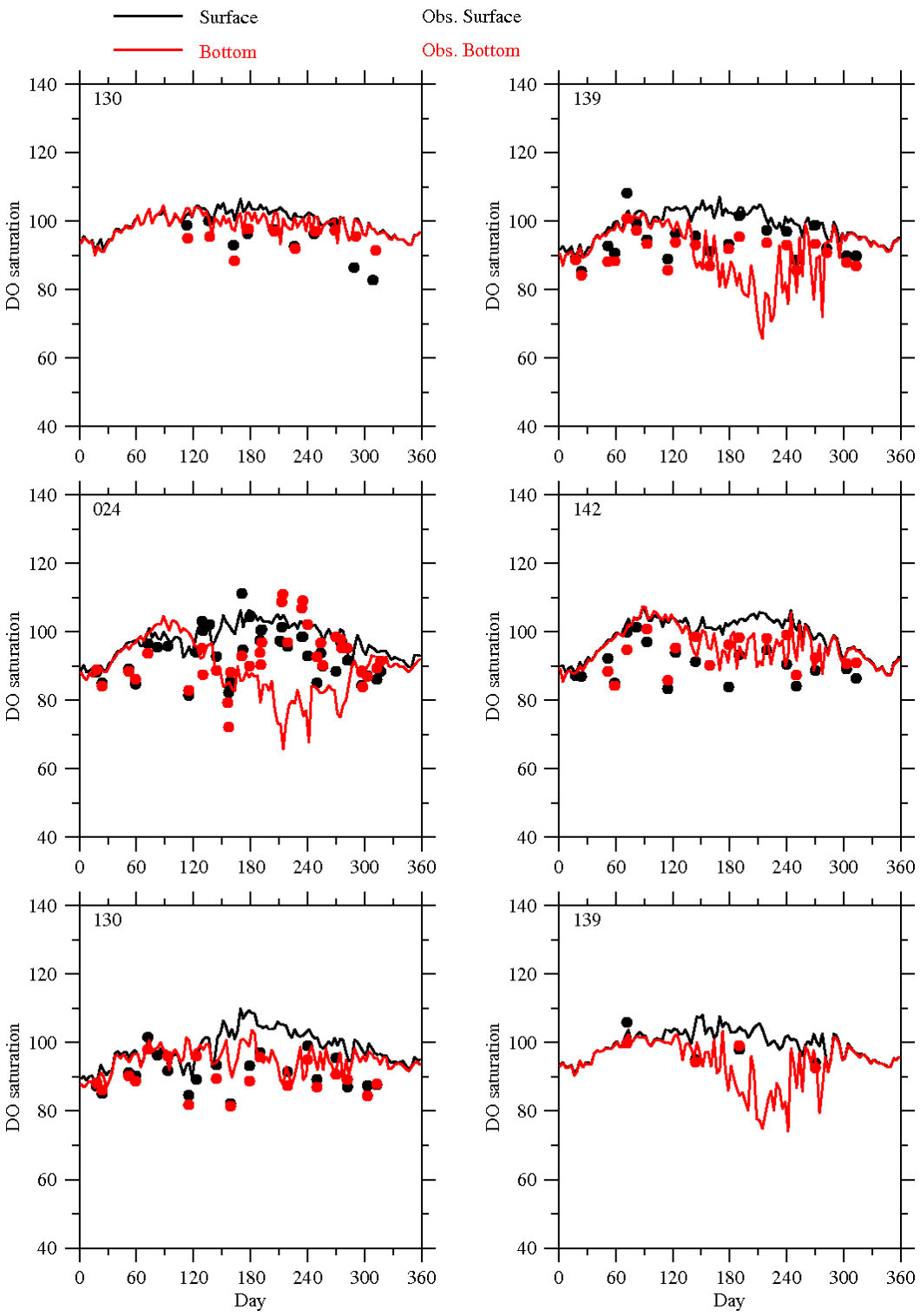

Figure 3.36 Comparison of observed (dots) and modeled (lines) time-series data of DO saturation at the Boston Harbor monitoring stations in 2007.

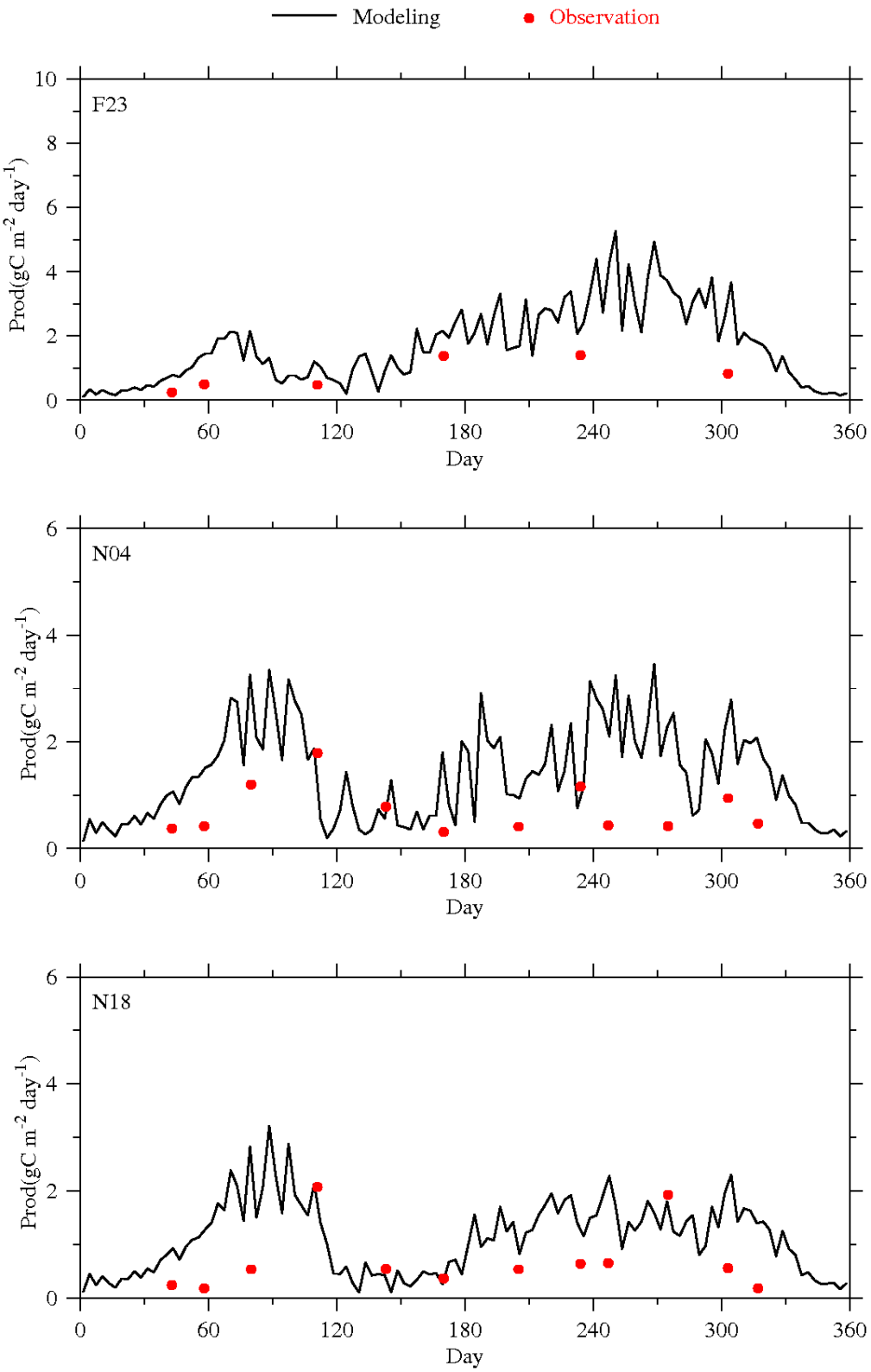

Figure 3.37 Comparison of observed (dots) and modeled (lines) time-series data of integrated primary production at MWRA monitoring stations in 2007.

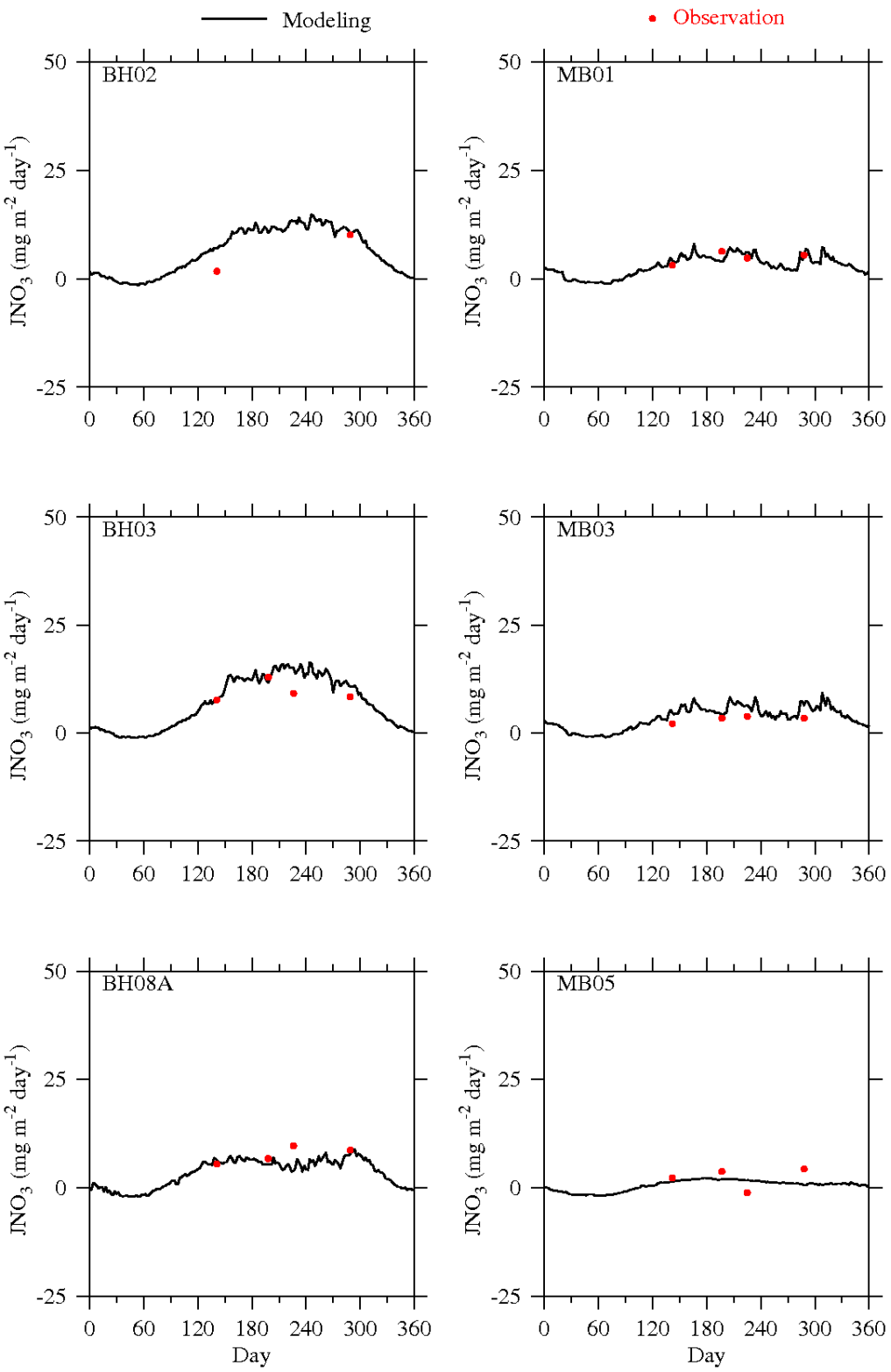

Figure 3.38 Comparison of observed (dots) and modeled (lines) time-series data of sediment NO_3^- flux at the MWRA monitoring stations in 2007.

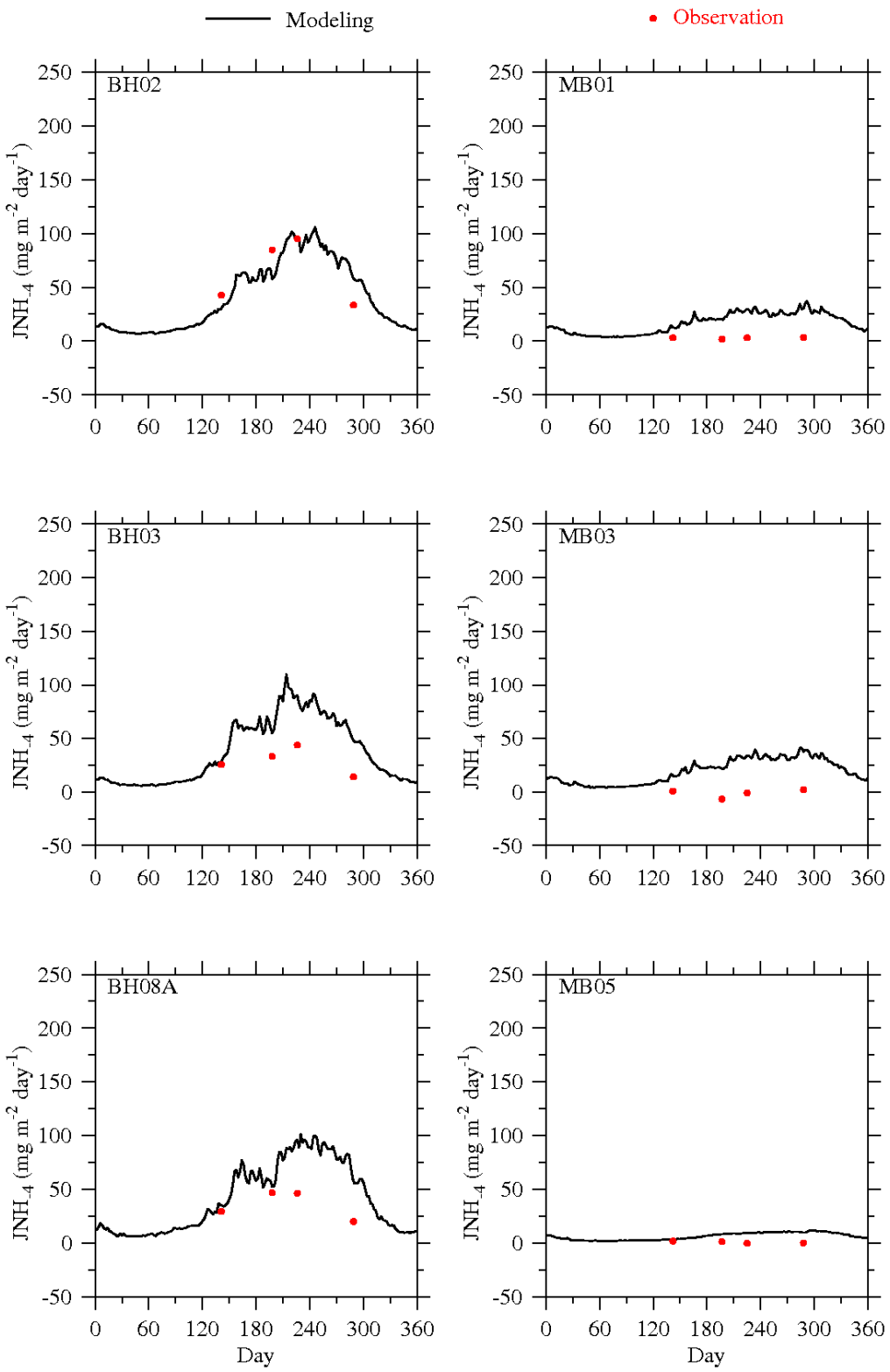

Figure 3.39 Comparison of observed (dots) and modeled (lines) time-series data of sediment NH_4^+ flux at the MWRA monitoring stations in 2007.

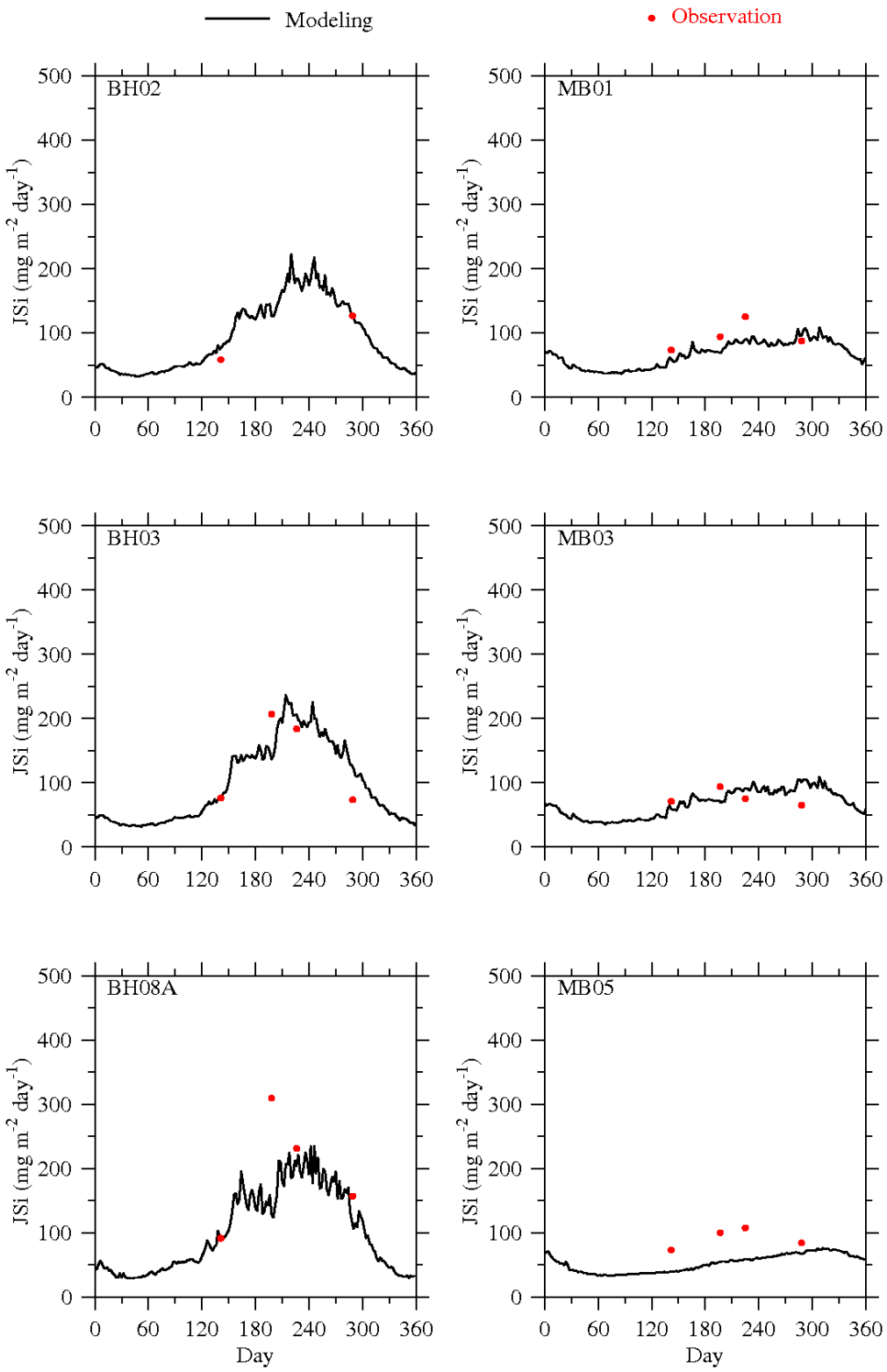

Figure 3.40 Comparison of observed (dots) and modeled (lines) time-series data of sediment $Si(OH)_4$ flux at the MWRA monitoring stations in 2007.

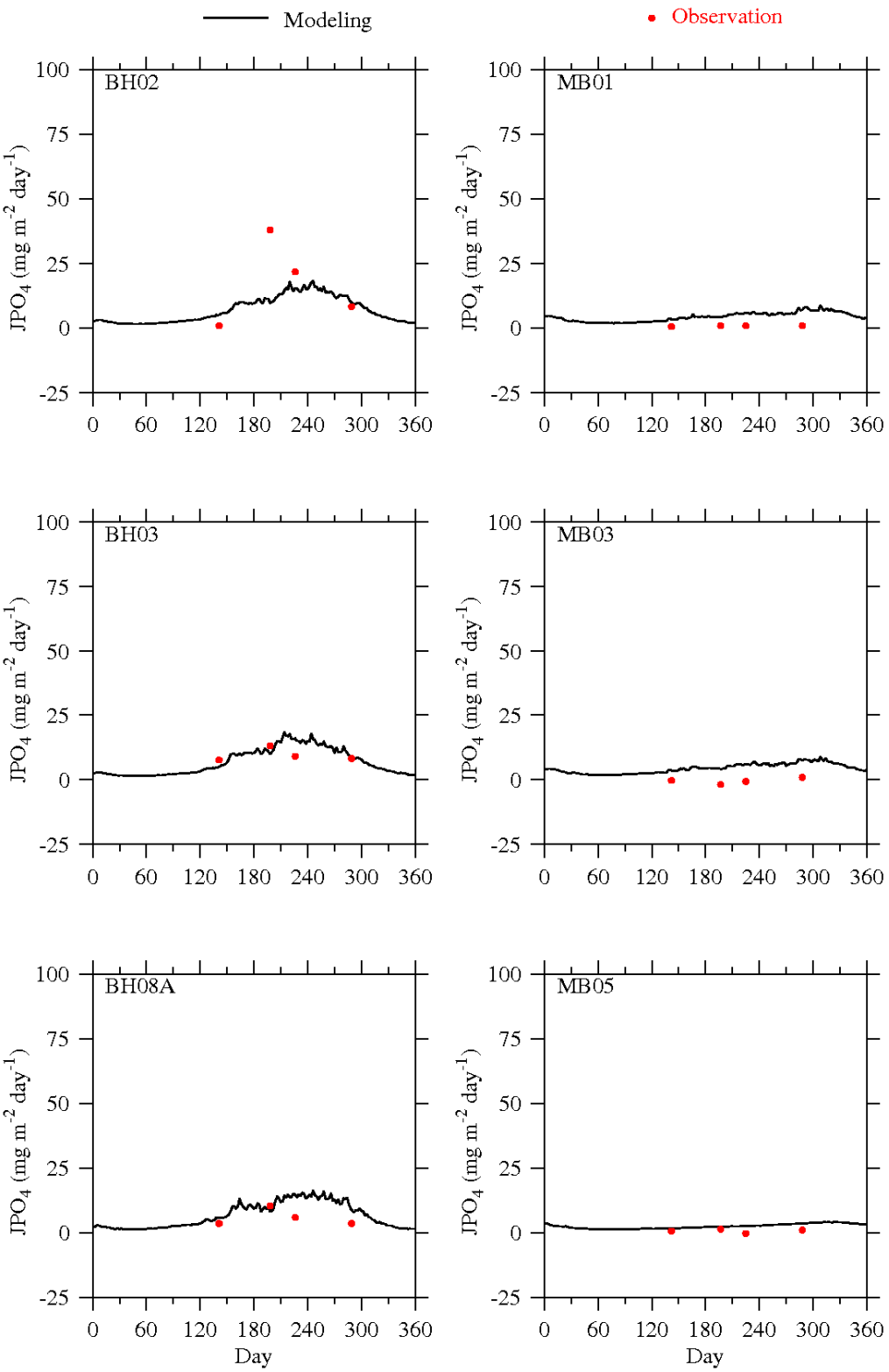

Figure 3.41 Comparison of observed (dots) and modeled (lines) time-series data of sediment PO_4^{3-} flux at the MWRA monitoring stations in 2007.

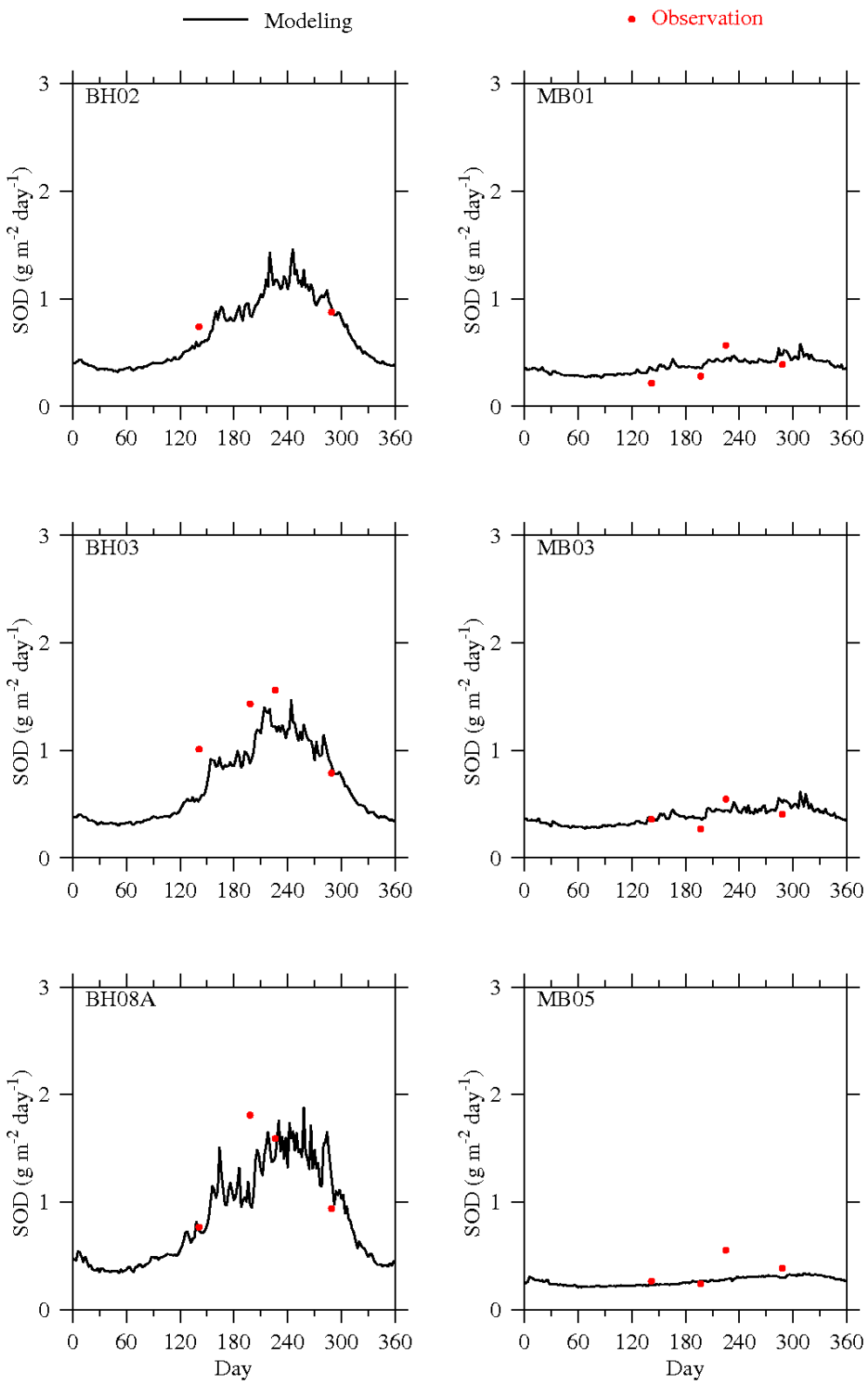

Figure 3.42 Comparison of observed (dots) and modeled (lines) time-series data of sediment SOD at the MWRA monitoring stations in 2007.

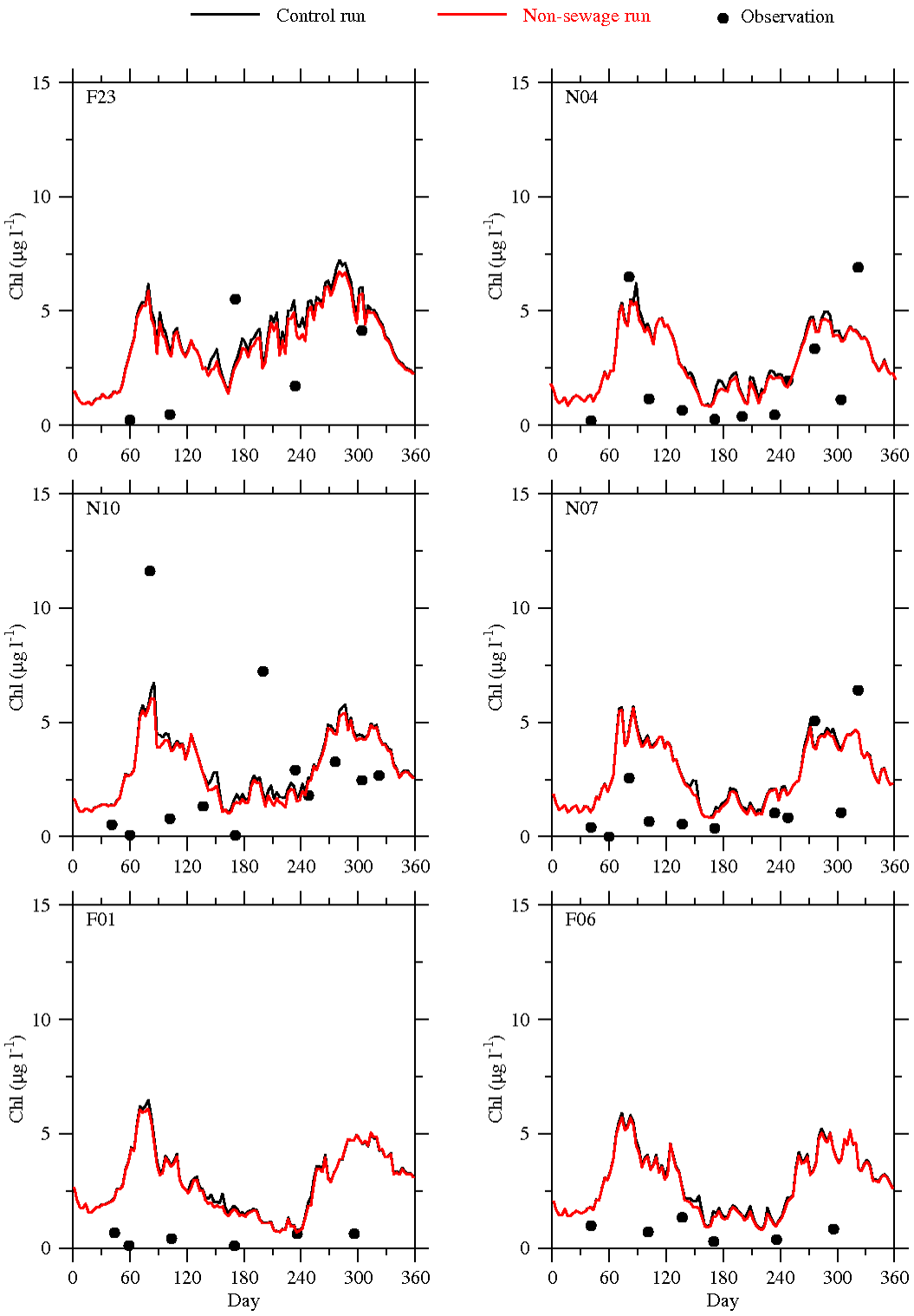

Figure 4.1 Comparison of surface chlorophyll concentration between the Control and Non-sewage experiments at the MWRA monitoring stations in 2006.

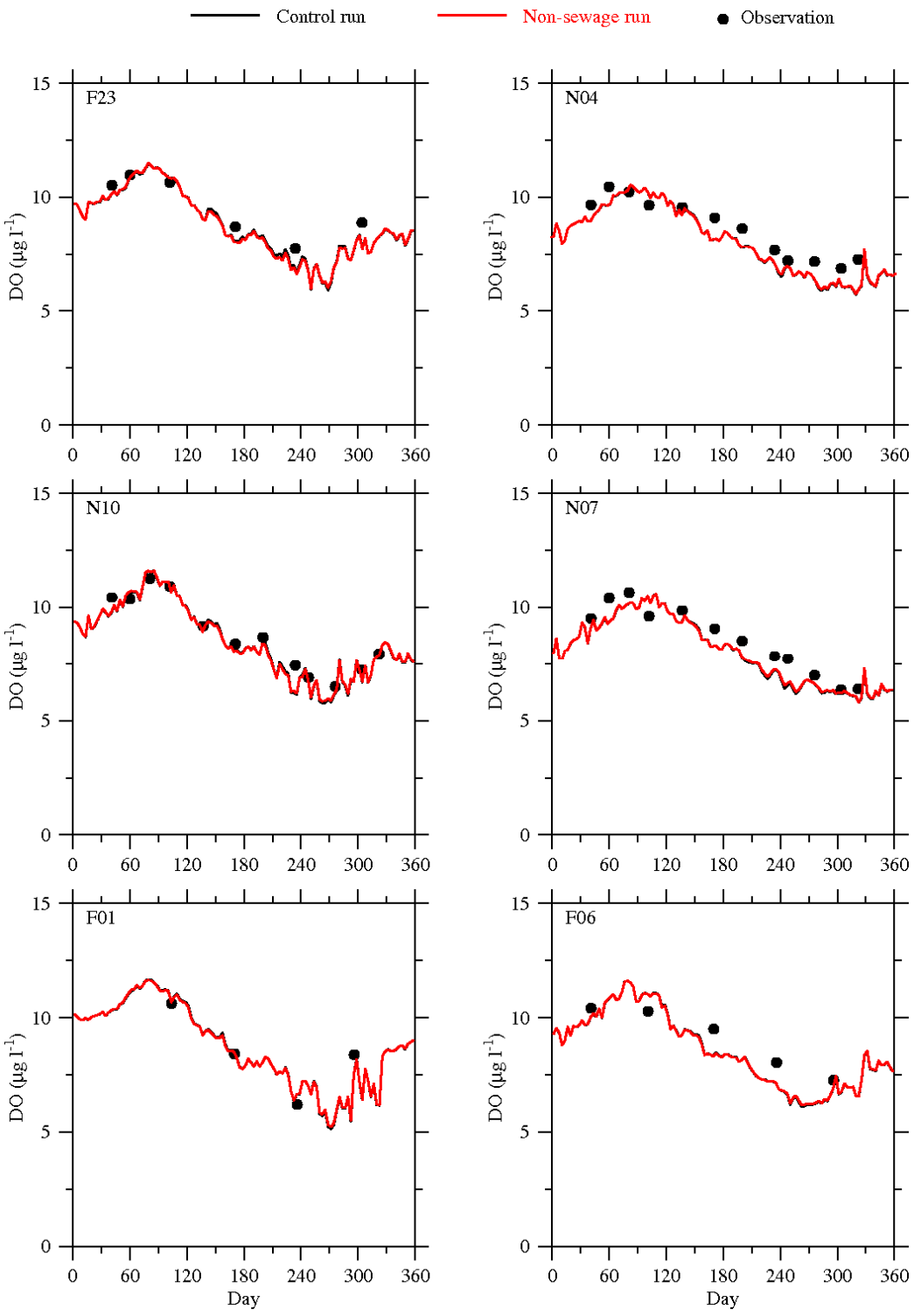

Figure 4.2 Comparison of bottom DO concentration between the Control and Non-sewage experiments at the MWRA monitoring stations in 2006.

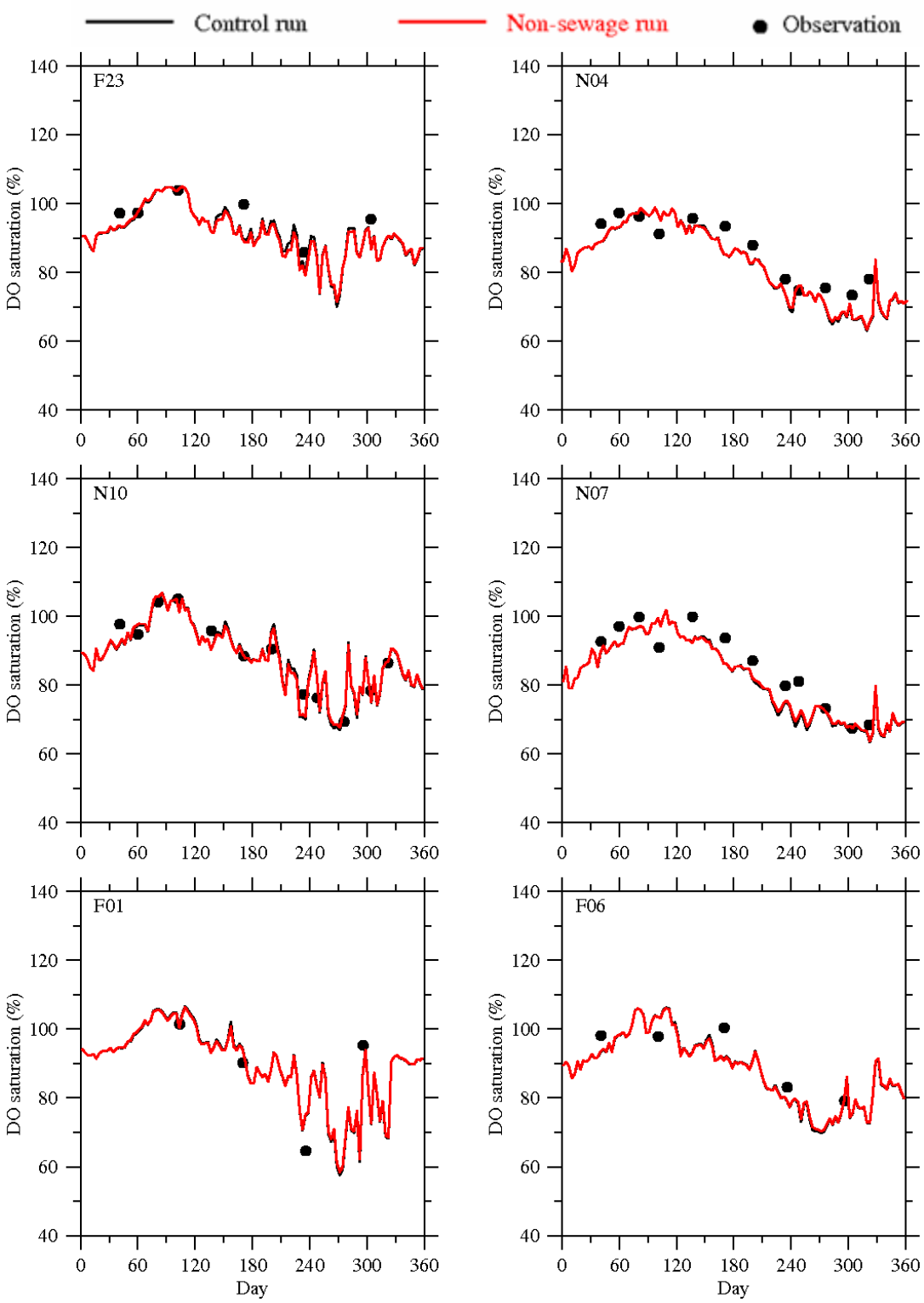

Figure 4.3 Comparison of bottom DO saturation between the Control and Non-sewage experiments at the MWRA monitoring stations in 2006.

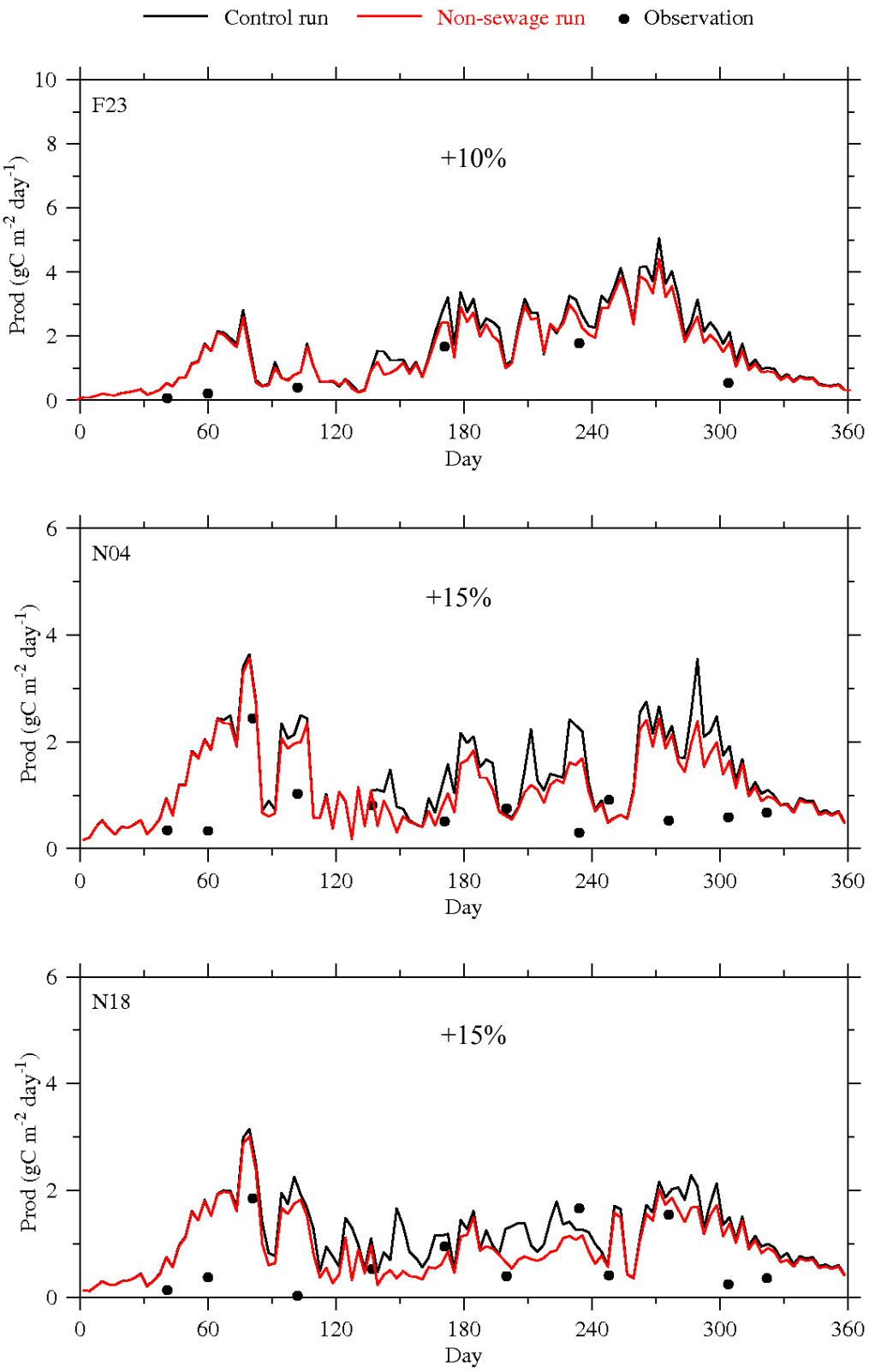

Figure 4.4 Comparison of integrated primary production between the Control and Non-sewage experiments at the MWRA monitoring stations in 2006.

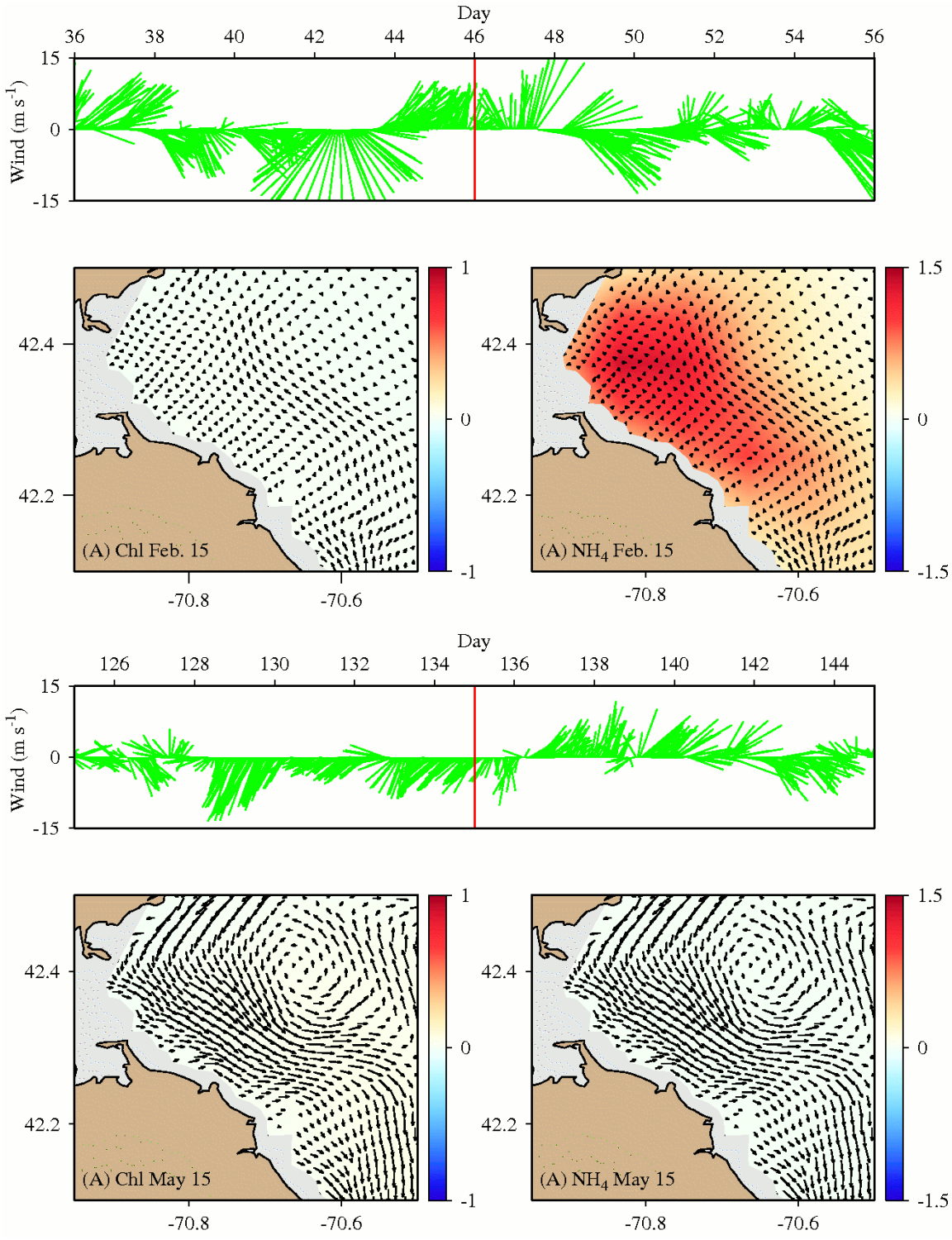

Figure 4.5 Current and differences of chlorophyll and NH_4^+ concentrations at 15-m depth on Feb 15 (upper panels) and May 15 (lower panels) between the Control and Non-sewage experiments in 2006.

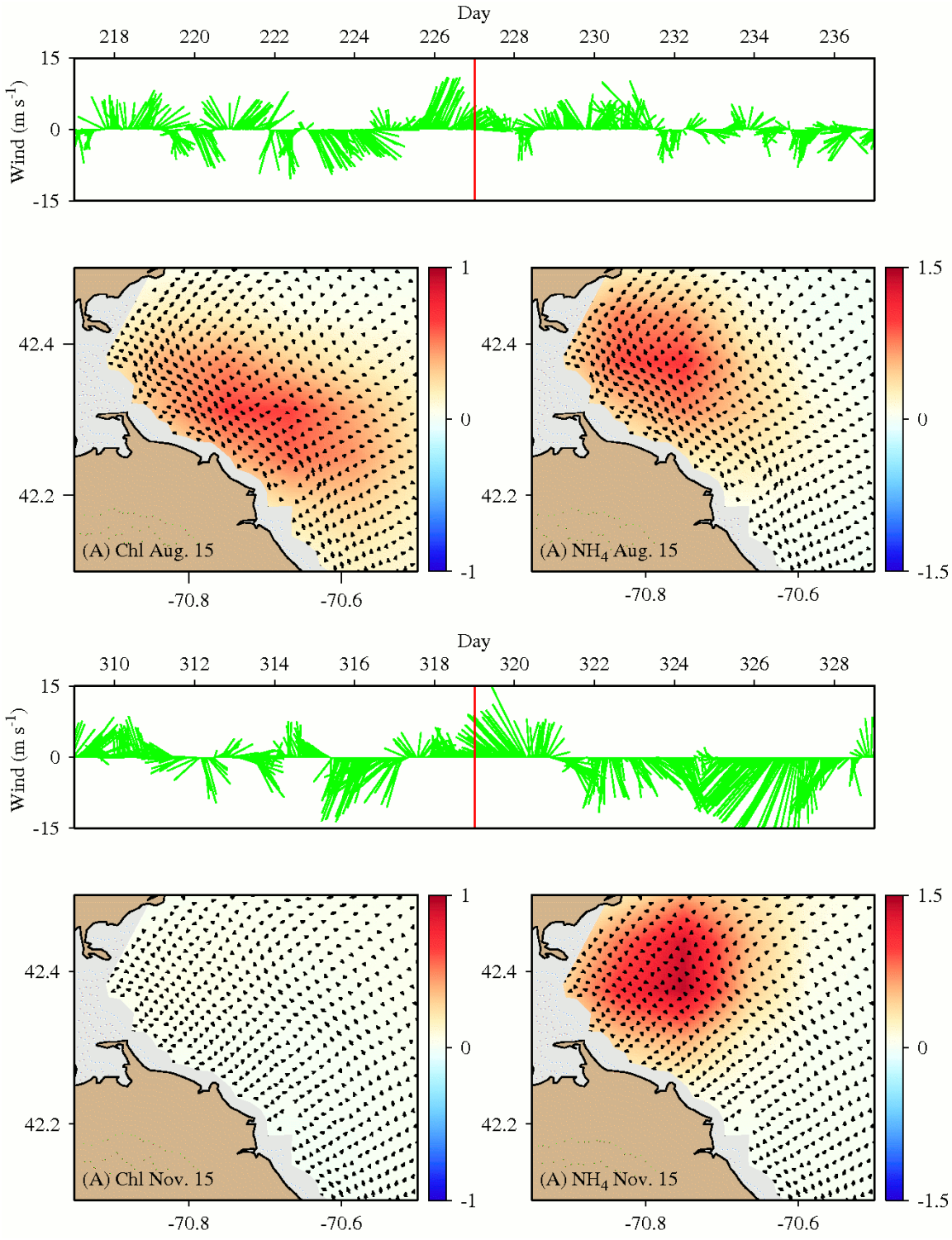

Figure 4.6 Current and differences of chlorophyll and NH_4^+ concentrations at 15-m depth on Aug 15 (upper panels) and Nov 15 (lower panels) between the Control and Non-sewage experiments in 2006.

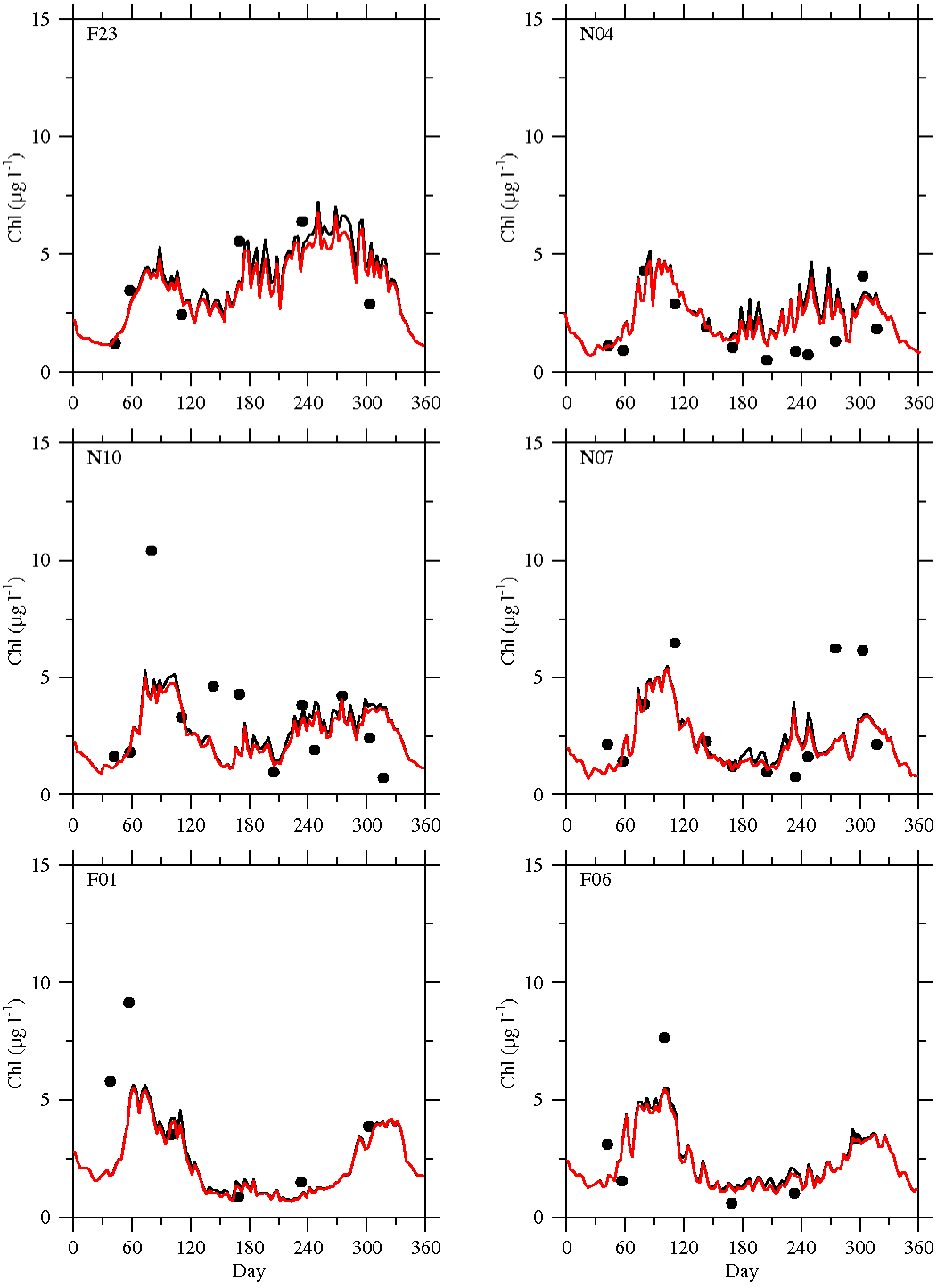

Figure 4.7 Comparison of surface chlorophyll concentration between the Control and Non-sewage experiments at the MWRA monitoring stations in 2007.

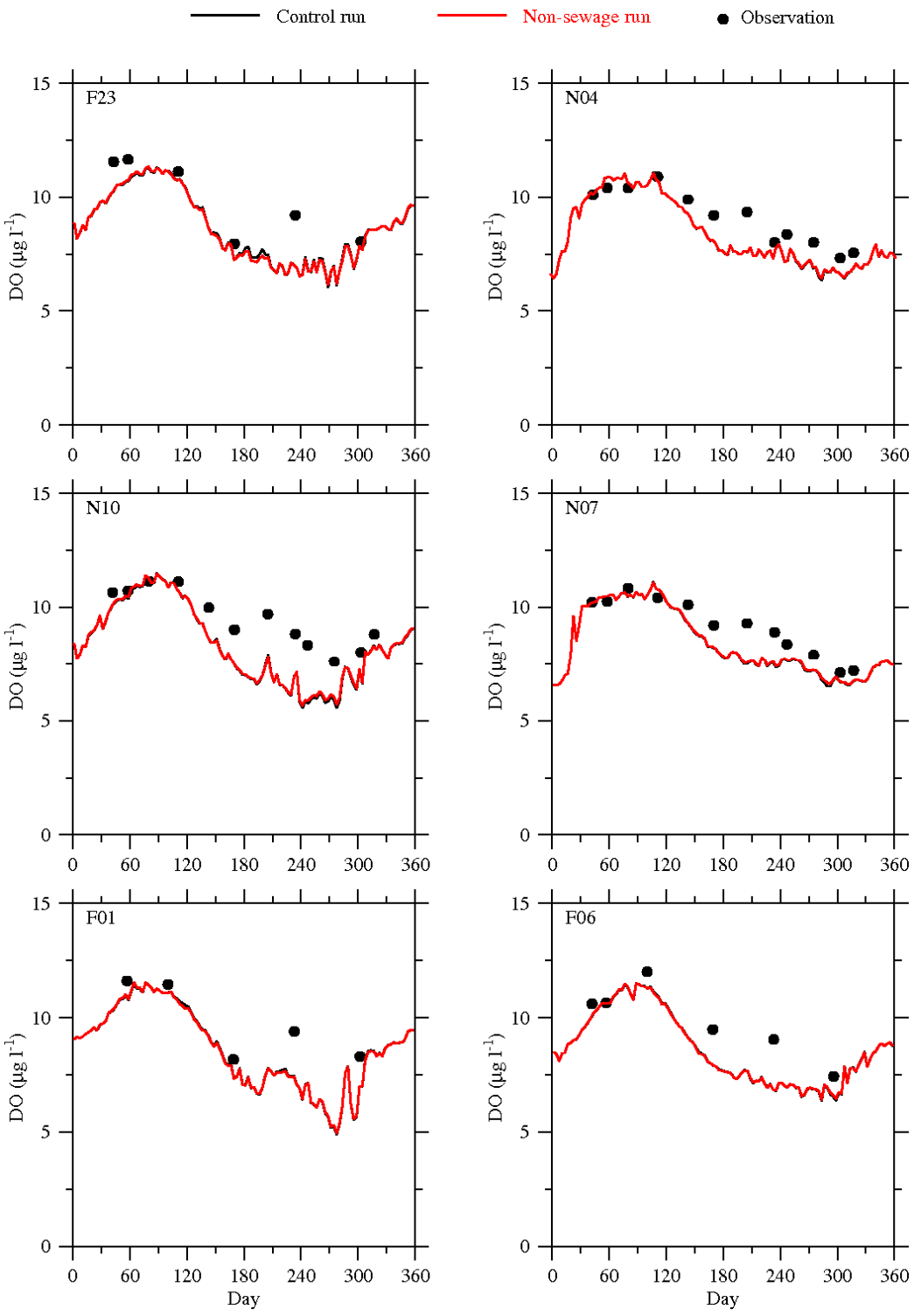

Figure 4.8 Comparison of bottom DO concentration between the Control and Non-sewage experiments at the MWRA monitoring stations in 2007.

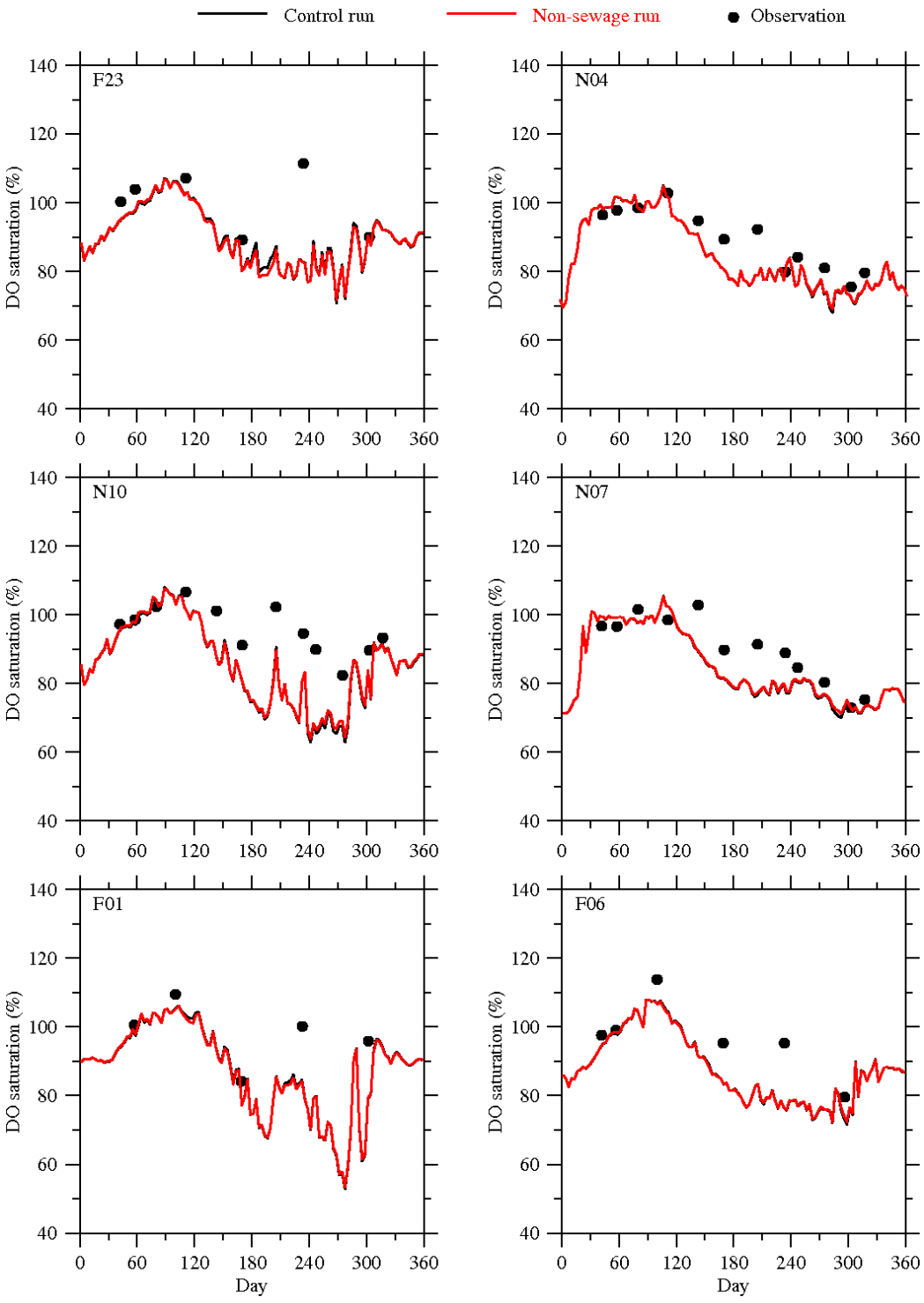

Figure 4.9 Comparison of bottom DO saturation between the Control and Non-sewage experiments at the MWRA monitoring stations in 2007.

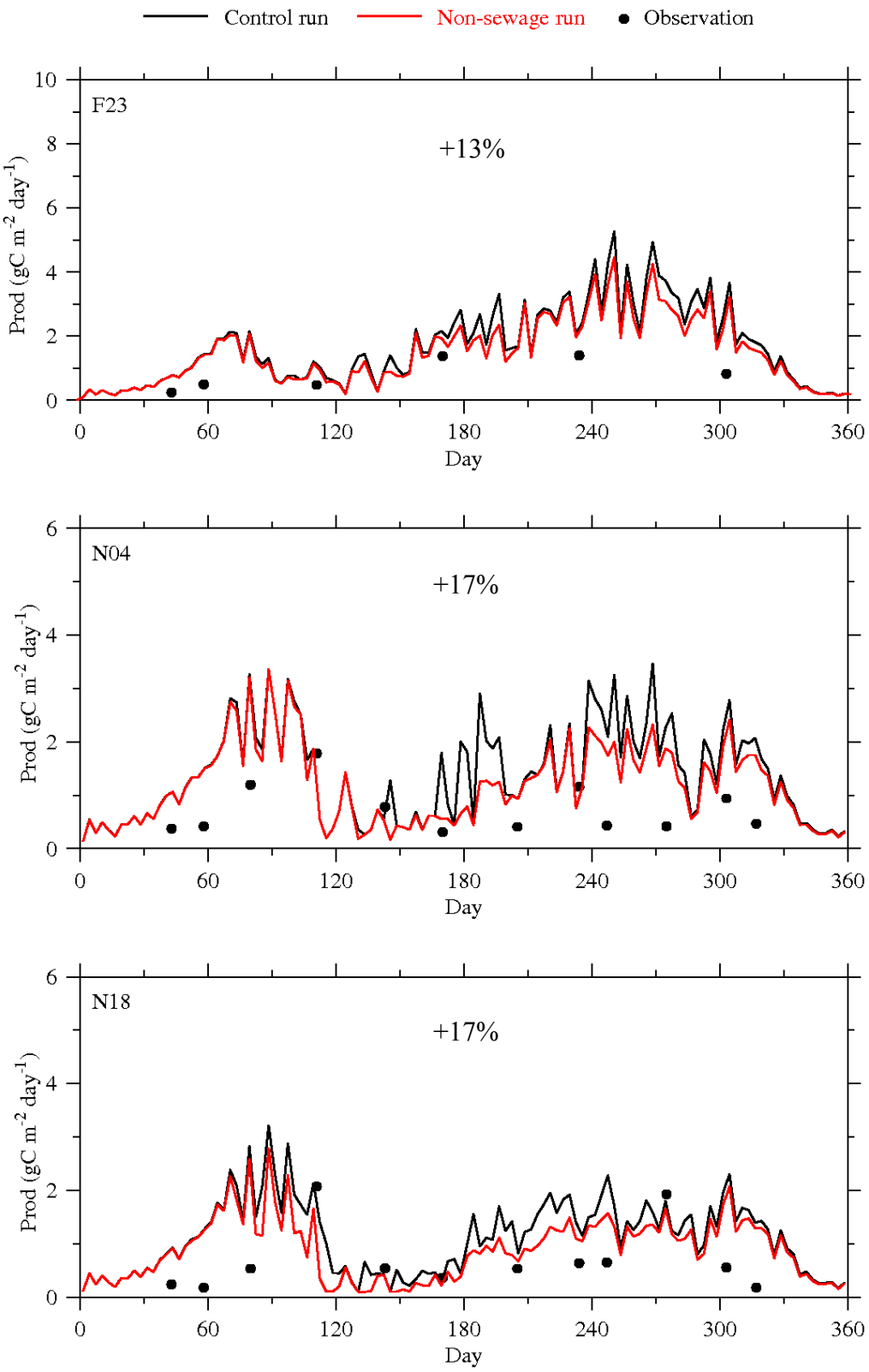

Figure 4.10. Comparison of integrated primary production between the Control and Non-sewage experiment at the MWRA monitoring stations in 2007.

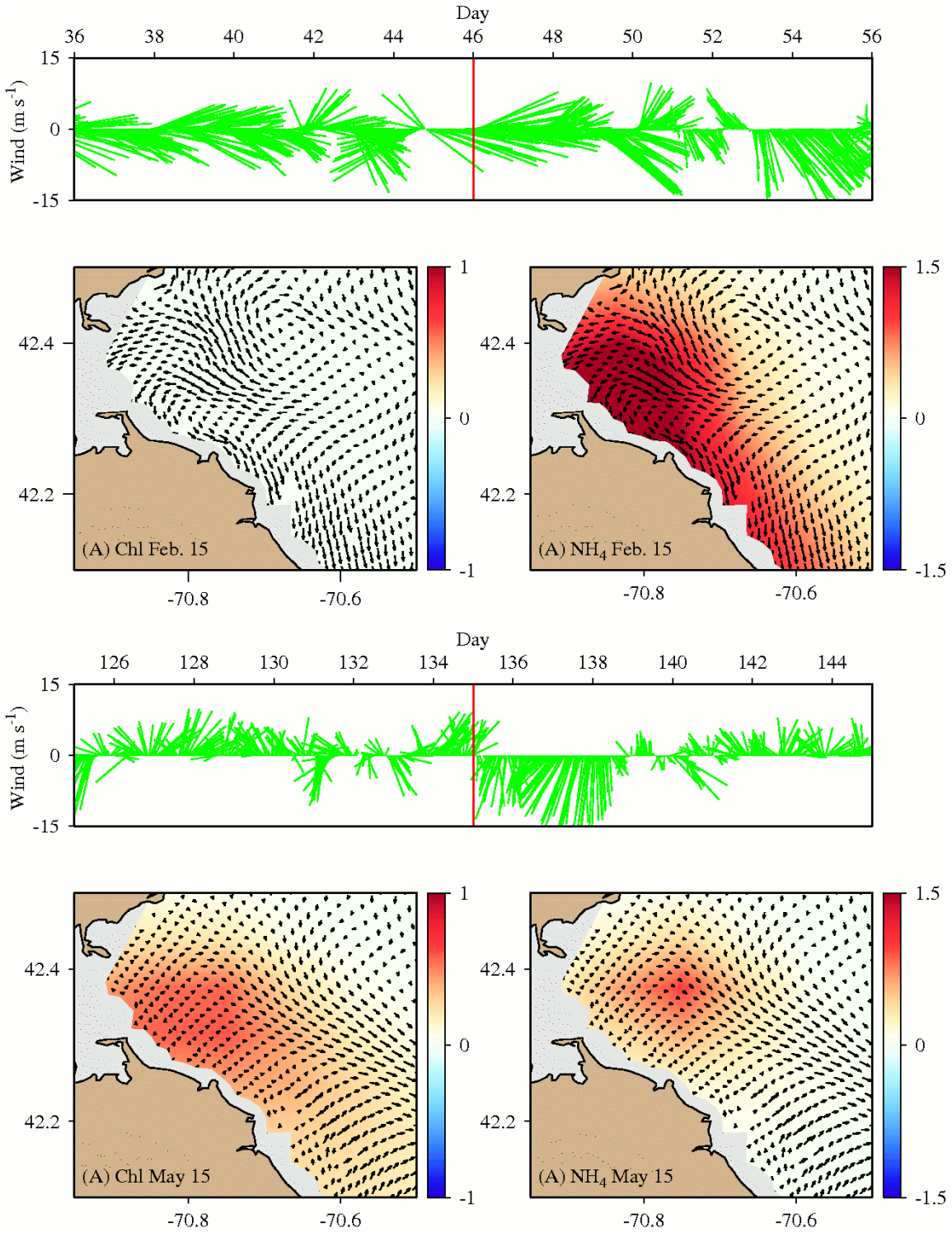

Figure 4.11 Current and differences of chlorophyll and NH_4^+ concentrations 15-m depth on Feb 15 (upper panels) and May 15 (lower panels) between the Control and Non-sewage experiments in 2007.

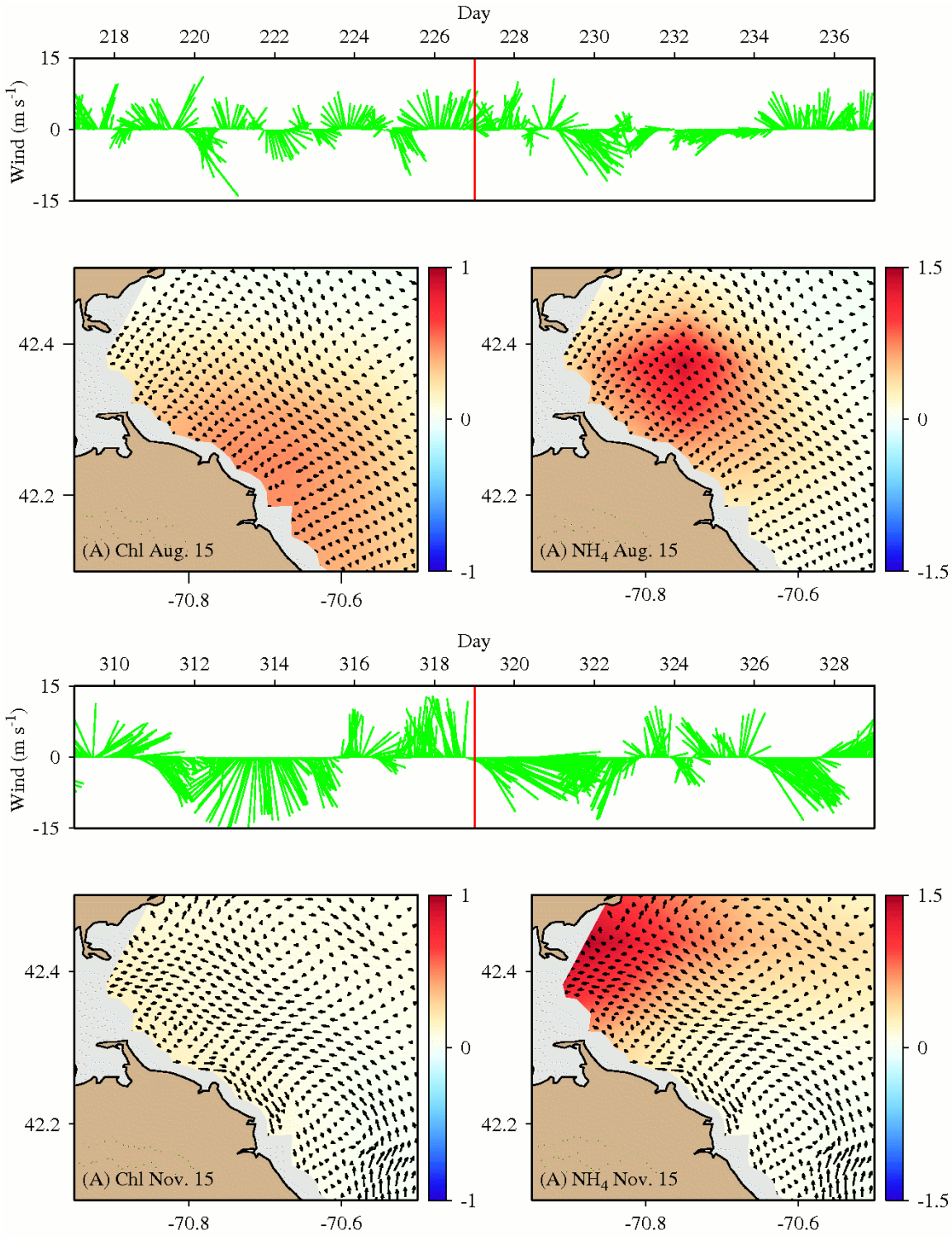

Figure 4.12 Current and differences of chlorophyll and NH_4^+ concentrations at 15-m depth on Aug 15 (upper panels) and Nov 15 (lower panels) between the Control and Non-sewage experiments in 2007.

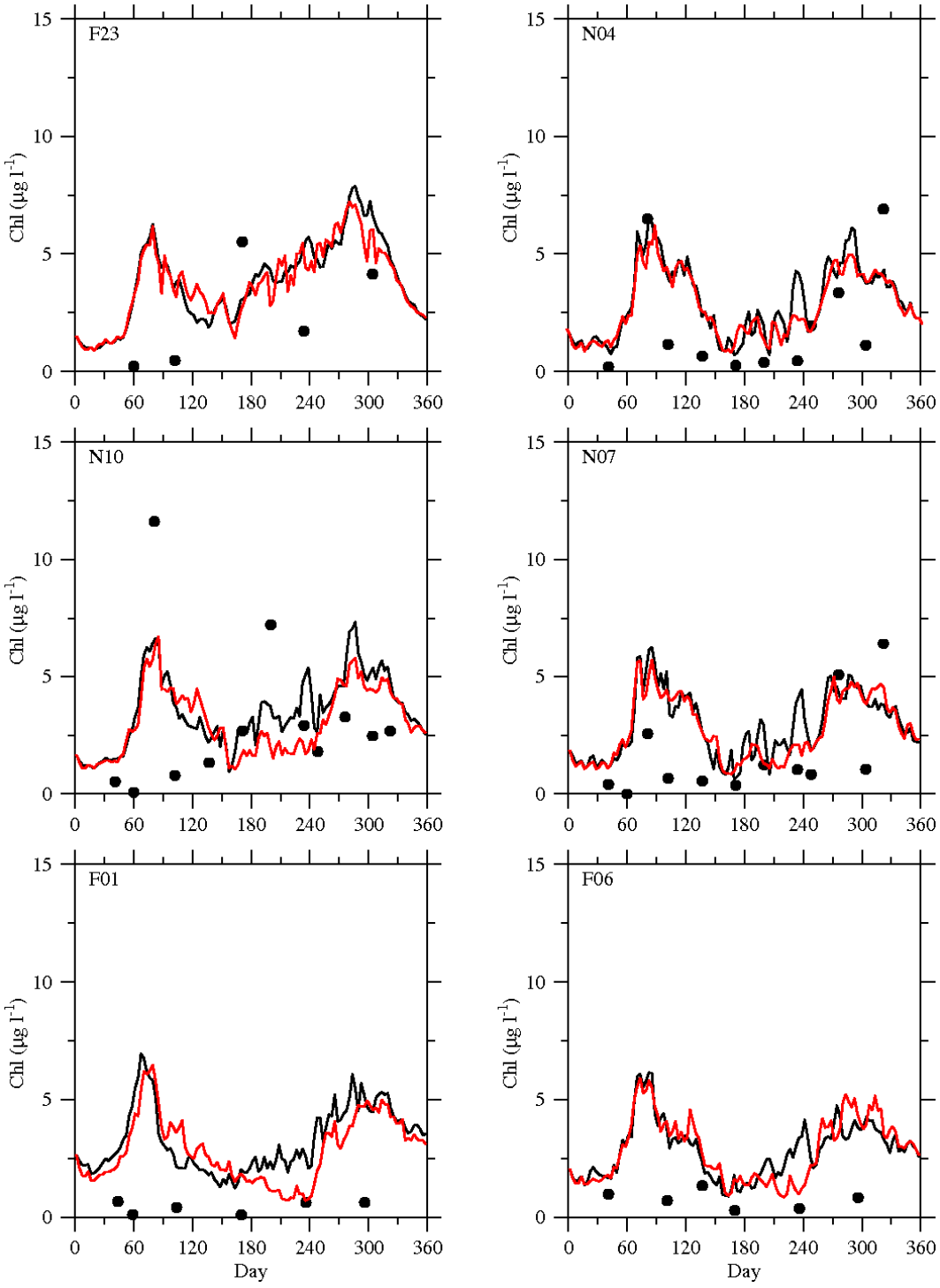

Figure 5.1 Comparison of surface chlorophyll concentration between the Wind-field (black lines) and Uniform-wind (red lines) runs at the MWRA monitoring stations in 2006.

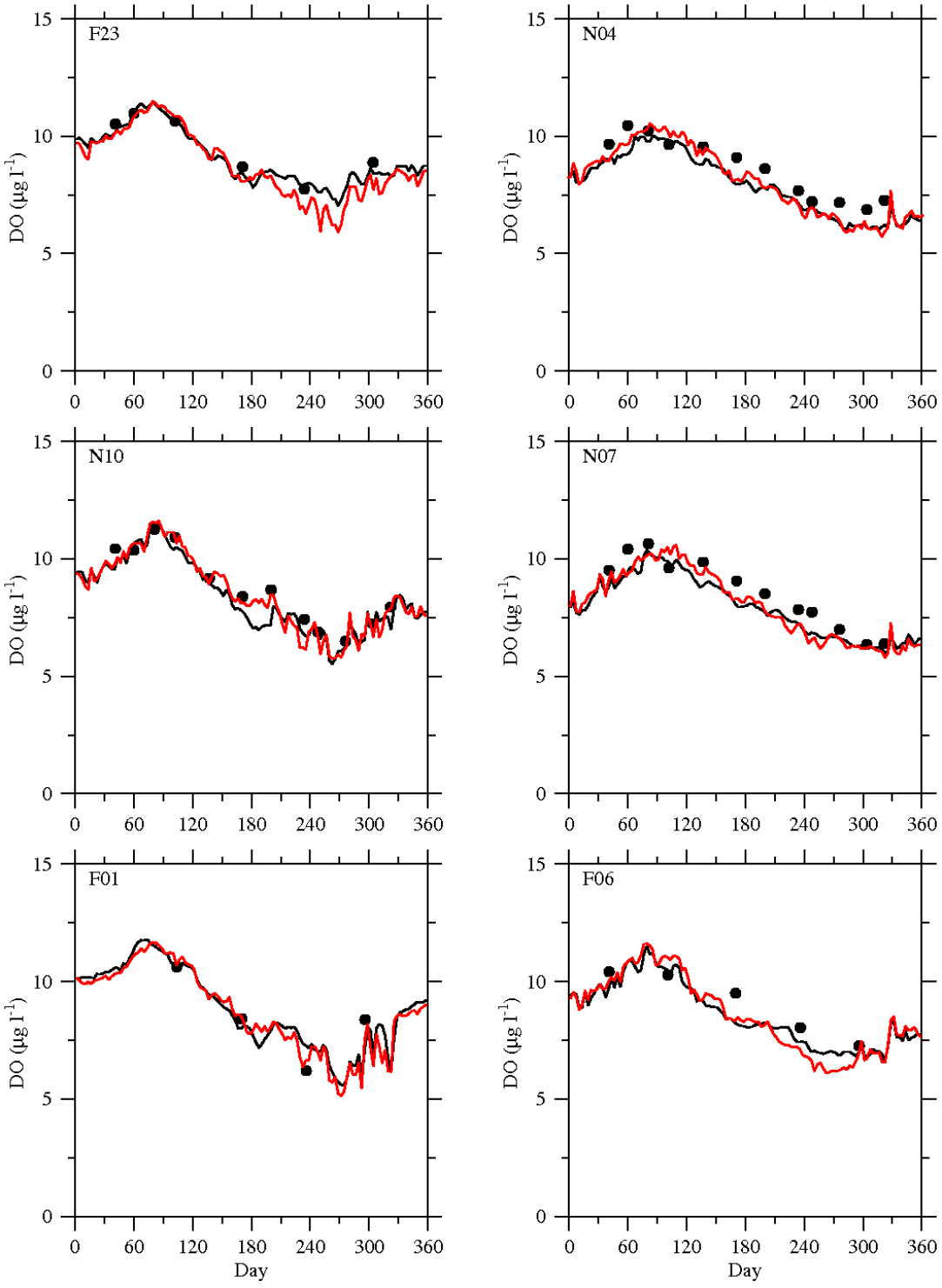

Figure 5.2 Comparison of bottom DO concentration between the Wind-field (black lines) and the Uniform-wind (red lines) runs at the MWRA monitoring stations in 2006.

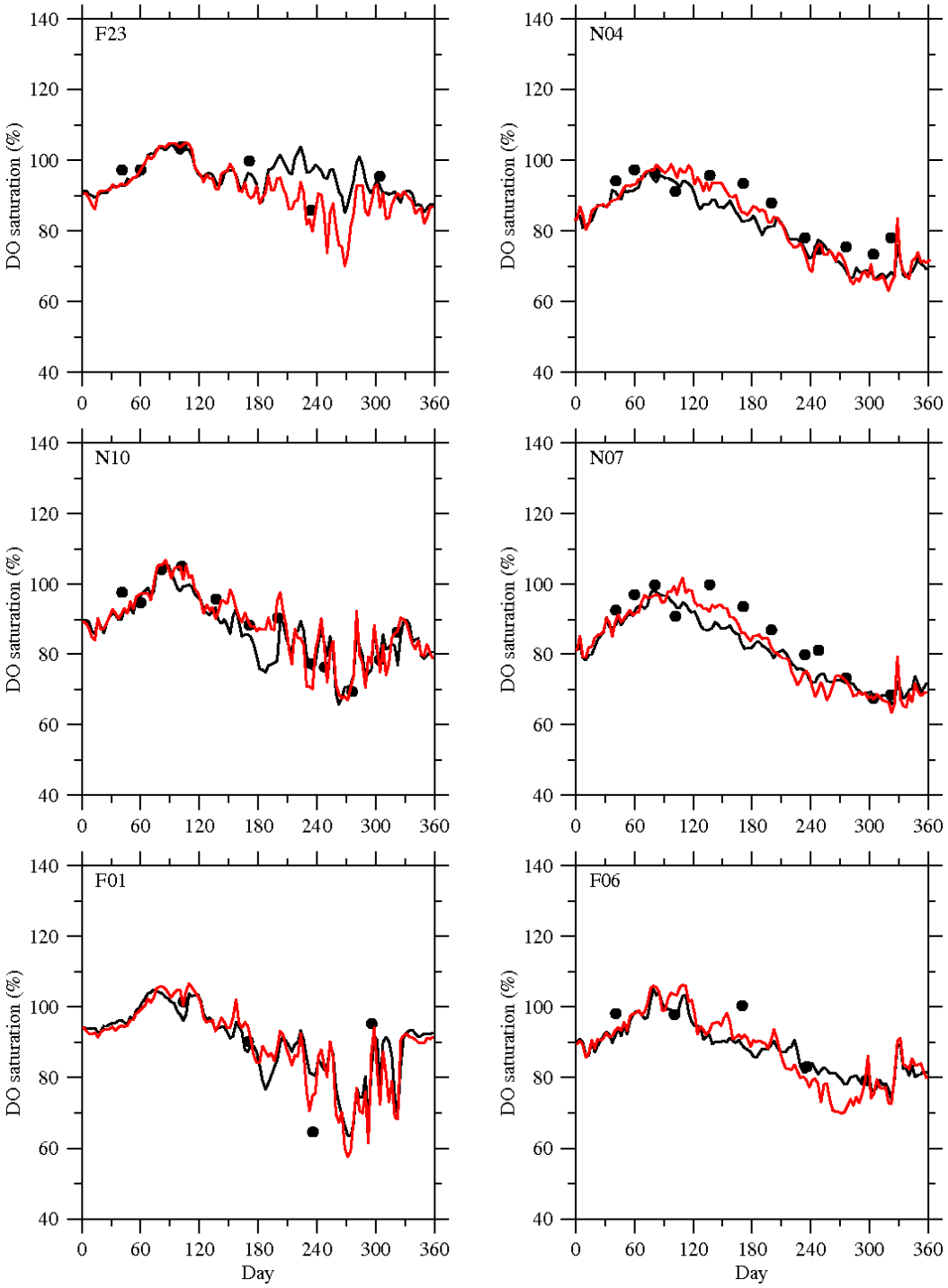

Figure 5.3 Comparison of bottom DO saturation between the Wind-field (black lines) and the Uniform-wind (red lines) runs at the MWRA monitoring stations in 2006.

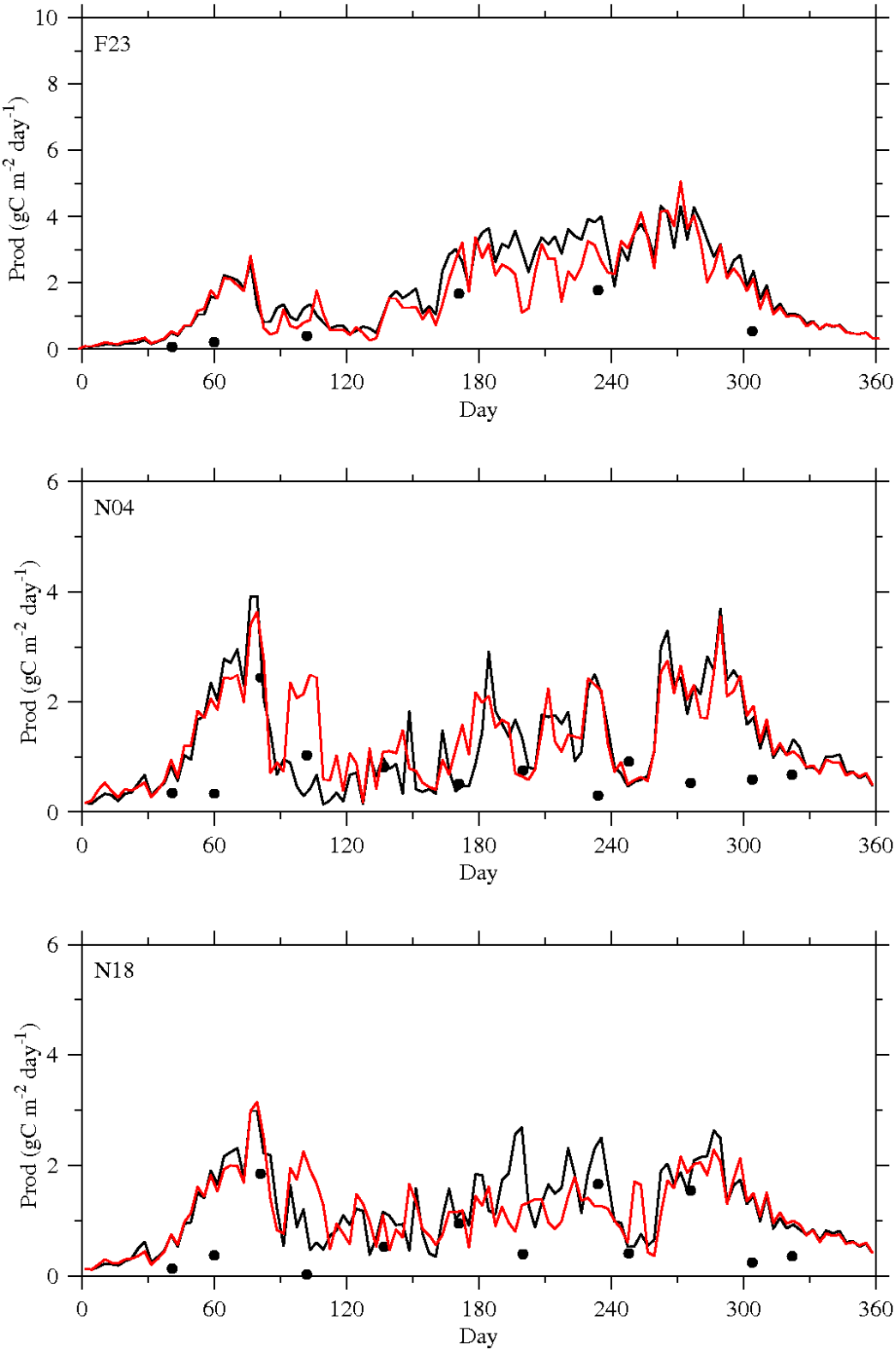

Figure 5.4 Comparison of integrated primary production between the Wind-field (black lines) and the Uniform-wind (red lines) runs at the MWRA monitoring stations in 2006.

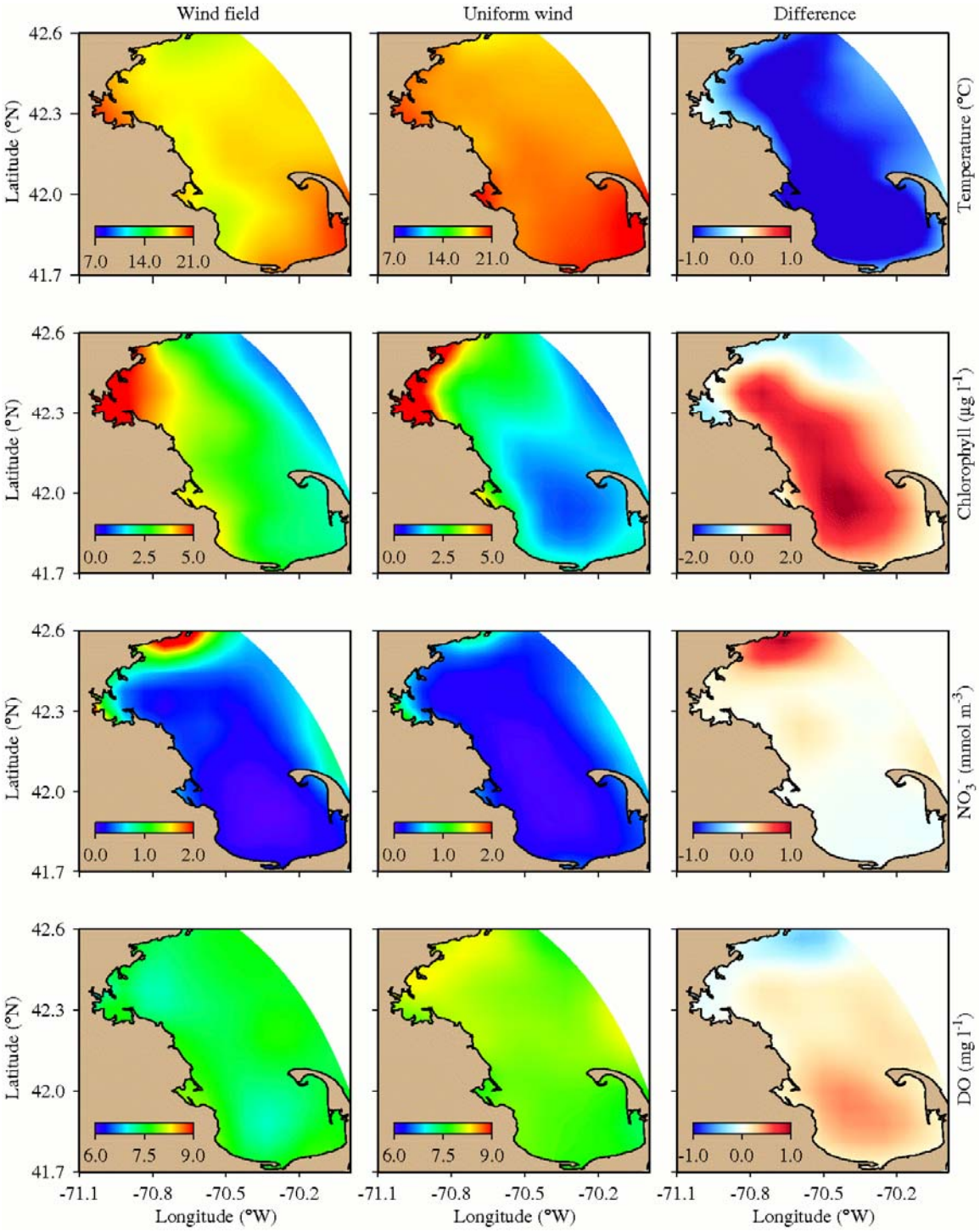

Figure 5.5 Comparison of temperature, chlorophyll, and NO_3^- in surface waters and DO in bottom waters predicted by the Wind-field run (left), the Uniform-wind run (middle) and the difference between the two simulations (Wind-field minus Wind-field prediction) during a cyclone event on Aug 20 2006 (Chen et al., 2009).

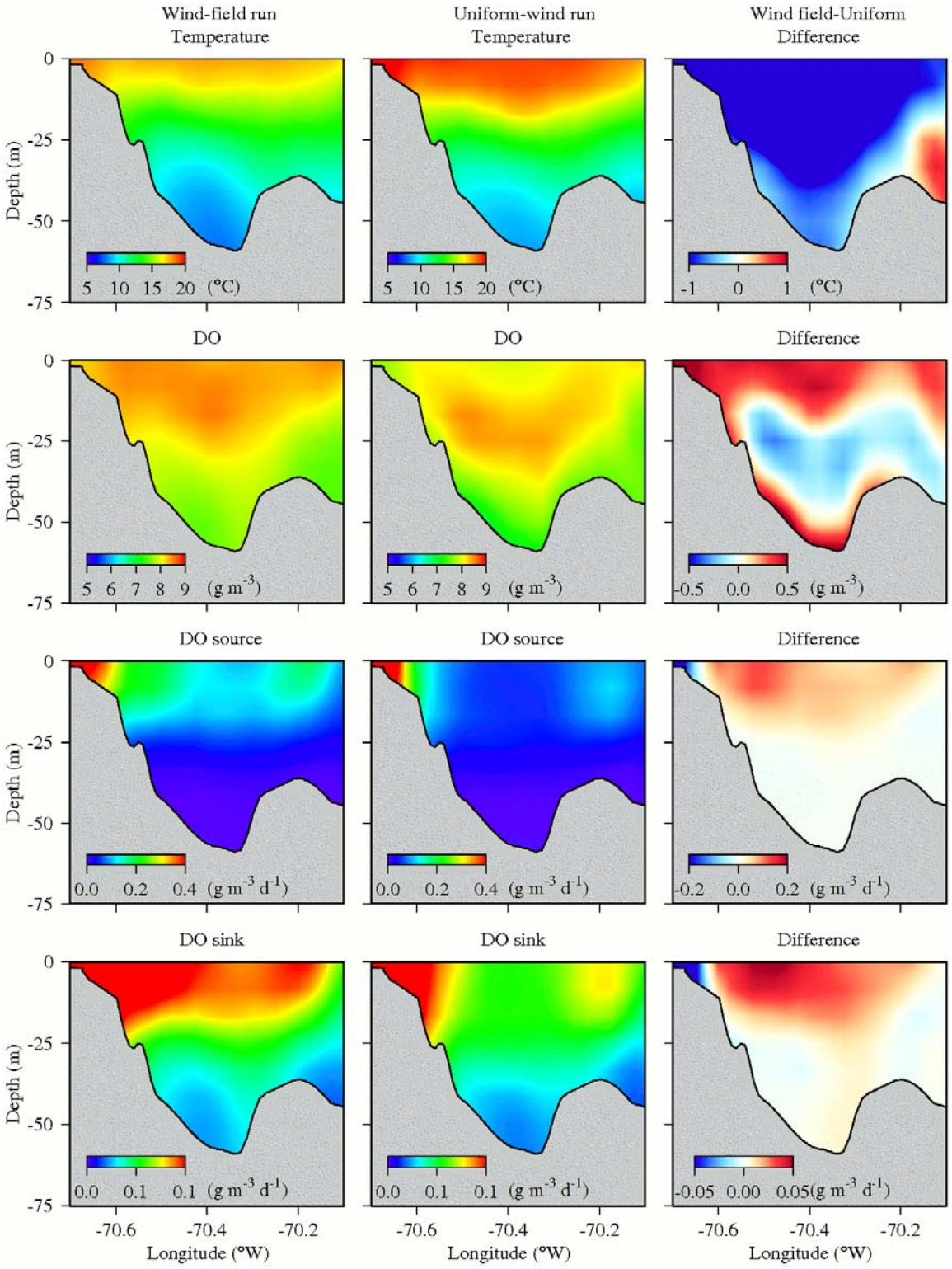

Figure 5.6 Transect of temperature, DO concentration, source and sink terms along the 22nd latitudinal grid (looking north from Cape Cod Bay) during a cyclone event on Aug 20 2006.

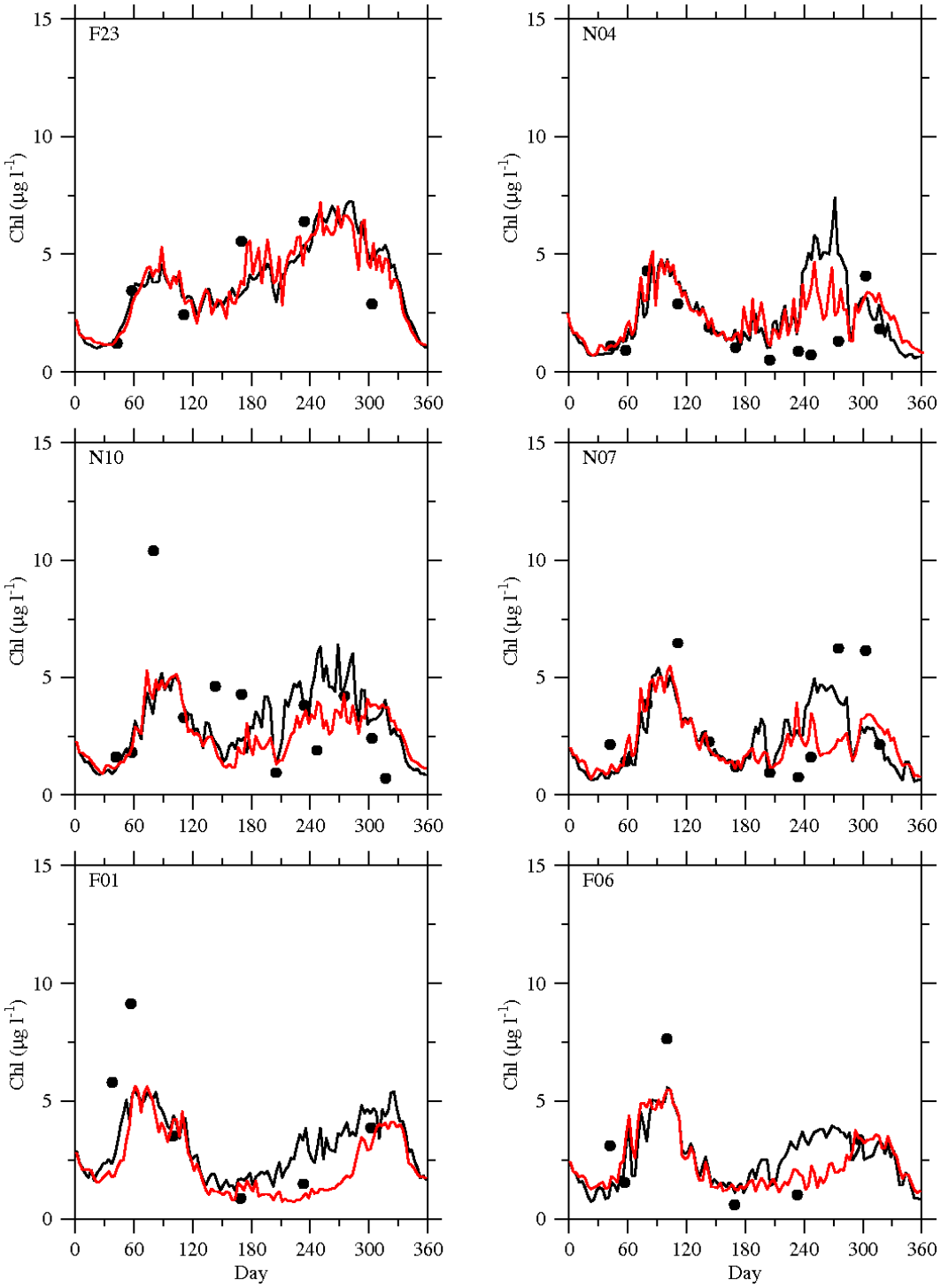

Figure 5.7 Comparison of surface chlorophyll concentration between the Wind-field (black lines) and the Uniform-wind (red lines) runs at the MWRA monitoring stations in 2007.

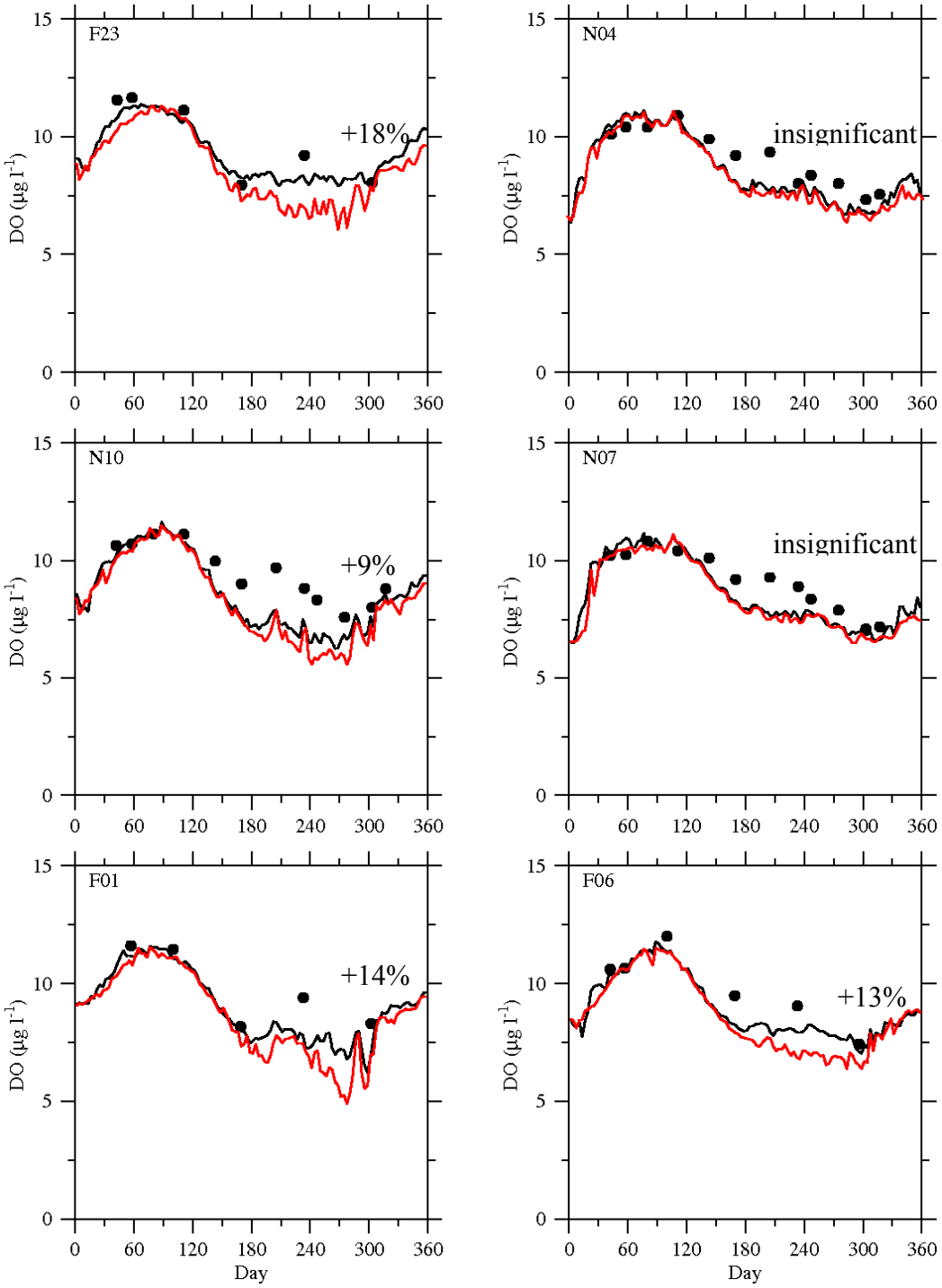

Figure 5.8 Comparison of bottom DO concentration between the Wind-field (black lines) and the Uniform-wind (red lines) runs at the MWRA monitoring stations in 2007.

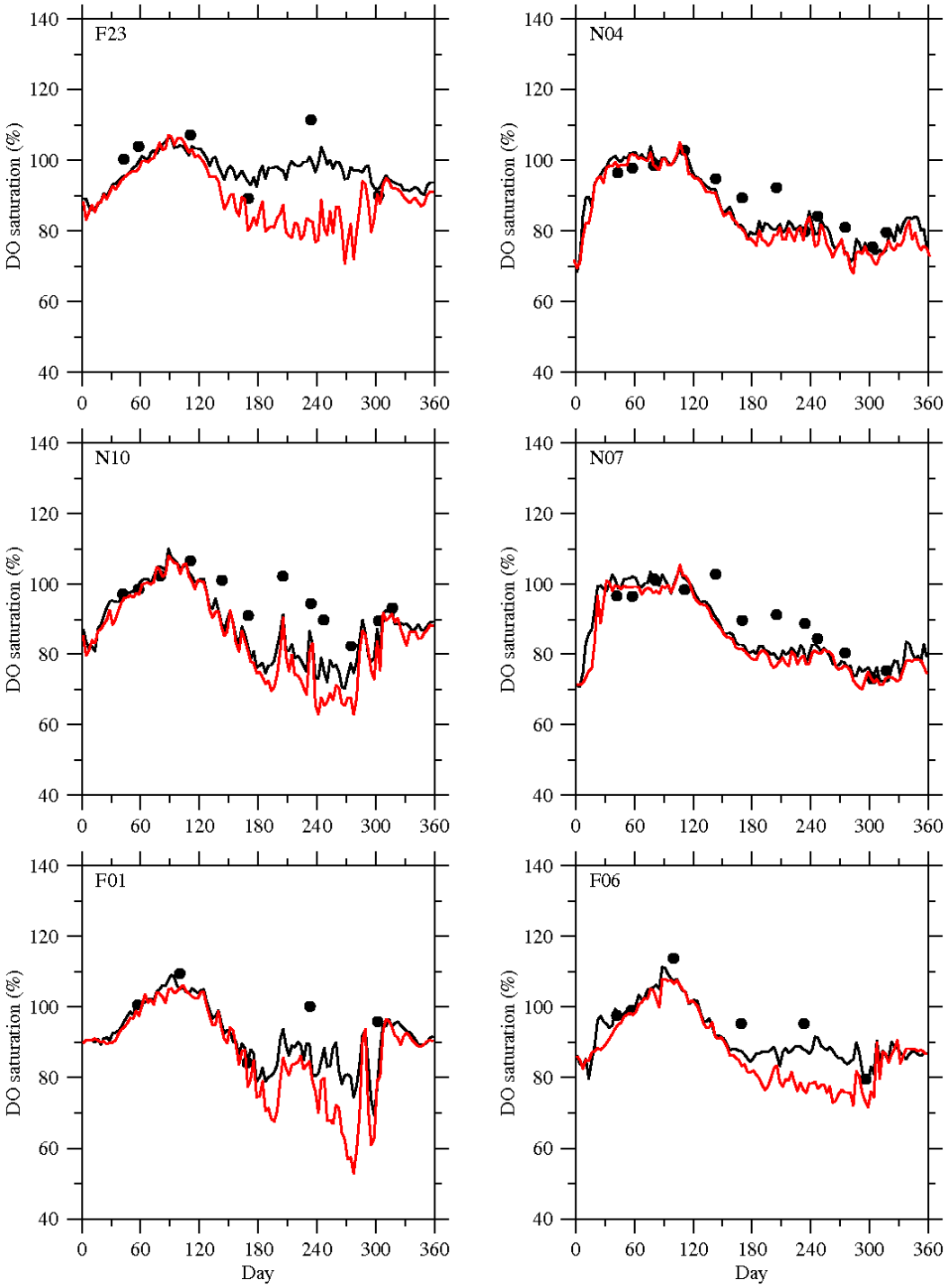

Figure 5.9 Comparison of bottom DO saturation between the Wind-field (black lines) and the Uniform-wind (red lines) runs at the MWRA monitoring stations in 2007.

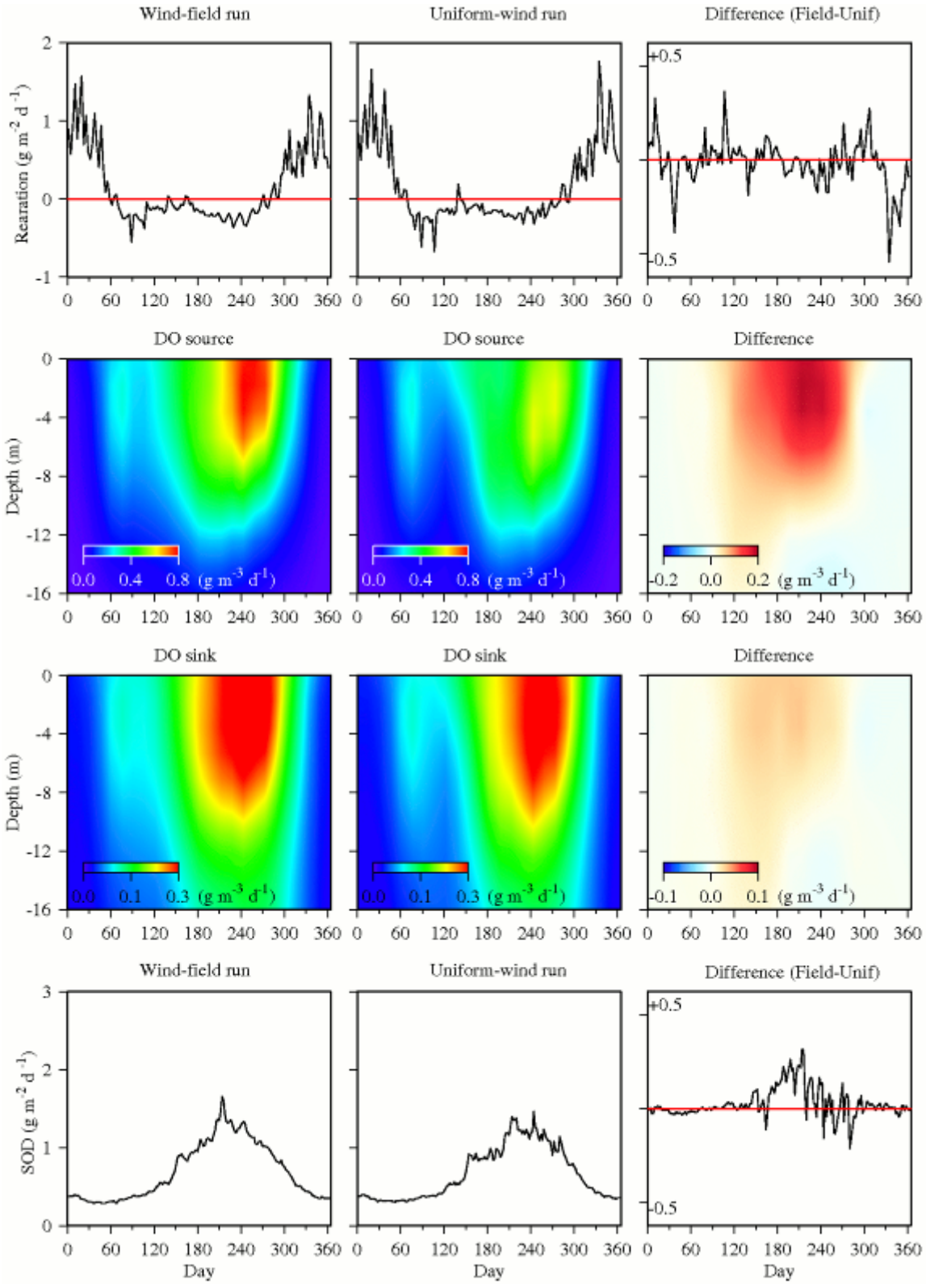

Figure 5.10 DO sources and sinks and difference between the Wind-field and the Uniform-wind runs at Station F23 in 2007.

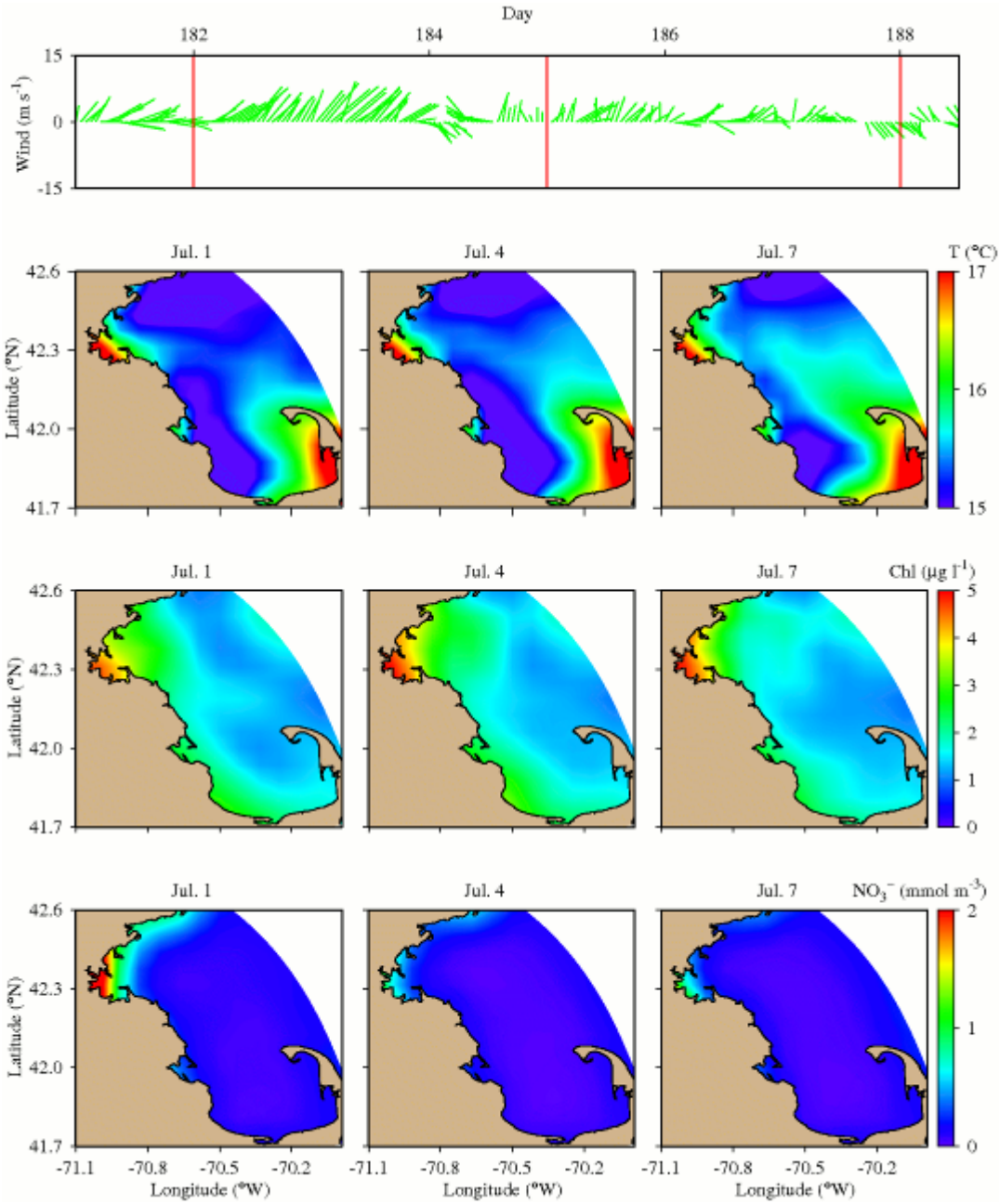

Figure 6.1 Biological response to an upwelling event from Jul 1 to 7 in 2006 reflected in the distribution of surface temperature, chlorophyll and nitrate.

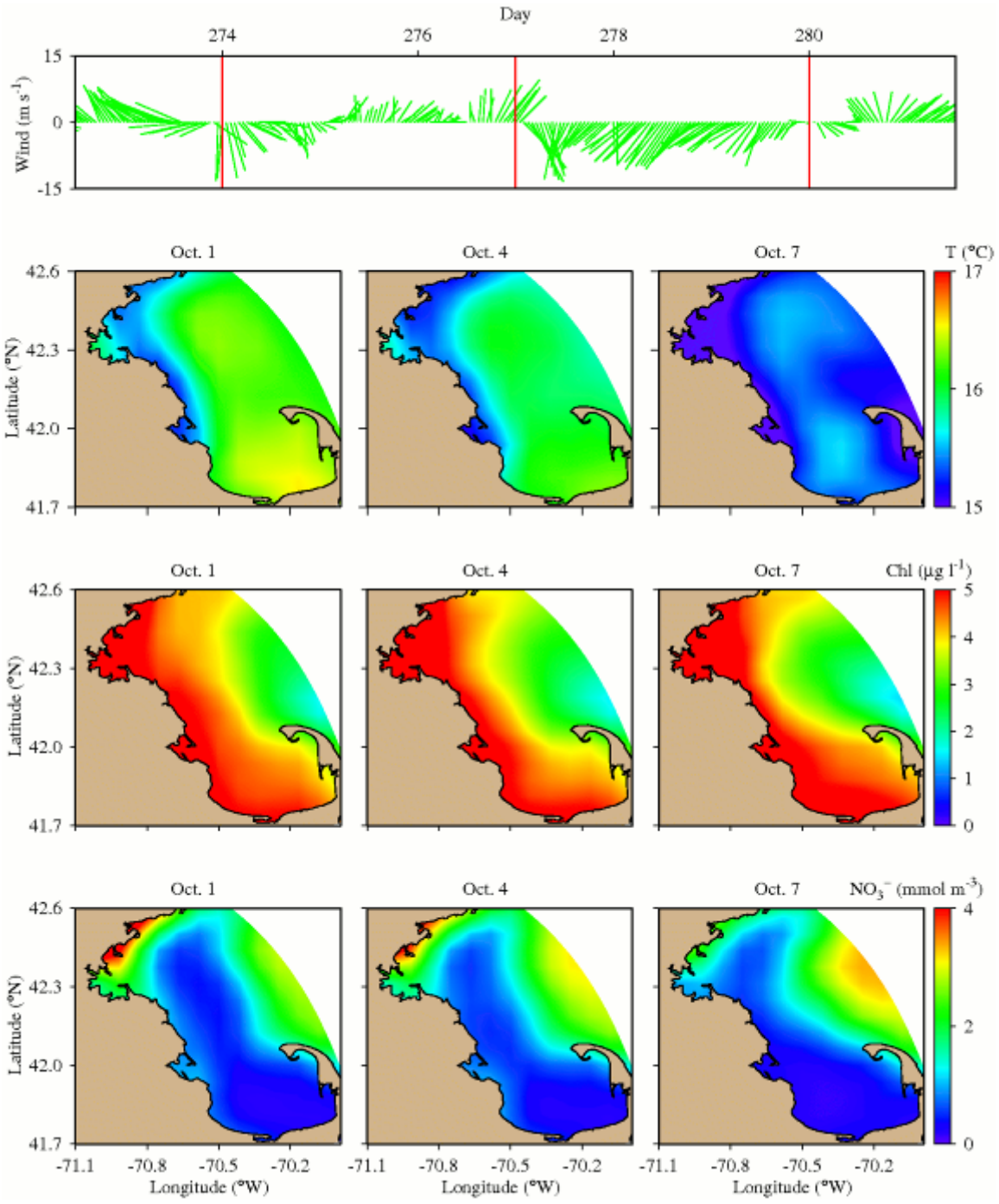

Figure 6.2 Biological response to an upwelling event from Oct 1 to 7 in 2006 reflected in the distribution of surface temperature, chlorophyll and nitrate.

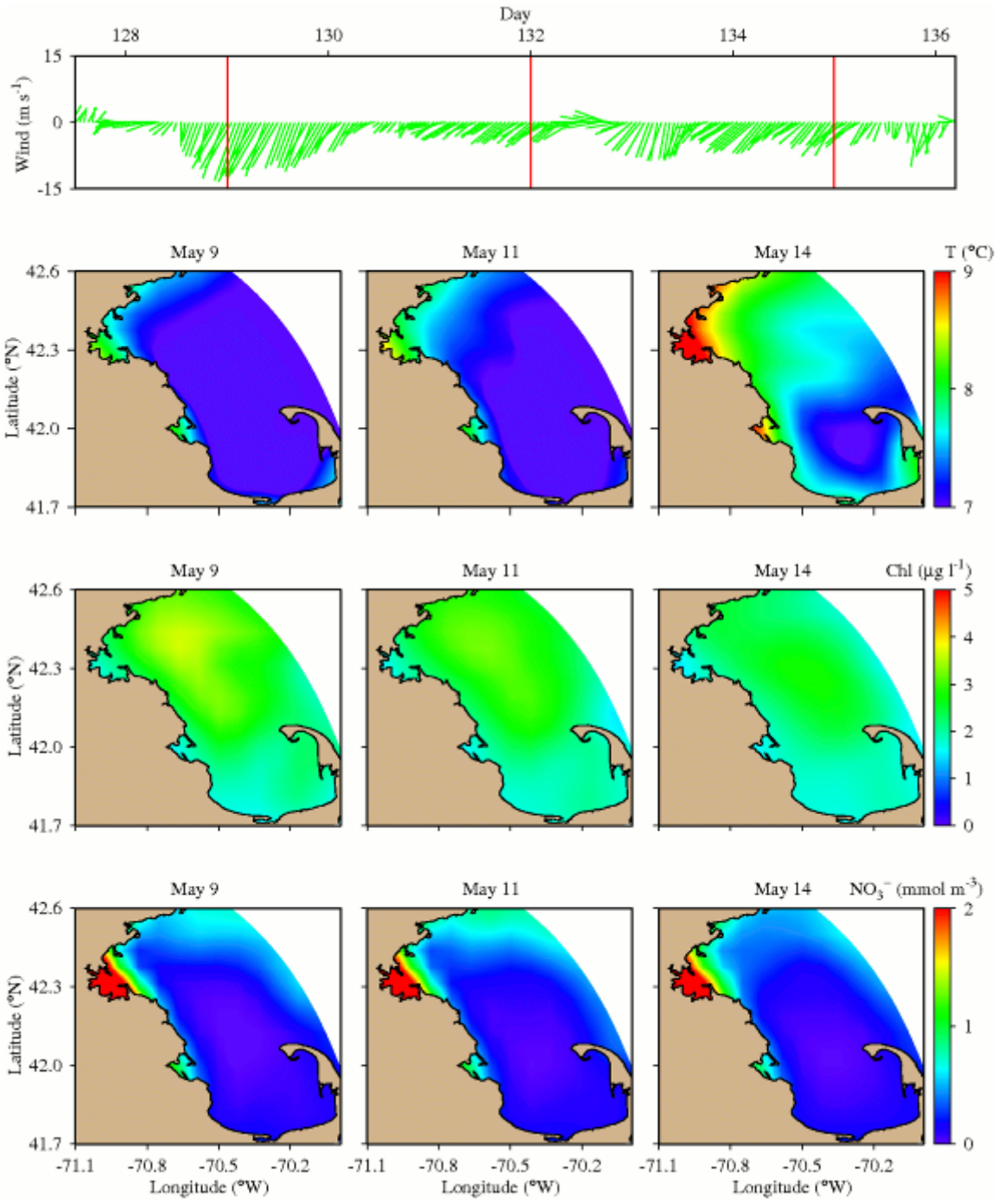

Figure 6.3 Biological response to the passage of a cyclone from May 9 to 14 in 2006 reflected in the distribution of surface temperature, chlorophyll and nitrate.

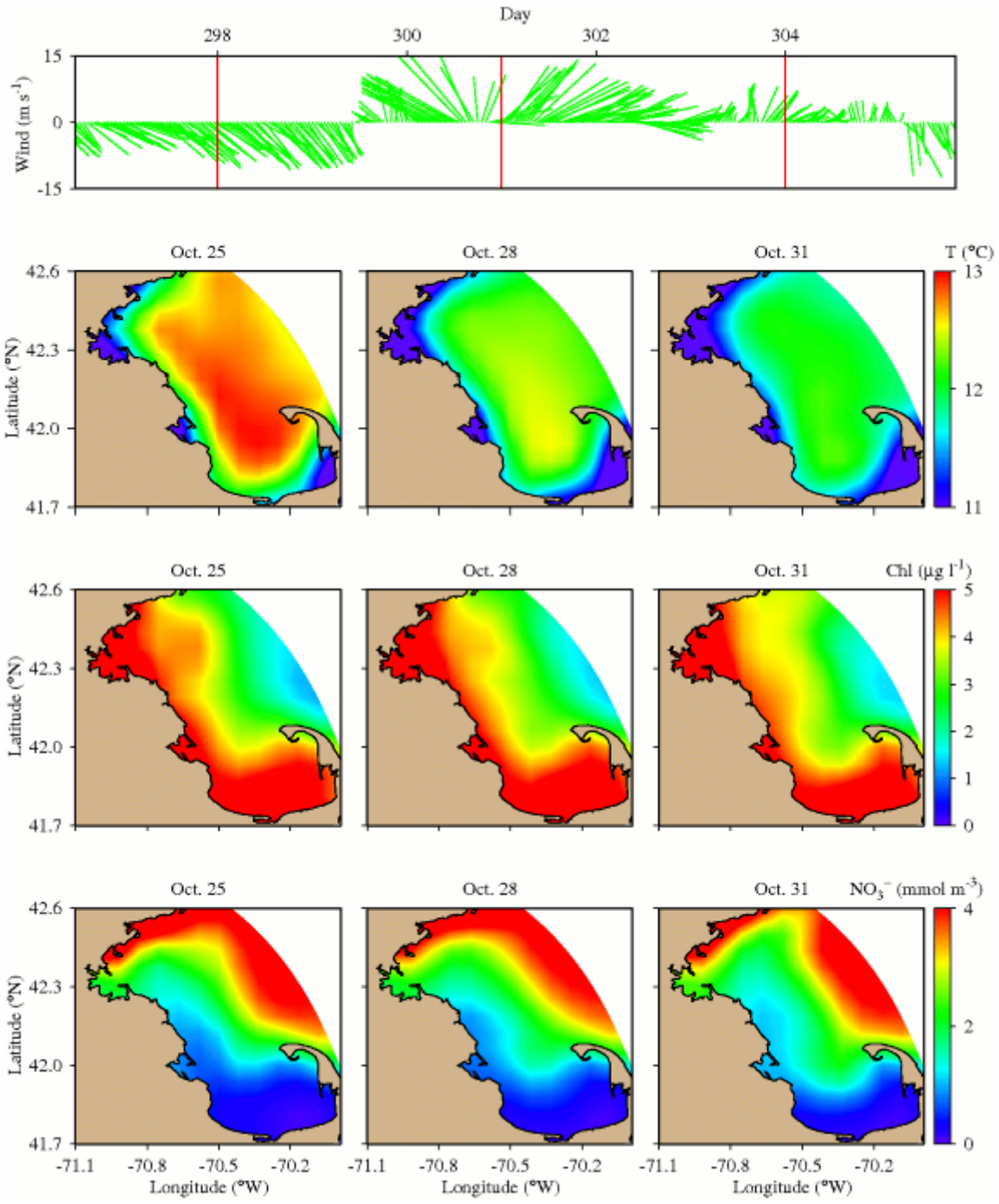

Figure 6.4 Biological response to the passage of an anticyclone from Oct 28 to 31 2006 reflected in the distribution of surface temperature, chlorophyll and nitrate.

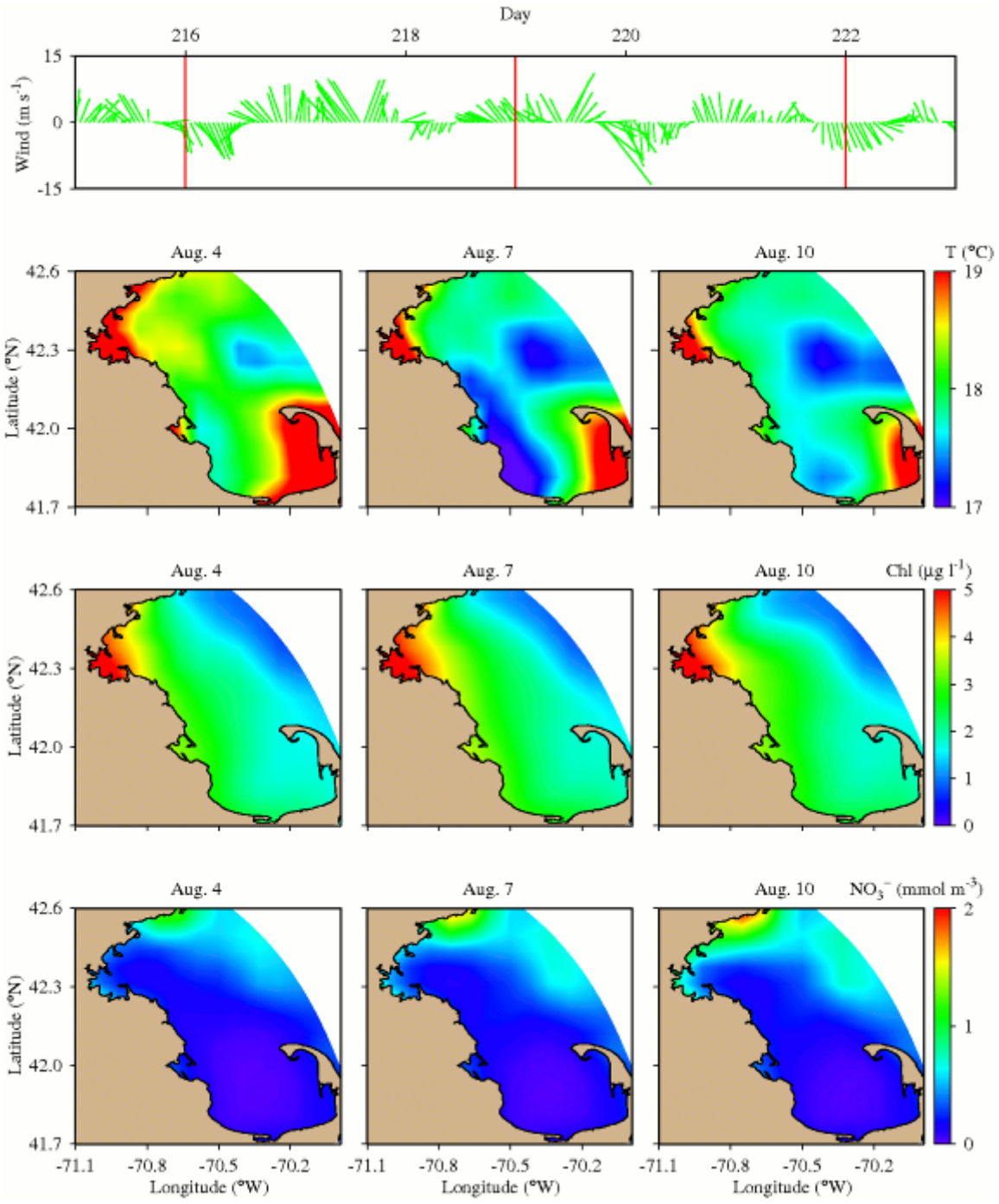

Figure 6.5 Biological response to an upwelling event from Aug 4 to 10 in 2007 reflected in the distribution of surface temperature, chlorophyll and nitrate.

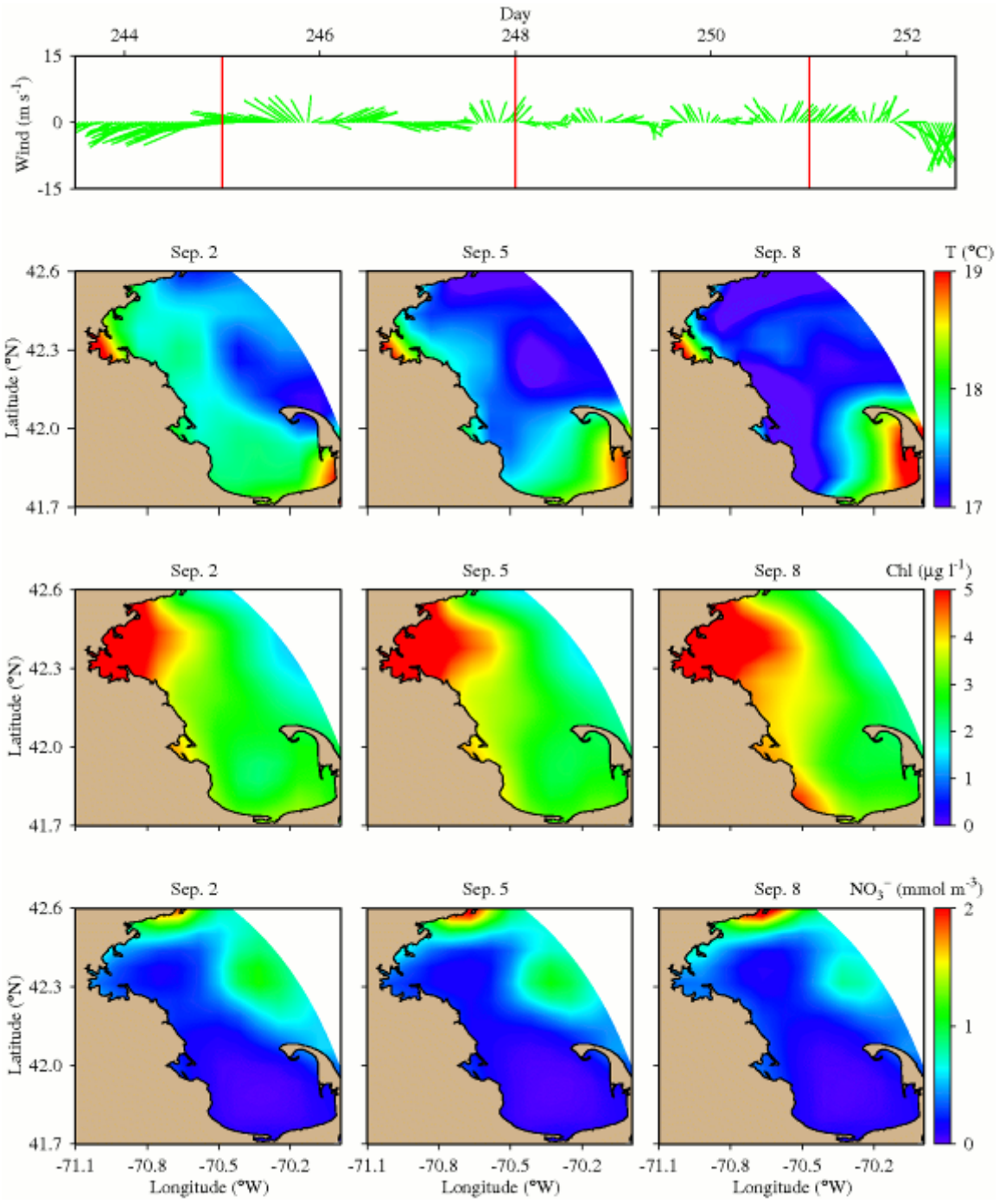

Figure 6.6 Biological response to an upwelling event from Sep 2 to 8 in 2007 reflected in the distribution of surface temperature, chlorophyll and nitrate.

Massachusetts Water Resources Authority
Charlestown Navy Yard
100 First Avenue
Boston, MA 02129
(617) 242-6000
http://www.mwra.state.ma.us